

## Chapter 6

# Thermolysis of Metallopolymers and Their Precursors as a Way for Synthesis of Nanocomposites

In this book we analyse all the types of metallopolymer used as precursors for obtaining nanocomposites via thermolysis. This method is an easy, reproducible and well-controlled route to prepare the nanocomposite materials. The research into the thermal decomposition of organic (metallo)polymers has long prehistory. Back during the Second World War, works on the design of polymers stable up to 870 K were started by the order of the USA air forces (cited from Ref. [1]). The attention was focused on the coordination polymers because the stability of organic compounds was known to increase upon their coordination to metal ions. Thus N-hydroxyethylethylenediamine rapidly decomposes under the action of hot nitric acid, while its complex with CoII withstands long-term (several hours) refluxing in concentrated nitric acid. Similarly,  $\beta$ -diketimine, which decomposes at moderate temperatures, starts to slowly decompose only at 620 K when complexed with copper. Although at that time the search for thermally stable coordination polymers has not met with success (in some cases, very short polymer chains were formed; in other cases, the organic groups connecting the metals were destroyed, etc.), they laid the foundation for the studies that recently resulted in the production of metallopolymer nanocomposites. Currently, various methods for the formation of the 'core-shell' type composites have been developed. These include, for example, sonochemical synthesis techniques [2], electrochemical methods [3], laser-induced reactions in the melt [4] and catalytic growth [5, 6], vapour-phase transport [7], IR pyrolysis [8, 9], polymer sol-gel synthesis [10], intercalation, 'wet' chemical methods [11, 12] etc. [13–15]. Controlled thermolysis was recognized as the simplest and most efficient, economical and versatile method. This process is usually carried out at temperatures from 500 to 1,300 K. It is environmentally clean and serves as a method for polymer waste disposal. An important application of the thermolysis is the preparation of carbon nanomaterials (for example, single- and multiwalled nanotubes, nanorods, nanospheres, etc.). Depending on the nature of the polymer and conditions of thermolysis, various carbon structures can be formed, including graphite- and diamond-like structures.

The thermal stability of a polymer usually determines its upper operating temperature limit in the environment. It is related to kinetic parameters: the initial temperature and the rate of destruction [16]. The knowledge of these parameters is necessary for the application and storage of polymers [17]. Thermolysis of polymers is a complex process involving a number of chemical reactions: destruction, cross-linking, transformations of functional groups and intramolecular rearrangements. For stabilizing a polymer and decreasing its reactivity, chemical or physical insertion of metal-containing particles is sometimes used. This affords new materials and composite systems. The simultaneous synthesis of finely dispersed particles (at their fairly high relative concentration) and the stabilizing polymer shell, together with process simplicity and controllability are the advantages of this approach. Although these studies have been carried out since the mid-twentieth century [18], let us note here the most interesting recent works [19–21] and references therein. The routes of thermolysis of polymers are versatile [22–24].

On the stage of thermolysis the different additives can be incorporated into polymers including metal-containing one which both influence the mechanism of thermolysis and lead to the quite number of interesting products, for example, polymer derivatives of ceramics. Thus, by thermolysis of polyvinyl alcohol (PVA) the polymer with conjugated bonds similar to polyacetylene is obtained. When the additives such as lead and bismuth formates, silver oxalate, potassium iodide or sodium hydroxide are introduced to the PVA a doped conjugated polymer is formed [25]. The metal nanoparticles formed promote electron transfer between the polymer chains and thus polymer conductivity is enhanced. The additives of  $\text{TiO}_2$ ,  $\text{ZnO}$  or  $\gamma\text{-Al}_2\text{O}_3$  considerably influence the thermolysis at 340–390 K of acrylic and fluorine-containing polymers and copolymers [26].

For stabilizing a polymer and decreasing its reactivity, chemical or physical insertion of metal-containing particles is sometimes used. This affords new materials and composite systems. The simultaneous synthesis of finely dispersed particles (at their fairly high relative concentration) and the stabilizing polymer shell, together with process simplicity and controllability are the advantages of this approach.

Numerous methods for the preparation of metal-containing polymeric composites are known. The key method is thermolysis of metal compounds that are readily decomposed both in the pure state and in the polymer matrix (carbonyls, nitrosyls, thiolates, saturated carboxylic acid salts, organometallic and complex compounds) where destruction of the organic part affords the polymeric shell. Other methods are also widely used, in particular, introduction of metal-containing powders with various degrees of dispersion into the ready polymeric matrices and mixing them with oligomers; heteroadagulation or spraying of nanoparticles on polymer powders, films and fibres; evaporation of the solvent from a solution containing the polymer and the metal-containing precursor or hardening of their melts in liquid media; extraction substitution and soon. However, all of these methods have drawbacks. The main drawbacks include the statistical pattern of distribution and spatial inhomogeneity of the metal-containing particles in the matrix and the lack of

control over the reaction at the dispersed phase – polymeric medium level. However, in all cases, the polymeric shell which separates the metal particles from one another and from the environment functions as a stabilizing agent, which may be represented by a natural (proteins, polysaccharides) or synthetic material obtained by polymerization or polycondensation. Of particular interest are the macromolecular metal complexes in which the metal is chemically bound to a polymer containing active functional groups (carboxylate, nitrile, amino, amido, imino and hydroxy groups and so on) but studies of the thermal transformations of such systems are only at the early stage of development.

Of particular interest are the macromolecular metal complexes in which the metal is chemically bound to a polymer containing active functional groups (carboxylate, nitrile, amino, amido, imino and hydroxy groups and so on) but studies of the thermal transformations of such systems are only at the early stage of development.

Relatively recently, a new approach has been developed [27] based on the use of metal-containing monomers as precursors. In this case, polymerization and synthesis of metal-containing nano-sized particles occur simultaneously during the thermal transformation. This field of research developed most intensely in recent years was called ‘polymer-mediated synthesis’ in our study [28] or it is called ‘combined solid-state polymerization – thermolysis.’ For the systems considered here, ‘dry’ methods for the composite formation are mainly used.

Note that quantitative studies of the thermolysis giving matrix-stabilized nanoparticles are few. These works are mainly qualitative and aim at describing the averaged characteristics and size distributions of the particles.

## 6.1 Kinetic Approaches to the Investigation of Thermolysis of (Metallo)polymer Systems

The kinetic approaches to the studies of thermolysis of (metallo)polymer systems provide quantitative knowledge about the course of transformations in each step for relatively slow processes at temperatures below 1,370 K. In recent years, thermogravimetric methods such as differential thermogravimetry (DTG) and differential thermal analysis (DTA), differential scanning calorimetry (DSC), thermodilatometry and thermomechanical analysis, dielectrical analysis, micro- and nanosized thermal analysis (including atomic force microscopy and scanning thermal microscopy) have been widely used, in particular, to study the thermolysis of (metallo)polymers. Recent achievements in the field of thermal analyses are summarized in the monograph [21].

Any thermal process is accompanied to a certain extent by the change in the inner heat content of the system, i.e., heat absorption or evolution. During the low-temperature thermolysis of most condensed polymer systems, the transformation rates are relatively low and the temperatures are low at rather intense heat transfer. Irrespective of the heat effect, these processes occur with time in the

spatially isothermal mode [29] i.e., the temperature of the surface of a condensed sample ( $T_a$ ) coincides with the ambient temperature ( $T_s$ ). In this case, the isothermal methods of classical chemical kinetics are applicable and the process conditions are formulated in view of scaling requirements, in particular, the ratio of the characteristic times of heating ( $\tau_h$ ) and transformation ( $\tau_r$ ).

The kinetics of thermal transformation of metallopolymer systems is generally described by the macrokinetic equation:

$$W(T, \eta) = k(T) \times \varphi(\eta), \quad (6.1)$$

where  $W(T, \eta)$  is the reaction rate ( $s^{-1}$ ),  $T$  is the temperature (K),  $k(T)$  is the temperature-dependent rate constant determined by the reaction mechanism ( $s^{-1}$ )<sup>1</sup>,  $\varphi(\eta)$  is a kinetic function. The last-mentioned value depends on the reaction mechanism and reflects the relationship between the concentrations of unreacted and reacted compound.

$$\varphi(\eta) = (1 - \eta)^n \quad (6.2)$$

where  $n$  is the order of the reaction,  $\eta$  is the degree of conversion ranging from 0 to 1.

Then the characteristic time of the reaction

$$\tau_r \approx W(T, \eta)^{-1}.$$

Since the transformations occur in the condensed phase, it is expedient to use as  $\tau_h$  the characteristic time of sample warming-up traditional for macrokinetics: [30]

$$\tau_h \approx d^2/a,$$

where  $d$  is the sample diameter,  $a$  is the sample temperature conductivity. In this case, for obtaining reliable kinetic results, the following condition should be met:  $\tau_h \ll \tau_p$ .

As a rule, thermolysis of polymers is a multistage process. Its mechanism is studied using various types of kinetic models. In a pseudo-single-component model, the material is considered to be ordered and single-component, and the mass loss is described by studying the kinetics of the solid- or gas-phase reaction over the whole temperature range [31]. However, this model does not describe the possible changes in the kinetics and mechanism upon the change in the temperature of thermolysis.

The pseudo-multicomponent summary model analyzes the material as consisting of a number of pseudo-components each of them being a separate real component or mixture of several components and the polymer thermolysis is

<sup>1</sup>The rate constant for the reaction can be expressed by the Arrhenius dependence  $k(T) = A \exp(-E_a/RT)$ , where  $A(s^{-1})$  is the pre-exponential factor ( $s^{-1}$ ),  $E_{a,eff}$  is the effective activation energy ( $kJ mol^{-1}$ ),  $R$  is the universal gas constant.

modelled by superposition of decompositions of these components. However, this approach considerably complicates the kinetic studies of thermal destruction. For example, in the case of thermolysis of polyaryl sulfides, the weight loss takes place in two stages [32]. The pseudo-two-component first-order stage-separated model considers the material as being decomposed in two temperature regions, which are described by different kinetic models. The temperature corresponding to the minimum in the derivatogram is the separation point between the two stages of weight loss. This method is considerably complicated when the two peaks are not completely separated but overlap.

The non-isothermal method is widely used to describe the kinetics and the mechanism of reactions in the condensed phase. Since the rate of thermolysis depends on the temperature, the change in the sample weight can be presented as the dependence:

$$\frac{d\eta}{dt} = k(T)\varphi(\eta) = A \exp\left(-\frac{E_a}{RT}\right)\varphi(\eta) \quad (6.3)$$

When the sample temperature is controlled by a constant heating rate  $\beta$  ( $\beta = dT/dt$ ), this equation has the form:

$$\frac{d\eta}{dt} = \frac{A}{\beta} \exp\left(-\frac{E_a}{RT}\right)(1-\eta)^n \quad (6.4)$$

In the integral form, expression (6.4) looks as follows:

$$g(\eta) = \int_0^\eta \frac{d\eta}{(1-\eta)^n} = \frac{A}{\beta} \int_0^T \exp\left(-\frac{E}{RT}\right) dT = \frac{AE}{\beta R} P(u) \quad (6.5)$$

and

$$\ln \left[ \frac{g(\eta)}{T^2} \right] = \ln \frac{AR}{\beta E_a} - \frac{E_a}{RT}. \quad (6.6)$$

For  $n = 1$

$$\ln \left[ -\ln \frac{1-\eta}{T^2} \right] = \ln \frac{AR}{\beta E_a} - \frac{E_a}{RT} \quad (6.7)$$

For  $n \neq 1$  in the most cases expression (6.7) is solved numerically.

Equations (6.5) and (6.6) are the fundamental expressions for calculating the kinetic parameters from thermogravimetric (TG) data. These are analyzed using the Kissinger, Flynn - Wall - Ozawa (FWO), Coat - Redfern, van Krevelen (vK), and Avramy-Erofeev methods in the differential and integral forms (see, for example [33–35]).

The dynamic parameter of thermal decomposition under linear heating is determined from the modified Kissinger equation at  $T_{\max}$ , i.e., the temperature corresponding to the maximum conversion in the TG curves. The straight-line plot  $\ln(\beta/T_{\max}^2) - 1,000/T_{\max}$  is used to calculate the activation energy and the pre-exponential factor. Equations (6.5) and (6.6) describe the thermolysis at 473 K of polymer networks and star-like polymers based on ethylene glycol dimethacrylate containing degradable acryl groups to give low-molecular-mass products [19]. Also the kinetics of nonisothermal decomposition of polypropylene filled with both mineral additives such as calcium carbonate, dioxide of silicone, zinc oxide, carbon black and fibers [36, 37] and organic ones as rice husk [38, 39] is well described by these equations. The degradation kinetics of the LDPE stabilized by cobalt stearate was investigated with the Flynn-Wall-Ozawa method [40, 41]. Several kinetic methods were used to investigate the thermal decomposition of chromium polyacrylate complexes [42, 43]. Under comparable conditions, the initial temperatures for the polymer and the metal complex were 628 and 591 K, respectively, and the final temperatures were 806 and 813 K; the temperature peaks in the derivatogram were observed at 713 and 690 K, the weight losses (%) were 53.40 and 65.56, and the activation energies of decomposition (at  $0.05 < Z < 0.90$ ) were 187.8 and 122.5 kJ/mol. The orders of reaction differed from unity for all of the decomposition models. These parameters depend to some extent on the storage time of the aged (for 1–5 weeks) macrocomplex.

At relatively low temperatures (for instance, the decomposition of metal carbonyls such as  $\text{Cr}(\text{CO})_6$ ,  $\text{Fe}(\text{CO})_5$ ,  $\text{Co}_2(\text{CO})_8$  in toluene at 363 K [44]) the study of kinetics can be carried out with spectral methods, in particular, by FTIR analysis on the decreasing of the band intensity at  $1,977 \text{ cm}^{-1}$  (at  $1,996$  and  $2,019 \text{ cm}^{-1}$  for iron and cobalt carbonyls, respectively).

Nonisothermal kinetic modeling of thermolysis of natural fibers commonly used in industry and their composites [45] showed the good agreement between the calculated kinetic parameters and experimental data in the rather wide range of temperatures.

Formal kinetics method [46, 47] in combination with the Netzsch-Thermokinetics programme allows one to describe the behavior of the system analysed; the data obtained are most informative in the study of complex multistage processes as thermolysis (Table 6.1).

**Table 6.1** The kinetic models and parameters for different stages of thermolysis

The kinetic model	$E_a/R \cdot 10^3 \text{ K}$	$\log A$	$N$
Prout Tompkins	$14.17 \pm 0.18$	$9.12 \pm 0.14$	$1.37 \pm 0.02$
$n$ th-order reaction	$16.71 \pm 0.16$	$9.85 \pm 0.12$	$1.43 \pm 0.02$
Prout Tompkins	$15.45 \pm 0.12$	$8.18 \pm 0.09$	$1.28 \pm 0.04$

$E_a/R$  is the temperature coefficient of the reaction rate,  $A$  is the pre-exponential factor,  $n$  is the effective reaction order

Thermal treatment considerably changes the structure and properties of a polymeric material. This is due, first of all, to the physical and chemical processes that accompany the polymer destruction. The physical destruction processes (crystallization, recrystallization, etc.) are usually reversible and do not lead to cleavage or cross-linking of polymer chains. The chemical processes are irreversible and are accompanied by chemical bond cleavage, cross-linking of macromolecules, changes in the chemical structure or decrease/increase in the molecular mass [48, 49].

For the design of metallopolymer compositions, the thermal stability of polymer matrices is important. It can be estimated from the strength of the bond between atoms. According to the Boltzmann law, the bond strength is determined by the expression  $S = E_b/RT^2$ , where  $E_b$  is the bond energy (in kJ/mol). The dependence of  $S$  on  $\gamma = (E_{X-Y} - E_{C-C})/E_{C-C}$ , i.e., the change in the bond energy between the atoms X and Y ( $E_{X-Y}$ ) relative to the average carbon-carbon bond energy ( $E_{C-C}$ ) in organic polymer, shows that organic homo- and heterochain polymers are least thermally stable. Inorganic matrices (clays, hexagonal boron nitride, silicate glasses, zeolites, etc.) having no carbon backbone and graphite are distinguished by enhanced thermal stability and mechanical strength. The bond energies between most typical atoms of the organic and inorganic matrices are summarized in Table 6.2. Polymeric compounds have especially strong Si-O, B-N and B-O bonds (note that the probability of chemical bond cleavage depends also on temperature).

A different kinetic picture is observed at relatively high temperature. In the case of high-temperature thermolysis, the time  $\tau_r$  related to the temperature  $T_a$  decreases and  $\tau_h$  does not depend on  $T_a$  and remains constant. Then in the case of exothermic reaction at  $\tau_h \approx \tau_r$ , thermal explosion is possible, and at  $\tau_h \gg \tau_r$ , ignition occurs well before the studied compound has been warmed-up and has time to react in the area adjoining the

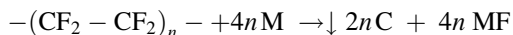
**Table 6.2** Bond energy between the atoms in the polymer matrices [50, 51]

Bond	Bond energy, kJ/mol	Bond	Bond energy, kJ/mol
Carbon-containing matrices			
C-C	336	C-B	372
C-O	327	Al-N	363
C-N	277	Si-O	364
C-Si	241	B-O	500
C-Al	258	B-N	387
Inorganic polymer matrices			
C-C	715 <sup>a</sup>	Ti-O	933
Al-O	1,027.6	B-O	1,047
Al-N	1,121	B-N	1,289
Si-O	586		

<sup>a</sup>For crystalline graphite

hot surface [29]. In the case of fast endothermic reactions,<sup>2</sup> no-self ignition takes place upon increase in  $T_a$ , and the temperature profile for the studied compound is not spatially isothermal. It depends on both the reaction coordinate and time, and the temperature assignment of the detected transformation becomes uncertain.

In particular, metal-polytetrafluoroethylene (M/PTFE) mixtures represent condensed high-energetic materials in which vigorous exothermic reactions take place according to the idealized scheme:



The PTFE is chemically and thermally stable due to the high energy of the C–F bond (481 kJ/mol). The composites can be used as oxidation agents because in many cases the strength of metal-fluorine bond is even more than that for C–F bond. The rate of thermolysis depends on the size of the reacting particle and concentration of reduction agent in the mixture [52–55]. Such composites are widely used as igniters of solid propellants and pyrotechnics [55, 56]. Self-propagation heat waves, associated with the oxidation of metals at heating rates at  $10^6$  K/c can yield new materials resulting from these ultra-fast reactions. High temperatures of thermolysis (theoretically exceeding 3,000 K for Mg/PTFE [57]) and specific conditions for fast product growth favour the formation of nanostructures and polyynes ( $-C\equiv C-$ )<sub>n</sub>.

Calorimetric studies (Fig. 6.1) showed that thermolysis proceeds in a self-sustaining high-temperature regime [58]. The heats of the reaction range from very low (less than 1,000 kJ/kg) for Zn/PTFE composites enriched with a metal to very high (more than 8,000 kJ/kg) for the reactants containing  $Al_3Mg_4$  at a concentration close to the postulated stoichiometry. Nevertheless, these numbers account for only ca. 70 % of the theoretical exothermal effect calculated assuming the chemical equilibrium of the thermolysis.

Hence, the classical isothermal methods are inapplicable to the kinetics of fast high-temperature processes. These processes are to be studied using the approaches of nonisothermal chemical kinetics the foundations of which were laid in the fundamental works: N. N. Semenov, D. A. Frank-Kamenetsky, Ya. B. Zeldovich, A. G. Merzhanov and were considered in detail in the book [29].

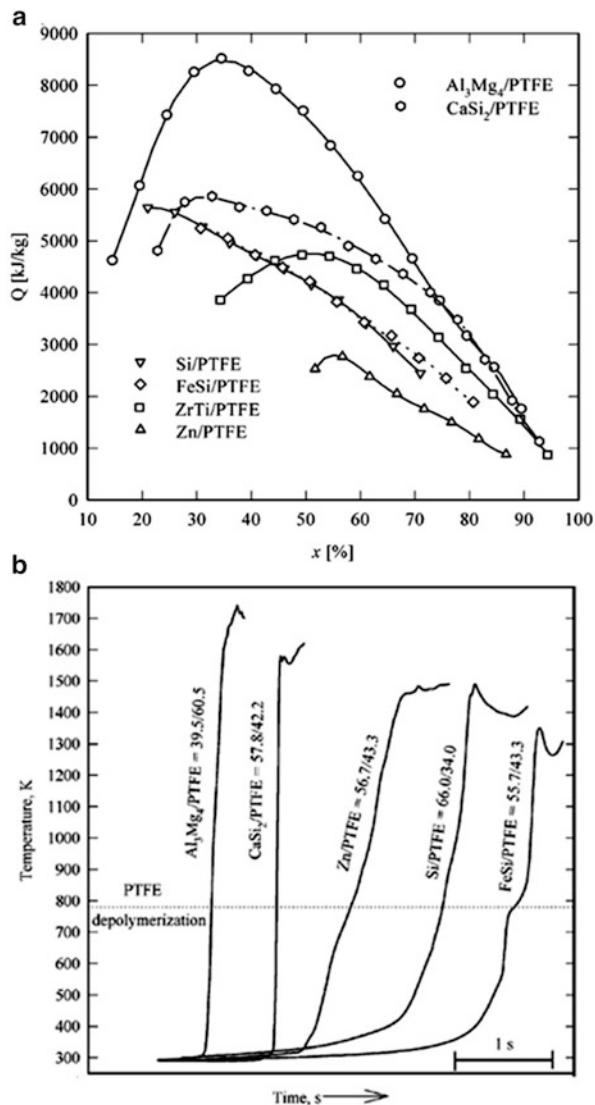
## 6.2 General Characterization of the Principal Methods of Thermolysis of (Metallo)polymers and Their Precursors

Thermal transformation of (metallo)polymers and their precursors are studied using external (or internal) heating under isothermal (or non-isothermal) conditions in a closed (or open) system. Depending on the task, the degree of conversion of the

<sup>2</sup>An example is forced high-temperature destruction of the polymer binders of the thermal protection covers of space vehicles, which accompanies the combustion of solid rocket propellant components.



**Fig. 6.1** Heats of reaction for M/PTFE mixtures as a function of metal (M) content (a) and change of temperature during ultra-fast burning reaction of the PTFE mixtures (b)



reactant is determined by a variety of methods. They are classified into gravimetric (thermogravimetric) and volumetric methods and determine the selection of the experimental gear.

Development of the instrumentation for measuring the kinetics of thermolysis has started since the first quarter of the twentieth century; the approaches to the design of instruments and protocols were analyzed in detail about 50 years ago in a monograph [59], which is still not out of date (see also the recently appeared review [21]). In recent years, integrated (synchronous) devices that combine several

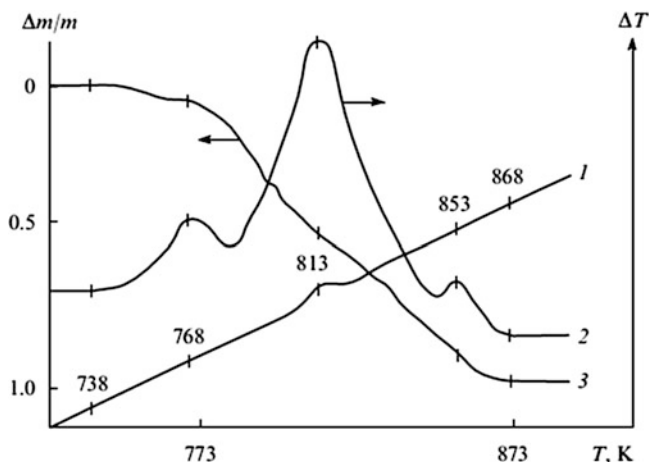
methods for monitoring the reactant conversion with automation and utilize the potential of modern computers within one instrument have started to appear. The specific features of the principal methods used to measure the kinetics of formation of nanoparticles are briefly analyzed below.

### 6.2.1 Thermogravimetric Methods

Thermogravimetric methods measure the relative change in the substance weight during the transformation as a function of temperature. Most often, the sample experiences programmed temperature change with a linear dependence on time. In some cases, thermogravimetry is combined with tensimetry and gas evolution is simultaneously measured. As a rule, these measurements are carried out under isothermal conditions in a dynamic vacuum and with recording in both continuous and discrete modes. For example, a study of the kinetics of consumption of volatile fractions formed in the pyrolysis of non-fractionated 230 kDa polystyrene was carried out using spring balance [59]. The resulting kinetic curves were S-shaped with a maximum transformation rate at  $\eta = 0.35\text{--}0.55$ . A modern thermobalance is suitable for continuous (automated) recording of the temporal variation of the sample weight ( $\Delta m$ ), and with known law of time variation of temperature, these dependences can be displayed via a computer. The TG methods are mainly based on traditional non-isothermal variants of linear heating.

In recent years, thermogravimetric methods such as differential thermogravimetry (DTG) and differential thermal analysis (DTA) have been widely used, in particular, to study the thermolysis of (metallo)polymers. In the former case, the first-order derivative of thermogravimetric curve is found either with respect to time ( $dm/dt$ ) or with respect to temperature ( $dm/dT$ ). In the latter case, the temperature difference between the substance and the reference is measured as a function of temperature, the substance and the reference being programmed heated. The development of DTA toward increase in the accuracy of quantitative determination of process heats led to the advent of the new investigation technique called differential scanning calorimetry (DSC) [60].

The combined use of thermogravimetric analysis (TGA) and DTA is illustrated by the data on thermooxidative destruction of polytetrafluoroethylene (PTFE) [61]. By DTA measurements (Fig. 6.2), it was shown for the first time that the transformation of PTFE in air proceeds in three stages with a complex heat evolution pattern in the temperature range of 735–870 K; the last two stages with characteristic temperatures of 810–820 and 850–860 K are accompanied by the loss of 94–95 % of the sample weight. The exothermic character of each stage attests to partial oxidation of the products formed upon PTFE destruction with air oxygen. The average apparent activation energy of the main period (735–850 K) calculated from the data of a non-isothermal experiment using TG curves is 295 kJ/mol, being independent of the heating rate or the particle size of the polymer. Meanwhile, at 735–870 K, the results of thermooxidative destruction of PTFE in the isothermal



**Fig. 6.2** Derivatogram of polytetrafluoroethylene [61]. (1) Temperature change, (2) DTA data, (3) TGA data

mode up to a degree of conversion of 0.9 are described satisfactorily by the 2/3-order reaction kinetics (the ‘compressing’ sphere equation [62]). In the temperature range of 735–870 K, the reaction rate increases 20-fold at  $\eta = 0.35$  and sixfold at  $\eta = 0.7$ . The activation energies are 24 kJ/mol in the temperature range of 735–770 K and 102 kJ/mol in the temperature range of 770–870 K. These values are considerably (more than 2.5 times) lower than the values obtained in the dynamic mode, which raises doubts on the correctness of determination of the kinetic data from PTFE destruction experiments performed in the non-isothermal mode.

The vast majority of the procedures used to determine the kinetic parameters from the DTA-TGA experiments carried out in the linear heating mode are based on the solution of the mathematical problem with allowance for only one kinetic equation. The mathematical simplicity of this scheme accounts for its popularity. However, during the experiment, the system is self-heated, which may generally surpass the quasi-stationary temperature difference by a large factor or even by orders of magnitude [63]. In the case of programmed heating rate, the kinetic characteristics of the process include the temperature of the decomposition onset, the decomposition stages, and temperature ranges of stability of the intermediate compounds [60]. Ignoring the specific features of exo- and endothermic reactions and the effect of heat-exchange parameters (heat transfer coefficient, heating rate, reaction heat, sample weight, etc.) affects the legitimacy of using a particular method for kinetic data acquisition.

For reducing the distortions introduced by the noncontrolled pressure and by the permanently increasing temperature, a new TG experiment was developed and served as the basis for the quasi-isothermal quasi-isobaric thermogravimetry technique [60, 63]. This implies fine adjustment of heating in such a way that the rate of variation of either weight or pressure is maintained constant.

**Table 6.3** Characteristics of thermoanalytical methods [64]<sup>a</sup>

Method	Measured characteristics	Application
Common methods		
Thermogravimetry	Weight	Phase destruction, dehydration, oxidation
DTA, DSC	Temperature difference between the reference and the tested compound	Phase transitions (temperature and heat) and chemical reaction (heat capacity)
Thermomechanical analysis (TMA)	Deformation	Mechanical changes, deformations
Thermooptometry	Optical properties	Phase changes, surface reactions, colour changes
Dielectric thermal analysis	Dielectric constant	Phase changes, changes in polymers
Specific methods		
Synchronous thermal analysis	Combines two or more methods of sample investigation	
Thermal analysis with a specified process rate	The rate of the change of sample properties is maintained constant	

<sup>a</sup>Note: In some cases, these methods are used in a reducing atmosphere, for example, in a 92:8 (by volume) N<sub>2</sub>:H<sub>2</sub> mixture

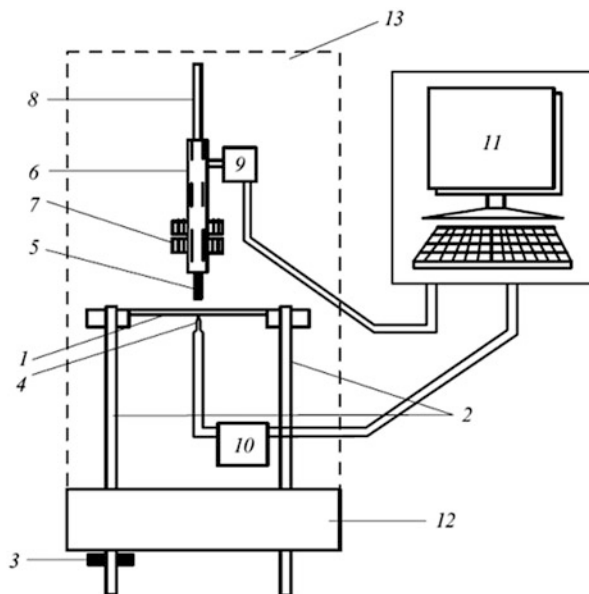
It is noteworthy that until recently all determinations of the kinetic parameters have been performed by ‘discrete’ type procedures using a small fraction of the ‘continuous’ information embedded in the set of DTA–TGA curves. For strict approximation to the real process, the kinetic equation should be considered together with the heat balance equation.

The best known thermoanalytical methods and their applications are indicated in Table 6.3.

### 6.2.2 Linear Pyrolysis Method

Linear pyrolysis (LP) is a steady-state one-dimensional propagation of the thermal reaction front of a condensed substance with heat supply from an external source [29]. Depending on the relationship between the effective ( $E_{\text{eff}}$ ) and true ( $E_{\text{tr}}$ ) activation energies, LP can occur in either of two regimes: kinetic (the macrokinetics of pyrolysis coincides with the true kinetics of decomposition,  $E_{\text{eff}} \approx E_{\text{tr}}$ ) or internal diffusion regime (by heat,  $E_{\text{eff}} \approx E_{\text{tr}}/2$ ). The development of this method was caused by the need for investigating the kinetics of fast high-temperature processes in condensed media where transition from one temperature region to another is accompanied by a change in the rate-limiting step of the reaction. In addition, the knowledge of the regularities of forced high-temperature decomposition of polymers

**Fig. 6.3** Schematic diagram for linear pyrolysis. (1) Heater plate, (2) conducting planes, (3) current lead, (4) thermocouple, (5) sample, (6) sliding piston, (7) ring loads, (8) guide bar, (9) photodiode block for process rate recording, (10) control and heater plate temperature recording block, (11) computer block with a monitor, (12) massive vinyl plastic plate, (13) cover



is important for the development of modern space rocket facilities. They are necessary for solving problems related to combustion and decomposition of polymers, energetic compounds, ablation (evaporation) of the thermal protection cover of spacecrafts, etc. [29].

The principle of action of the devices used for LP experiments is presented in Fig. 6.3. A sample of the tested compound is pressed upon the surface of the heating plate at constant temperature. During the experiment, the temperature of the heater surface ( $T_0$ ) and the velocity of sample migration ( $U$ ) equal to the linear decomposition rate are recorded. When the rate of the linear pyrolysis related to the experiment parameters is below some limiting value (which is true for most of the real conditions), the temperature of the hot sample surface can be considered to be  $T_0$  without considerable error. For a condensed substance with low thermophysical characteristics, LP is fairly fast.

Under conditions of low heat exchange with the environment, its rate is determined (for a zero-order reaction) by the Merzhanov relation [29]:

$$U = \sqrt{\frac{ak_0RT_s^2 \exp(-E/RT_s)}{E[(T_s - T_0) \pm Q/2c]}} \quad (6.8)$$

where  $a$  and  $c$  are the temperature conductivity and the heat capacity of the compound, respectively,  $k_0$  is the pre-exponential factor in the Arrhenius equation,  $T_s$  is the temperature of the environment and of the opposite surface of the sample,  $Q$  is the reaction heat.

**Table 6.4** Kinetic parameters of high- and low-temperature destruction of PMMA from linear pyrolysis and isothermal method [59]

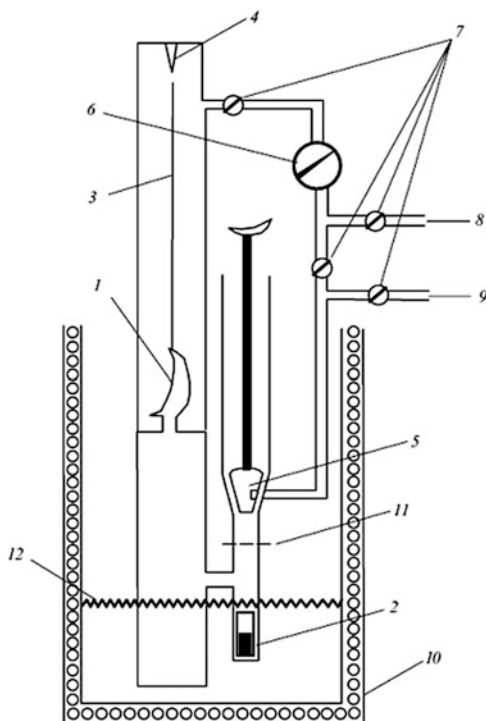
Polymer	$T, K$	$E, kJ/mol$	$\lg k_0 [k_0, c^{-1}]$
Linear pyrolysis			
PMMA	723 ÷ 793	179.7 ± 12.5	13.3 ± 1.0
	>803	≥292.6 ÷ 364.4	≥22 ÷ 23
PMMA + 2 % TEGM	763 ÷ 863	179.7 ± 12.5	12.5 ± 1.0
	>873	≥292.6 ÷ 364.4	≥21 ÷ 22
PMMA + 10 % TEGM	763 ÷ 863	179.7 ± 12.5	12.5 ± 1.0
	>873	≥292.6 ÷ 364.4	≥21 ÷ 22
Isothermal method			
Linear PMMA	493 ÷ 523	129.6	9.5
	499 ÷ 529	125.4	8.6
	563 ÷ 613	177.6	12.5
	653 ÷ 703	179.7	13.0
PMMA + 2 % TEGM	583 ÷ 633	181.8	12.1
PMMA + 10 % TEGM	583 ÷ 633	182.1	12.3

We emphasize that the data on low-temperature thermal decomposition kinetics of polymers are hardly applicable to the high-temperature pyrolysis. For example, decomposition of poly(methyl methacrylate) (PMMA) at temperatures  $\leq 620$  K follows first-order kinetics (for degree of conversion  $\eta > 0.2$ ) with the activation energy  $E_a \approx 167$  kJ/mol [59]. Then for LP rates from  $10^{-3}$  to  $10^{-2}$  m s $^{-1}$ , Eq. (6.8) gives the temperature of the polymer surface ranging from 1,070 to 1,170 K. However, the calculated values from the results of thermocouple measurements far exceed the real values. These examples are quite numerous. Table 6.4 gives the results of measurements of the rate constants for high-temperature and low-temperature destruction of PMMA with added triethylene glycol methacrylate (TEGM). Their comparison demonstrates that extrapolation of the data obtained for PMMA transformation in the low-temperature region using usual kinetic methods to the high-temperature region (for example, to the polymer combustion region) should be done with caution.

### 6.2.3 Volumetric Methods

Volumetric methods are used to detect small amounts of a substance, i.e., to study the process at early stages of transformation. The time dependence of the volume of the evolved gas  $[V(t)]$  can be measured either discretely or continuously. The key drawback of pressure gauge units is the possibility of direct contact of gas evolution products, which are often chemically corrosive, with the corroding metallic parts and mercury. An obvious advantage of these setups is the use of glass membrane type pressure gauges devoid of metallic parts. They have short response times and

**Fig. 6.4** Schematic diagram of the reaction vessel with a Bourdon pressure gauge for kinetic measurements. (1) Quartz crescent-shaped membrane, (2) tested compound, (3) rod, (4) zero indicator (zero reader), (5) vacuum valve, (6) recording mercury pressure gauge, (7) valves, (8) compensating gas inlet, (9) pumping out, (10) high-temperature thermostat, (11) vacuum sealing-off position, (12) position of the reaction vessel relative to the thermostat in the non-isothermal scheme



thus they are suitable for studying the rates of fast processes in a close reactor space by means of a Bourdon membrane-type pressure gauge (Fig. 6.4). A deformable highly sensitive membrane 1 separating the reaction space from the compensating space of the reactor serves as the pressure transducer. The gas pressure is determined either from the calibration curve which relates the membrane deformation value to the vapor pressure or by the compensation method (as a zero reader in the compensating circuit). Gas evolution during the transformation takes place in a self-generated atmosphere (SGA). Recently this method has been called RAPET (Reaction under Autogenic Pressure at Elevated Temperature) (see, for example, Ref. [65]). The reaction volume occurs under static isothermal conditions and is fully thermostated. The pressure created in the reaction chamber deforms membrane 1 and this induces bending of rod 3 welded to it. If a compensating gas is fed to the compensating chamber via valve 8 under pressure equal to the pressure of the gases evolved from the sample, rod 3 returns to the starting position, which is detected by pointer 4.

This reactor manufactured of quartz glass having a sealed-off reaction chamber is suitable for studying the kinetics of thermolysis of metallopolymers at fairly high temperatures (1,270–1,470 K) under fully isothermal conditions and for analyzing and interrupting gas evolution at any transformation stage. The number of moles of

the evolved heated gas ( $n_{\text{exp}}$ ) reduced to the number of moles ( $n_{\Sigma}$ ) evolved at room temperature ( $T_r$ ) is found from the equation

$$n_{\text{exp}}/n_{\Sigma} = (V_{\text{exp}}/V_{\Sigma})(T_r/T_{\text{exp}}).$$

Usually the reactor is designed in such a way that the ratio of the heated volume ( $V_{\text{exp}}$ ) to the total reactor volume ( $V_{\Sigma}$ ) is 1–5 %.

### 6.2.4 Thermolysis Induced by High-Energy Radiation

The thermal methods considered in the previous Section are based on the external heating of the tested sample. High-frequency (HF) electric fields can be used as an alternative source of heating [66–68]. On the one hand, polar groups and fragments of polymer molecule (dielectric material) placed in a variable electric field orient themselves following the change in the field polarity. On the other hand, thermal motion and non-polar groups and molecules prevent this orientation. The energy spent for overcoming the material disorientation is dissipated in the material and heats it. The intensity of heating increases with an increase in the oscillation frequency and electric field strength.

The key advantage of the HF heating is that heating occurs throughout the whole sample bulk without a contact. High-frequency treatment at 100–300 MHz (warming-up temperature may reach 510 K) of thermosetting oligomers containing finely powdered conductive fillers (iron, aluminium or copper powders, metal salts, complex organometallic compounds or soot) with particle size of less than 500  $\mu\text{m}$  in an amount of up to 85 % of the weight produces homogeneous composite materials. They can be used for injection moulding, production of adhesives and electrically conducting articles for motor-vehicle construction, aircraft industry, microelectronics.

When amorphous titanium, zirconium and hafnium hydroxides are heated in a muffle microwave kiln or exposed to a 2,450 MHz electromagnetic field with a 700 W power, the warming-up temperature reaches 495–770 K [69]. The obtained metal oxide powders have well crystallized structure, highly developed surface (>500  $\text{m}^2/\text{g}$ ) and nanometre-range particle size.

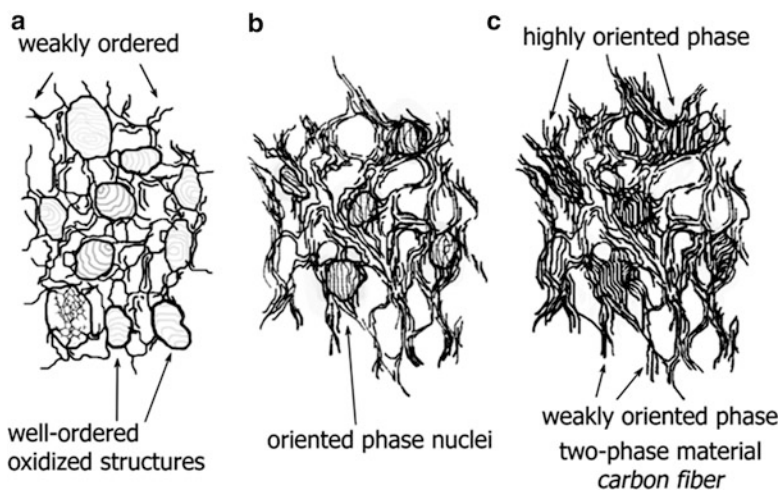
A promising approach is the thermal treatment of metallopolymer materials under the action of lasers or accelerated electrons [70]. Laser ablation is also applicable. Carbon nanotubes were produced from polyacrylonitrile (PAN), PTFE, acrylonitrile and methyl methacrylate copolymers, etc. by a number of methods (arc discharge, laser or magnetron radiation, plasma treatment and so on) [71, 72]. In some cases, the polymer incorporates a metal-containing component, which affects considerably the nature of carbon structure: this gives carbon nanotubes with a metal nanoparticle shell. In particular, nanocrystalline Co particles with diameter of 4–7 nm and bimetallic Co–Pt particles in the carbon matrix are formed on exposure of (bi)metallic and carbon plates to an argon ion beam



[73]. Gold and ruthenium nanoparticles were obtained from metallized polymer precursors by electron beam treatment [74, 75].

Let's consider thermolysis of the PAN fiber in more detail. Commercial PAN fiber is a triple copolymer of acrylonitrile, methylacrylate and itaconic acid, the contents of the monomer units are equal to 93.0, 5.7 and 1.3 %, respectively. Thermolysis is carried out in an oxidizing atmosphere. Oxygen promotes the hydrogen elimination from the structure of the carbon chain polymer followed by the formation of intra- and intermolecular cross-linking and polyconjugated bonds. Cyclization of nitrile groups occurs at 150 °C yielded the conjugated C=N-bonds, but the system of conjugated C=N-bonds is formed at 200–220 °C. The gaseous products evaporate vigorously in the initial stage of carbonization (pre-carbonization). The loss of heteroatoms results of the formation of polyconjugates carbon structures accompanied by the hybridization of residual  $sp^3$ -carbon into  $sp^2$ -form. Further heating leads to the formation of ordered phase nuclei and ordered structures as well as a total polyconjugated system. These processes are approximated by Avramy-Erofeev equation of n-th order. The apparent activation energy is relatively low. Subsequent stages are accompanied with the formation of nanocrystalline structures of different dimensions and defects. At carbonization temperatures (1,300–1,400 °C) the layered nanocrystallites of graphene fragments are obtained [76, 77] (Fig. 6.5).

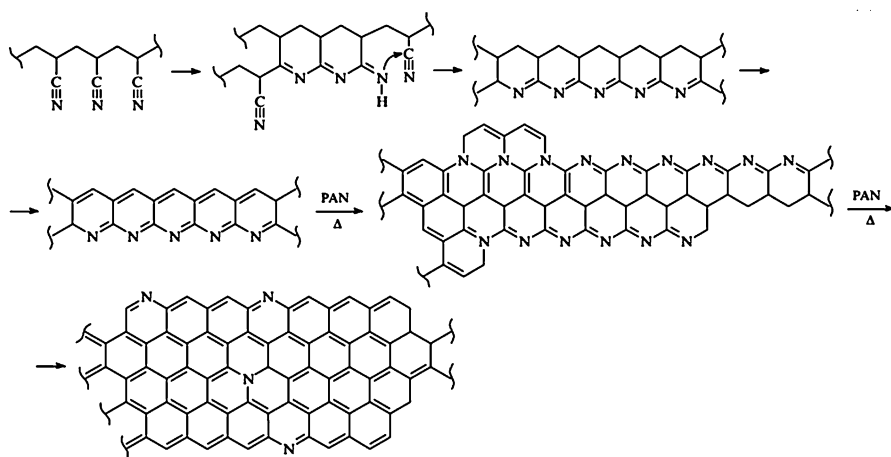
Considering its mechanism, IR thermolysis also belongs to this group of methods. However, in this case, the rates of chemical reactions are much higher, which is related to selective action of IR radiation on the vibrational energy of particular bonds of the macromolecule. For example, above mentioned thermolysis of PVA at 200 °C is accompanied by dehydration of macromolecules followed with the formation of polyconjugated bonds system. In this case anisotropic



**Fig. 6.5** A scheme of structural transformations of the PAN during carbonization. (a) an oxidized fiber; (b, c) – formation of ordered clusters in the volume of material

polarizability and decreasing of the vibration band in Raman spectrum associated with the vibration of atoms along a polymer chain and an increase of the band of deformation transverse vibrations are observed [78].

The IR thermolysis of PAN is best studied. At only 473 K, the polymer nitrile groups start to undergo cyclization caused by the mobility of the hydrogen atom at the tertiary carbon atom and its migration to the nitrile group to form an imine bond ( $>NH$ ). The cyclization is facilitated by hydrogen bonding of the imine with the nitrile group [8]. At 708 K a vigorous IR-pyrolysis of PAN occur. This is accompanied by restructuring of the material yielded the formation of pyrolyzed conducting film, particularly, in the case of its doping [79]. It is of interest that in the case of IR pyrolysis of the PAN/Co metallopolymer system, the structure of the resulting carbon phase is perfected at the expense of the carbon present in the polymer. Hence, the cobalt nanoparticles catalyze the formation of crystalline graphite [80]. The hypothetical sequence of transformations is shown in Scheme 6.1.



**Scheme 6.1** A scheme of pyrolysis of PAN

Most likely, such structures are stacked into layers. Probably, carbonization of other polymers, for example, polybenzimidazole, polyphenylcarbyne, and so on, proceeds in a similar way. The preliminary annealing is carried out in air at 473 K and then under argon at 673–1,373 K. The precursor is a solution in DMF containing simultaneously three components: PAN,  $PtCl_4$  and  $Ru$  (Re, Rh) $Cl_3$ . Under these conditions, the salts form complexes with PAN and the products of its transformation. Already at 513 K the complexes are destroyed; however, the reduced metal atoms are surrounded by a polymeric structure, which restricts their mobility and prevents aggregation during the subsequent pyrolysis. This factor is responsible for the formation of rather small and uniform nanoparticles in the composite. The size of spherical nanoparticles is 2–18 nm, the presence of the  $Pt_{13}Ru_{27}$  intermetallic and alloy formation throughout the whole homogeneity range of Pt solid solutions were also detected.

Other metal – carbon nanocomposites were obtained in a similar way using uranium nitrate, ammonium heptamolybdate, etc. IR-thermolysis of mixtures of PAN,  $\text{FeCl}_3 \cdot 6\text{H}_2\text{O}$  and  $\text{NiCl}_2 \cdot 6\text{H}_2\text{O}$  yields  $\text{FeNi}_3/\text{C}$  nanocomposite with controlled electrophysical and magnetic properties [81, 82]. The particles were 10–80 nm in size and homogeneously distributed in a carbon matrix. Mechanism of the nanocomposite formation is multistage. Dehydration of the starting components takes place at 150 °C, the chemical bond of iron and nickel with nitrile groups of PAN appears up to 250 °C, the  $\text{NiFe}_2\text{O}$  and  $\text{FeNi}_3/\text{C}$  occur at 400 °C and 600 °C, respectively, and finally,  $\gamma\text{-(Fe,Ni)}$  forms at 800 °C.

### 6.2.5 Spray Pyrolysis

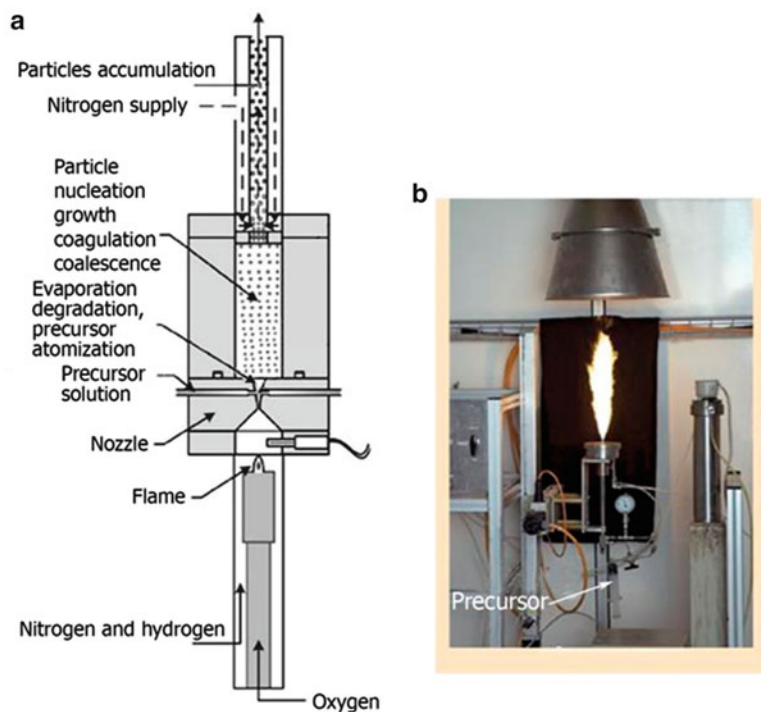
As regards the character and the equipment used, spray pyrolysis differs from the procedures considered above. This is an aerosol process that is used efficiently on a large scale to obtain metal and metal oxide nanoparticles and powdered ceramics and nanostructured materials [83, 84]. This technique has proved itself good in materials science and chemical and food industry.

Spray pyrolysis includes five key stages. The first stage is generation of the spray from a liquid precursor using an appropriate drop generator. Then it is followed by spray transport by an air or inert gas stream during which the solvent evaporates. The next stage is precipitation of the solute after the critical supersaturation limit has been reached in the drops. The key stage is thermolysis of the precipitated substance giving nanoporous particles followed by calcination to obtain dense structures. The extraction of particles from the gas stream completes the process. In some cases, sol-gel synthesis and spray pyrolysis techniques are combined. Other techniques such as ultrasound-, plasma-, and laser pyrolysis as well as flame spray-pyrolysis are also widely used [85–87]. The latter method has been proven to be more effective for obtaining zinc oxide in comparison with other known approaches such as CDV, sol-gel synthesis, etc. [88]. It is interesting to note that  $\text{ZnO}$ <sup>3</sup> [89–95] is the third pigment on production volume (next of carbon black and titanium dioxide), its production exceeds 600,000 t/year. Introducing it into elastomers the materials with the developed specific surface can be obtained to apply for pharmaceutical, cosmetic, catalytic purposes, etc. [96]. Flame spray-pyrolysis synthesis of nanostructured  $\text{ZnO}$  (diameter of particles of 10–20 nm) can be represented by a principal scheme (Fig. 6.6) [97, 98].

The gas – particle conversion methods and the liquid–solid phase transformations followed by thermolysis and pulverization have important advantages. These

---

<sup>3</sup> In turn, nanocrystalline zinc oxide is one of widely investigated nanomaterial [89–95]. This is a large-band-gap semiconductor (with a band gap of 3.37 eV at 300 K and a large exciton binding energy of 60 meV) and a multifunctional material with the unique set of mechanical, electrical and luminescent properties. Quasi-one-dimensional structures of  $\text{ZnO}$  are the significant building blocks of different nanodevices such as light-emitting, sensor (including biosensor), piezoelectric, solarvoltaic arrays etc.

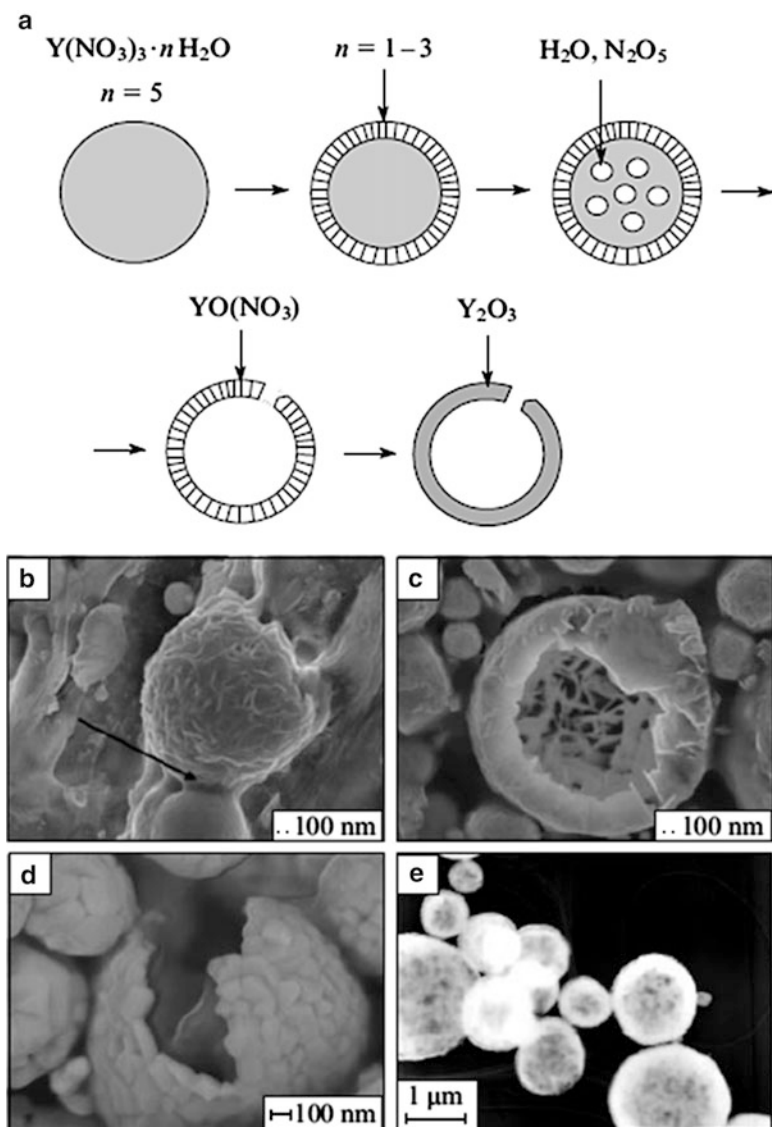


**Fig. 6.6** A scheme of flame spray pyrolysis (a) and a view of the high-temperature stream reactor (b)

are the purity and the uniform chemical composition of the obtained material, narrow particle size and shape distributions, the possibility of synthesizing multicomponent systems, and the simplicity and scalability of the whole process. They are suitable for preparing particles of three different morphologies: [99] solid nanoporous, microporous and hollow ones (Fig. 6.7). The first (e.g.,  $\text{Al}_2\text{O}_3$ ) and third (e.g.,  $\text{MgO}$  and  $\text{ZnO}$ ) type particles are formed from the corresponding nitrates. Upon variation of the temperature of spray pyrolysis,  $\text{ZrO}_2$  particles of all types were obtained.

Currently, some stages of spray pyrolysis<sup>4</sup> [100] are being under detailed investigation, for example, drop formation [101], evaporation and drying stages [102]. However, it is still unclear how the change of reaction conditions (component concentrations, flow rates, evaporation – precipitation or thermolysis) affects the mechanism and the possibility of control of nanoparticle formation. It was noted [103, 104] that the addition of a polymer, e.g., poly(ethylene glycol), to the initial solution of the precursor can be used to prepare nanoparticles of europium-doped yttrium oxide of controlled morphology.

<sup>4</sup>To consider the spray-pyrolysis in the more detail including the formation of bioceramics and processes with organic components the recent rather comprehensive review can be recommended [100].



**Fig. 6.7** Schematic view of the change of the morphology of  $Y(NO_3)_3 \cdot nH_2O$  drops during spray pyrolysis (a); electron microscopic images of the products formed after drying and the first stage of thermolysis (390 K) (b), after thermolysis at 673 K (c), after thermolysis at 973 K and subsequent annealing at 1,673 (d) or 1,473 K (e) [99]

Nanoparticles and nanocomposites on the base of metal oxides obtaining by spray-pyrolysis are quite well characterized (see, for instance [105–112]).

New gas phase methods are extensively developed to obtain new ceramic materials. Flame spray pyrolysis combining with aqua and non-aqua sol-gel synthesis, hydro- and solvothermal methods, pyrolysis of polymer materials and high-pressure

techniques has great synthetic potential. Probably, the same way is suitable for synthesis of copper nanoparticles stabilized with graphene [113].

### **6.2.6 *Calorimetric Bomb as a Method to Study the Enthalpy of Combustion (the Enthalpy of Formation) of Nanoparticles***

This is one of the important methods for studying of thermochemical data by the burning of material in calorimetric bomb. This method is widespread and has been brought to perfection. The bomb calorimeters are widely used in a thermoanalysis to measure the enthalpy of reaction for many compounds. Here we have not analyzed the well-known method of Bartolo and its modifications as well as calorimetric bombs of Rossini and Prosen (the information can be found in the corresponding handbooks). Let's consider briefly a modified calorimetric bomb constructed in the thermochemical laboratory in Moscow State University (Fig. 6.8). The bomb is a hermetically sealed stainless steel vessel to withstand pressures of at least 40 atm. There are electrodes to carry an ignition current. The calorimetric bomb holds in a container (calorimeter) filled by 2–4 L of water, as a rule. Before a material with an unknown heat of combustion can be tested in a bomb calorimeter, the calorimeter must be calibrated with allowance of the energy contributed by the fuse. Benzoic acid is often used as a standard material with a known heat of combustion under controlled and reproducible operating conditions.

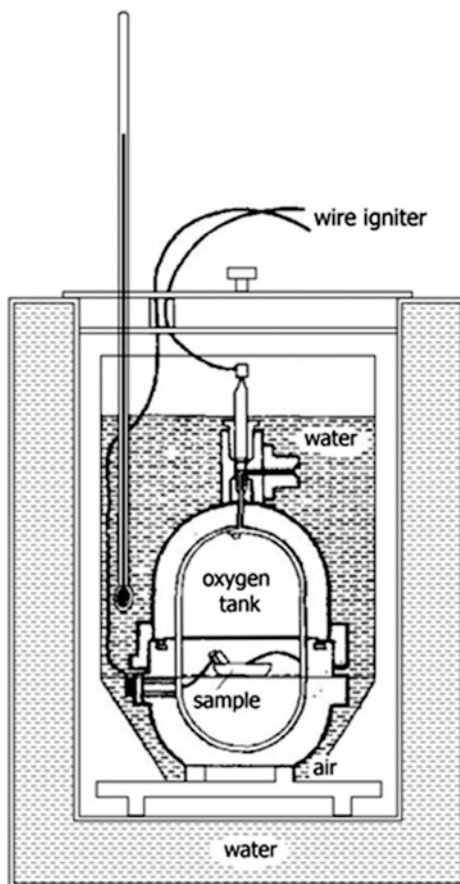
The standard enthalpy of combustion is the enthalpy change when 1 mol of a reactant completely burns in excess oxygen under the constant temperature and pressure yielded liquid water and gaseous dioxide carbon.

Thus, different methods for the preparation of nanocomposites and study of the kinetics of their formation have now been developed.

## **6.3 Thermolysis of Metalloprecursors**

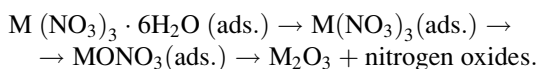
In this Section we consider the thermal decomposition of more particularly used precursors with a comparative analysis of their decomposition in polymer matrices. It should be noted that non-hydrolytic routes are the most popular to carry out the processes of thermolysis. This is a thermolysis of metal salts, metal oxysalts and their derivatives in high-boiling organic solvents. In addition, in many cases, it is difficult to compare the thermodynamic and kinetic data because the different conditions of experiments (inert and self-generated atmosphere or air, the different reaction rates, etc.).

**Fig. 6.8** A scheme of the calorimetric bomb



### 6.3.1 Metal Nitrates

Thermal decomposition of metal nitrates, as well as metal perchlorates, is used to prepare pure metal oxides, in particular, as parts of composites, for example, explosives [114]. Metal nanoparticles, for example, of aluminum in combination with ammonium nitrite and cyclotrimethylene trinitramine increase the rate and temperature of burning. Such energetic nanomaterials are of interest for a heterogeneous burning (see, for instance [115]). The mechanism of thermal decomposition of metal nitrates has been established; for actinides and lanthanides (except for cerium and samarium salts), it can be represented as follows:



High energy thermolysis of nitrate complexes of bis-ethylenediamine  $[M(EDA)_2](NO_3)_2$  ( $M=Cu, Co, Ni$  and  $Zn$ ) is investigated in detail [116]. Their decomposition proceeds in two stages. First, one EDA molecule and monoethylene diamine are evolved; formation of high-dispersed metal oxides completes the reaction:



The kinetics of the process is described by second- and third-order equations:  $1 - (1 - \eta)^{1/2} = kt$  and  $1 - (1 - \eta)^{1/3} = kt$ , respectively. The thermal stability and the activation energy of decomposition (88.8–108 kJ/mol) increases as follows:  $[Cu(EDA)_2](NO_3)_2 < [Co(EDA)_2](NO_3)_2 < [Ni(EDA)_2](NO_3)_2 < [Zn(EDA)_2](NO_3)_2$ . It is important that the initial complexes can be used as burning rate modifiers of solid propellants. By introducing 2 wt% of the complex into a composite of polybutadiene with terminal hydroxyl groups – ammonium perchlorate the rate of burning increases by 1.1–1.80 times. Still more activity is characteristic for the complexes of transition metal salts with 5-nitro 2,4-dihydro-3H-1,2,4-triazole-3-on [117]. In this case high-dispersed metal oxides are formed with the more developed surface that enhances the flame temperature.

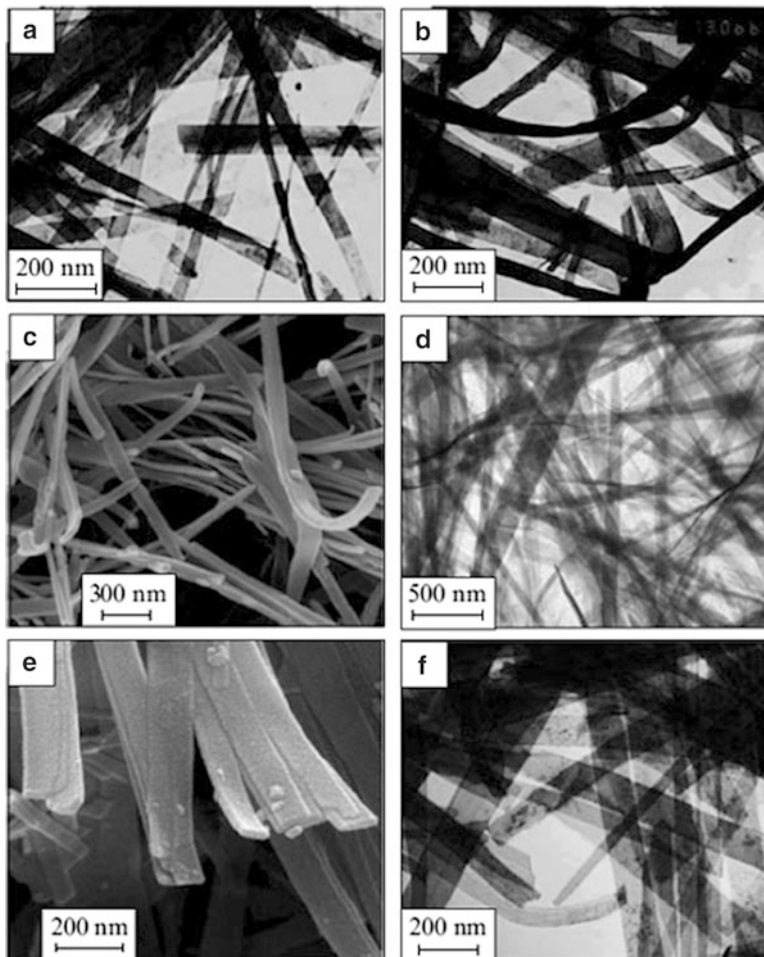
The interesting mechanism is revealed under thermal transformations in the system of  $Cu(NO_3)_2 \cdot 3H_2O$  – 1,2–ethandiol [118, 119]. At the comparative low temperatures and in an acid medium the spontaneous oxidation of 1,2–ethandiol occurs in a coordination sphere of metal caused by an equilibrium shift to the formation of the polynuclear coordinated product. The thermal conversion at 1273 K yields CuO.

Decomposition of anhydrous cerium nitrate to  $CeO_2$  (in the temperature range of 500–633 K) corresponds to second-order kinetic equation  $kt = [1/(1 - \eta)]^{-1}$ , the reaction enthalpy is 111.1 kJ/mol and the apparent activation energy is 104 kJ/mol (for comparison, these values for thermolysis of anhydrous  $Nd(NO_3)_3$ ,  $Dy(NO_3)_3$  and  $Yb(NO_3)_3$  are 33, 23 and 46 kJ/mol, respectively) [120]. Decomposition of the corresponding nitrates gave yttrium group rare earth metal sesquioxides ( $M_2O_3$ ,  $M=Y, Dy, Ho, Er$ ) with a controlled geometric structure as nanobelts [121–123] (Fig. 6.9).

The nanoparticle shape is considerably affected by the reaction conditions, specifically, the solvent composition, concentration of the precursor, temperature and time. Thus the mechanism of the hierarchical self-organization of cerium (IV) oxide nanoparticles [124] upon thermolysis of  $(NH_4)_2Ce(NO_3)_6$  in oleic acid – oleylamine mixture includes two key stages. First, during hydrolysis of the initial salt at 413 – 493 K,  $CeO_2$  cluster particles framed by surfactant and  $NO_3^-$  anion ligands are formed. The next stage (above 493 K) comprises spontaneous assembly of primary particles to flower-like structures (cubic, tetrapetalous, star-like and other structures) caused by the decrease in the concentration of the surface ligands as a result of fast decomposition of the precursor at high temperature.

Spray pyrolysis of cerium nitrate complexes gives rise to hollow spheres of  $CeO_2$ , [125] whereas  $Zn_2SiO_4$  and ZnO form microporous spheres [126]. Synthesis





**Fig. 6.9** Photomicrographs of lanthanide oxide nanobelts:  $\text{Dy}_2\text{O}_3$  (a, b),  $\text{Ho}_2\text{O}_3$  (c, d) and  $\text{Er}_2\text{O}_3$  (e, f) from scanning (a, c, e) and transmission (b, d, f) electron microscopy (TEM) [121]

of non-doped and doped with Cu (0.1–5 %) ZnO was carried out using  $\text{Zn}(\text{NO}_3)_2 \cdot 6\text{H}_2\text{O}$ ,  $\text{Cu}(\text{NO}_3)_2 \cdot 3\text{H}_2\text{O}$  and glycine [127]. The products possessed a hexagonal phase and symmetry of wurtzite.

Quasi-1D belt-like nanostructures are convenient objects for studying the fundamental physical and chemical properties of closed systems. They are obtained by various methods including thermolysis [128, 129]. For example, the thermolysis of  $\text{M}(\text{NO}_3)_3 \cdot x\text{H}_2\text{O}$  ( $\text{M} = \text{Dy}, \text{Ho}, \text{Er}$ ) in a dodecylamine–octadec-1-ene high-boiling solvent mixture is described [121]. Since the solubility of salts in this mixture is low, heat transfer between the liquid and solid phases takes place; dodecylamine plays the key role in controlling the structure formation in such ‘solid-liquid’ chemical systems with separated nucleation and particle growth stages. The ternary

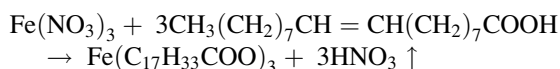
oxides such as  $\text{MAlO}_3$  and  $\text{M}_3\text{Al}_5\text{O}_{13}$  can be obtained in the same way. However, the authors did not consider the possibility of octadec-1-ene polymerization under these conditions (at temperatures of up to 600 K) or the formation of a protecting shell. It should be mentioned also thermolysis of silver nitrate [130].

### 6.3.2 Thermolysis of Metal Carboxylates

Metal salts of carboxylic acids have been widely used since ancient times. For example, calcium propionate is used as a preservative in food industry and in the soap and lubricant production. Its thermal behaviour has been studied in detail [131], as well as the behaviour of metal carboxylates with the number of carbon atoms ( $n$ ) in the aliphatic chain ranging from 12 to 18. (These salts are present, for example, in human gallstones [132]). The products of their thermolysis (metal nanoparticles, metal oxides or carbides) are of interest owing to a wide application as catalysts of basic organic synthesis reactions, inorganic pigments and so on (see [133–135]).

Metal carboxylates usually exist as monohydrates, their dehydration at the temperature  $T_1$  ( $>383$  K) being accompanied by a phase transformation and considerable loss of crystallinity [136, 137]. At temperature  $T_2$ , which decreases by an exponential law following increase in the number of carbon atoms (Table 6.5), the salts start to decompose over a broad temperature range extending beyond 573 K starts (Fig. 6.10).

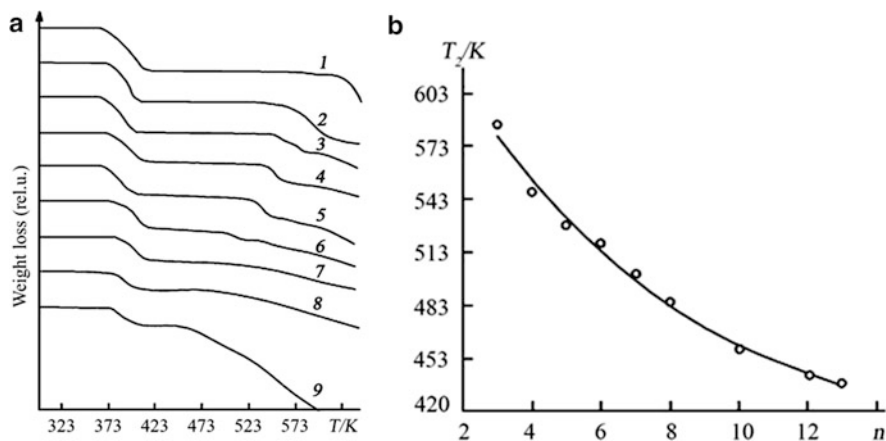
A typical scheme of the reaction in case of an anhydrous salt can be represented as follows:



Synthesis of the monodispersed product proceeds through two separated stages: nucleation and growth of the crystal. It is supposed that under thermolysis of

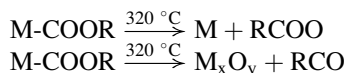
**Table 6.5** Temperatures of dehydration ( $T_1/\text{K}$ ) and onset of the decomposition ( $T_2/\text{K}$ ) of calcium carboxylates  $\text{Ca}(\text{n-C}_n\text{H}_{2n+1}\text{CO}_2)_2 \cdot \text{H}_2\text{O}$

Carboxylate	$T_1$	$T_2$
C3	386.3	585
C4	392.8	547
C5	389.9	517
C6	394.8	500
C8	391.9	485
C10	391.6	458
C12	394.2	443
C13	391.7	439



**Fig. 6.10** Profiles of the thermograms of decomposition of Ca(II) carboxylates (a) and initial decomposition temperature ( $T_2$ ) vs. the number of C atoms in the aliphatic chain (b) [136]. Heating rate  $10 \text{ deg min}^{-1}$ ;  $n=3$  (1), 4 (2), 5 (3), 6 (4), 7 (5), 8 (6), 10 (7), 12 (8), 13 (9)

hydrated iron carboxylate the nucleation initiates a thermal generation of free radicals from the metal carboxylate [138]:



The free radicals can recombine or form volatile products such as CO, CO<sub>2</sub>, H<sub>2</sub>O, ethers etc. Generally, the free radicals attack another M–COOR molecules and initiate the chain reactions. Carboxylic acids play a dual role in the synthesis of nanocrystalline iron oxide. Firstly, the carboxyl group is a ligand to bind iron ions into the precursor complex. Secondly, free oleic acid is a stabilizing agent covered the particles and yielding the fine dispersions in organic solvents. Nickel nanoparticles (with diameter of 7 nm and product purity of 74.3 %) were obtained by the thermal decomposition of nickel acetate in the presence of hexadecylamine surfactant or by the controlled evaporation of solution of nickel-oleylamine complex [139, 140]. In some cases, it has been possible to identify the intermediates such as nanocrystals of Ni<sub>3</sub>C [141].

Carboxylic acids derivatives of the types of potassiumferrous-carboxylate with general formula  $\text{K}_3[\text{Fe}(\text{L})_6] \cdot x\text{H}_2\text{O}$  (L is formate, acetate, propionate, butyrate) underwent thermolysis in air up to 1,173 K. After dehydration an anhydrous complex exothermally decomposed with the formation of different intermediates, in particular, of potassium carbonate. Further decomposition (above 973 K) led to  $\text{KFeO}_2$ . This product can be also obtained at 873 K if oxalyldihydrazide  $\text{C}_2\text{H}_6\text{N}_4\text{O}_2(\text{aq})$  as a complexing agent is added to the batch. Then a reaction mixture was ignited in a muffle [142]. Reduction of Fe(III) to Fe(II) being endothermal absorbs some heat that facilitates the formation of ferrites at more high temperatures. Such behavior is

similar to thermolysis of alkaline metal ferrioxalates. Both methods allow one to obtain the stoichiometric pure ferrites at lower temperatures and shorter reaction time. Besides, the additional grinding of the initial materials is not required that is necessary in synthesis of ceramics and may cause defects of the lattice and, in turn, effect permanent magnetic properties. Thermolysis of citrate of alkaline-earth metals and tris(oxalate/maleate/malonate ferrates (III) was investigated quite well. Different reasons cause the significant attention to thermolysis of strontium and barium citrate ferrates [143, 144]. It was shown by Mossbauer spectroscopy that isothermal and non-isothermal decomposition of  $M_3[Fe(C_6H_5O_7)_2]_2 \cdot 4H_2O$  ( $M = Sr, Ba$ ) includes three main stages [145]: dehydration of the complex, its thermal decomposition yielded  $\alpha\text{-Fe}_2O_3$  and metastable acetonedicarboxylate intermediate, and finally, oxidative decomposition of the intermediate and formation of the  $Ba_3[Fe(C_6H_5O_7)_2]_2$  ferrite. Analysis of isomeric schift and quadrupole splitting of Mossbauer spectra allowed proving the composition, structure and quantities of the products at 673 and 923 K ( $BaFe_2O_4$  and  $Ba_3Fe_2O_{7-x}$ ).





The most detailed mechanism of thermolysis of metal carboxylates of saturated carboxylic acids has been elucidated in a number works [146–149]. Thermal transformations of Fe(II), Fe(III), Ni(II), Cu(II), and Pb(II) formates of the formula  $M(HCOO)_n$  and the oxalates  $Fe_2(C_2O_4)_3 \cdot 5H_2O$  and  $FeC_2O_4 \cdot 0.5H_2O$  are temperature-separated successive processes consisting of dehydration and subsequent decomposition of the anhydrous carboxylate. The kinetic parameters of decomposition, the pattern of dependence of the decomposition rate on the degree of salt conversion and the corresponding approximating equations are presented in Table 6.6. The kinetics of isothermal decomposition in an SGA is affected by the temperature of the experiment ( $T_{exp}$ ), the rate of the preceding dehydration and the  $m_0/V$  ratio ( $m_0$  is the sample weight,  $V$  is the volume of the reaction vessel).

Thermolysis of iron and copper carboxylates follows two consecutive macrostages to give intermediately metal carboxylates with a low oxidation state of the metal; this is caused apparently by rather low redox potentials of the Fe(III)/Fe(II) ( $E^\circ = +0.771$  V) and Cu(II)/Cu(I) ( $E^\circ = +0.158$  V) pairs [51].

The composition of the volatile products obtained in a high-vacuum pyrolysis of copper formate in the cavity of a mass spectrometer [148] under conditions that rule out secondary reactions indicates that the transformation is a complex multichannel process. In the early stages (up to the degree of conversion  $\chi_\Sigma \sim 0.5$ ,  $\chi_\Sigma$  is the fraction of the total intensity of the principal mass peaks at the end of the decomposition,  $\Sigma$  implies summation over all components),  $CO_2$ ,  $CO$ ,  $H_2O$  and  $HCO_2H$  are formed simultaneously, and  $\chi CO_2 > \chi H_2O \approx \chi CO > \chi HCO_2H$ ; subsequently the evolution of  $H_2O$  and  $CO$  virtually stops, the rate of their accumulation being low and given by  $W_{min}(\chi_\Sigma)$ .

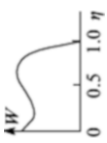

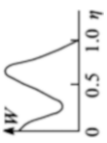
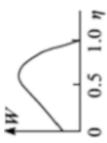
Thermolysis of Co(II) formate conditionally can be divided into two stages as well: dehydration and a subsequent decomposition. The first stage has been investigated rather in detail [150]. Thermal decomposition of the anhydrous product is accompanied by evolution of gaseous products  $H_2$ ,  $CO$  and  $CO_2$ ; water vapors formed yet during dehydration, as well as  $CH_3OH$ ,  $CH_3COOH$ , products of thermolysis of formic acid [151–153].

**Table 6.6** The kinetic parameters of thermal decomposition of metal salts of saturated carboxylic acids [149]

Compound ( $T_{\text{exp}}$ , K)	Pattern of the curve $W(\eta)$	Approximating equation $W(\eta)$	$k_i, \xi_0$ $(m_0/V) \times 10^3, \text{g cm}^{-1}$	$k(T) = k_0 \exp[-E_a/(RT)]$	
				$k_0/\text{s}^{-1}$	$E_a/\text{kJ mol}^{-1}$
$\text{Ni}(\text{COO})_2 \cdot 2\text{H}_2\text{O}$ (473–439 K)		Approximating equation $W(\eta)$ $W(\eta) = k_1(1 - \eta) - k_2\eta(1 - \eta)$ ( $m_0/V$ ) $\uparrow -k_1 \downarrow, k_2 \downarrow$ ; $W(0) = k_1$	$k_1$ $k_2$ 1.63	$1.5 \cdot 10^{20}$ $2.7 \cdot 10^{18}$	244.0 202.5
$\text{Fe}(\text{COO})_2 \cdot 2\text{H}_2\text{O}$ (513–553 K)		$W(\eta) = k(1 - \eta)(\eta + \xi_0)^2$ ( $m_0/V$ ) $\uparrow -\xi_0 \uparrow$ ; $k = \text{const}$ $W(0) = k\xi_0^2$	$k$ $\xi_0$ $W(0)$	$0.33 \cdot 10^2$ $5.6 \cdot 10^8$ $1.04 \cdot 10^{19}$	38.0 101.0 240.0
$\text{Fe}(\text{COO})_3$ (513–553 K)		$\eta = 0 \div 0.2$ ; $W(\eta) = k_1(\eta_{1\infty} - \eta)$ ; $\eta > 0.2$ ; $W(\eta) = k(1 - \omega)^2(\omega + \xi_0)$ , where $\omega = [\eta - \eta_{1\infty}(1 - e^{-k_1 t})]/(1 - \eta_{1\infty})$ ; ( $m_0/V$ ) $\uparrow -k_1 \uparrow, k_2 \uparrow$ ; $\eta_{1\infty} = 0.38 = \text{const}$ ; $\xi_0 = \text{const}$ ; $W(0)_1 = k_1\eta_{1\infty}$ ; $W(0)_2 = k\xi_0^2$	2.0 $k_1$ $k_2$ $\xi_0$ $W(0)_1$ $W(0)_2$	$7.1 \cdot 10^{17}$ $7.8 \cdot 10^{16}$ 0.63 $2.7 \cdot 10^{17}$ $4.9 \cdot 10^{16}$	221.0 210.5 8.4 221.0 228.0
$\text{Cu}(\text{COO})_2$ (393–453 K)		$\eta = 0 \div 0.3$ ; $W(\eta) = k_1(\eta_{1\infty} - \eta)$ ; $\eta > 0.3$ ; $W(\eta) = k(1 - \omega)(\omega + \xi_0)^2$ , where $\omega = [\eta - \eta_{1\infty}(1 - e^{-k_1 t})]/(1 - \eta_{1\infty})$ ; ( $m_0/V$ ) $\uparrow -k_1 \uparrow, k_2 \uparrow$ ; $\eta_{1\infty} = 0.42 = \text{const}$ ; $\xi_0 = \text{const}$ ; $W(0)_1 = k_1\eta_{1\infty}$ ; $W(0)_2 = k\xi_0^2$	1.3 $k_1$ $k_2$ $\xi_0$ $W(0)_1$ $W(0)_2$	$1.3 \cdot 10^{11}$ $3.5 \cdot 10^2$ $1.2 \cdot 10^3$ $5.5 \cdot 10^{10}$ $4.2 \cdot 10^5$	137.5 50.5 35.5 137.5 72.0

(continued)

Table 6.6 (continued)

Compound ( $T_{\text{exp}}$ , K)	Pattern of the curve $W(\eta)$	Approximating equation $W(\eta)$	$k_1, \xi_0$ $(m_0/V) \times 10^3, \text{g cm}^{-1}$	$k(T) = k_0 \exp[-E_a/(RT)]$	$E_a/\text{kJ mol}^{-1}$
$\text{Pb}(\text{COO})_2$ (478–503 K)		Approximating equation $W(\eta)$ $\eta = 0 \div \eta_{W_{\text{min}}}$ (0.16); $W(\eta) = k_1(\eta_{\infty} - \eta)$ ; $\eta = \eta_{W_{\text{min}}} \div \eta_{W_{\text{max}}}$ (0.5 – 0.7); $W = W_{\text{min}} + k_2(\eta - \eta_{W_{\text{min}}})$ ; $(m_0/V) \uparrow - W(0) \uparrow, k_2 \uparrow, W_{\text{min}} \uparrow,$ $W_{\text{max}} \uparrow, \eta_{W_{\text{min}}} \downarrow, \eta_{W_{\text{max}}} \uparrow$ ; $W(0) = k_1 \eta_{\infty}$	$k_1$ $\eta_{1,\infty}$ $k_2$ $W(0)$ $W_{\text{min}}$ $8.7 \cdot 10^{11}$ $117.0$	$4.7 \cdot 10^6$ $2.5 \cdot 10^4$ $4.2 \cdot 10^{10}$ $1.2 \cdot 10^{11}$ $8.7 \cdot 10^{11}$	74.0 39.0 104.5 113.0 117.0
Cocrystallite $\text{Fe}(\text{COO})_2$ and $\text{Ba}(\text{COO})_2$ [Fe]:[Ba] = 12 (543–583 K)		$\eta = 0 \div 0.3$ ; $W(\eta) = k(1 - \eta)(\eta + \xi_0)^2$ ; $W(0) = k\xi_0^2$	$k$ $\xi_0$ $W(0)$	$0.37 \cdot 10^3$ $2.8 \cdot 10^4$ $1.5 \cdot 10^{13}$	50.5 67.0 184.0
$\text{Fe}_2(\text{C}_2\text{O}_4)_3 \cdot 5\text{H}_2\text{O} = 2\text{FeC}_2\text{O}_4 \cdot 0.5\text{H}_2\text{O}$ + $2\text{CO}_2 + 4\text{H}_2\text{O}$ (398–423 K)		$\eta = 0 \div \eta_{W_{\text{min}}} (< 0.2)$ ; $W(\eta) = k_1(1 - \eta)$ ; $\eta = \eta_{W_{\text{min}}} \div \eta_{W_{\text{max}}}$ ; $W = W_{\text{min}} + k_2(\eta - \eta_{W_{\text{min}}})$ ; $(m_0/V) \uparrow - W(\eta) \approx \text{const}$ ;	2.7 $k_1$ $k_2$ $W_{\text{min}}$ $W_{\text{max}}$ $\eta_{W_{\text{min}}}$	$1.8 \cdot 10^4$ $1.0 \cdot 10^{16}$ $1.7 \cdot 10^{11}$ $8.3 \cdot 10^{15}$ $1.0 \cdot 10^7$	53.5 154.5 123.5 157.5 54.5
$\text{FeC}_2\text{O}_4 \cdot 0.5\text{H}_2\text{O}$ (573–608 K)		Before $W_{\text{max}}$ : $W(\eta) = W(0) + k_1\eta$ ; $k_1\eta$ ; after $W_{\text{max}}$ : $W(\eta) = k_2(1 - \eta)$ ; $(m_0/V) \uparrow - W(0) \uparrow, k_2 \uparrow, W_{\text{max}} \uparrow,$ $k_1 \approx \text{const}$	3.83 $k_1$ $k_2$ $W(0)$ $W_{\text{max}}$ 1.93	$1.3 \cdot 10^{24}$ $9.6 \cdot 10^{17}$ $4.7 \cdot 10^6$ $3.1 \cdot 10^{18}$	318.0 251.0 127.5 253.0

Note:  $W = dn/dt$  is the rate of conversion;  $W(0)$  is the initial rate of conversion;  $\eta = \alpha/\alpha_{\infty}$  is the degree of conversion;  $\alpha$ ,  $\alpha_{\infty}$  is the number of moles of the evolved gaseous products per mole of the initial compound at time  $t$  and at the end of transformation, respectively;  $V$  is the volume of the reaction vessel;  $\uparrow, \downarrow$  are increase and decrease of a parameter, respectively;  $\xi_0$  is the constant depending on  $m_0/V$  and  $T_{\text{exp}}$



**Table 6.7** Average particle size and thickness of the polymeric shell for decomposition products of metal carboxylates [149, 155]

Compound	$T_{\text{ex}}$ , K	$d_s^f$ , nm <sup>a</sup>	$d_{\text{EM}}$ , nm <sup>b</sup>	$\Delta L_{\text{shell}}$ , nm <sup>c</sup>	Product <sup>d</sup>
$\text{Fe}(\text{COO})_2 \cdot 2\text{H}_2\text{O}$	543	27.0	20.0	3–5	$\text{Fe}_3\text{O}_4$
$\text{Fe}(\text{COO})_3$	543	~25.0	–	–	$\text{Fe}_3\text{O}_4$
$\text{Ni}(\text{COO})_2 \cdot 2\text{H}_2\text{O}$	483	~30.0	50.0	~4.0	Ni
$\text{Cu}(\text{COO})_2$	413	~30.0	~30.0	–	Cu
$\text{Cu}(\text{COO})_2 \cdot \text{MEA}$ (see <sup>e</sup> )	398	–	69–75	–	Cu
$\text{Cu}(\text{N}_2\text{H}_3\text{COO})_2 \cdot 2\text{H}_2\text{O}$ (see <sup>f</sup> )	393	–	200–300	–	Cu
$\text{Fe}_2(\text{C}_2\text{O}_4)_3 \cdot 5\text{H}_2\text{O}$	583	35.0	30.0	–	$\text{Fe}_3\text{O}_4$
$\text{Pb}(\text{COO})_2$	493	~150.0	~3,000.0	–	Pb
$\text{Pb}(\text{COO})_2 \cdot \text{MEA}$	525	–	~3,000.0 (~46.0) <sup>g</sup>	–	Pb

<sup>a</sup>Particle diameter calculated from the specific surface area data for the solid products at the end of decomposition

<sup>b</sup>Average particle diameter calculated from EM data

<sup>c</sup>Polymer shell thickness

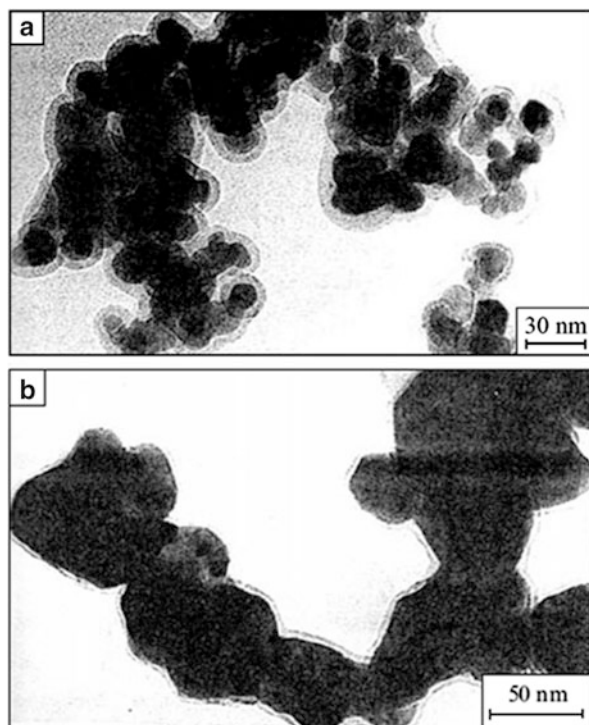
<sup>d</sup>Powder X-ray diffraction and electron diffraction data

<sup>e</sup>MEA is monoethanolamine

<sup>f</sup>Hydrazinocarboxylate

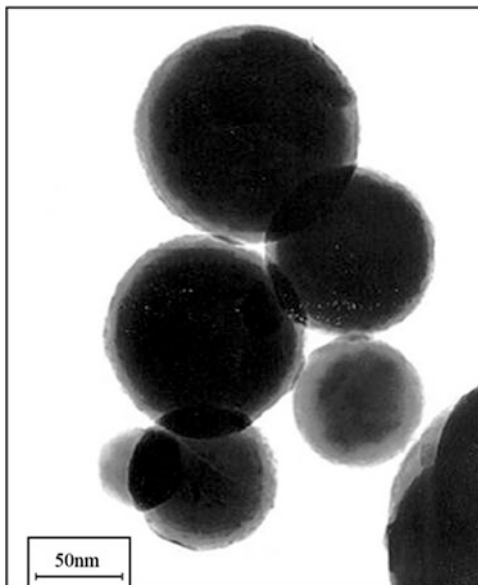
<sup>g</sup>After ultrasonic treatment

**Fig. 6.11** Polymeric shell on the particles formed upon decomposition of  $\text{Fe}(\text{HCO}_2)_2 \cdot 2\text{H}_2\text{O}$  (543 K) (a) and  $\text{Ni}(\text{HCO}_2)_2 \cdot 2\text{H}_2\text{O}$  (483 K) (b)





**Fig. 6.12** Electron microscopic image of the spherical particulates of bismuth metal formed upon reduction of bismuth stearate in the presence of high-boiling alcohol (<http://www.sbras.nsc.ru/win/sbras/rep/rep2003/tom1/nim.html>)

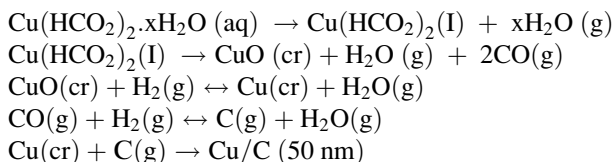


(e.g., benzyl alcohol), powdered nanocrystalline bismuth is formed, while in air bismuth oxide as various polymorphs or as a mixture with the metal is produced. Initially, nanosized (1–2 nm) bismuth particles in ordered layered structures with interlayer spacing of  $\sim 5$  nm are formed and subsequently they are converted to polymer-stabilized crystalline structures, which are enlarged to 50 nm (Fig. 6.12). The polymer probably arises due to thickening of the destruction products of the carboxyl fragment.

Homogenous thin films of ZnO with a controlled morphology of wurtzite deposited in a silicone support were obtained from solutions of zinc acetate or nitrate using the ultrasound treatment [157]. The thermal decomposition of zinc acetate on a silicone substrate is carried out at relatively low temperature (473–523 K) with the formation of nanoparticles, nanowires, and nanowalls as mono- or polycrystals [158]. Of interest is obtaining of ZnO by thermal decomposition at 473 K of coordination polymers of  $[\text{Zn}(4\text{-bpdb})(\text{NO}_2)_2]_n$  types (where bpdb is 1,4-bis(4-pyridil)-2,3-diazo-1,3-butadiene) [159] resulted of high-crystalline nanomaterials.

To obtain homogeneous hexagonal nanocrystalline ZnO, decomposition of Zn-oleate complex were investigated by the thermogravimetric analysis [160]. The decomposition starts at 523 K and ends at 763 K. Size of nanocrystallites depends time (from 1 to 10 h) and temperature of thermolysis; nanoparticles can be redispersed in non-polar organic solvents.

Flame pyrolysis of copper formate solution in the excess of hydrogen produced copper nanoparticles covered with carbon on the following scheme [161]:

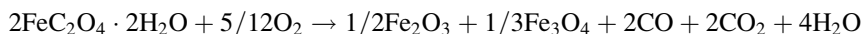


Thermolysis of oleate complexes solvating in 1-octadecene is widely applied (see, for example [162–165]). Significant efforts have been attempted to study different carboxylate salts of silver [166–170] including perfluorine carboxylates [171], oxalate [172], etc. [173]. As a rule, relatively low temperatures (393–523 K), a long-term reaction time (8–24 h), an inert atmosphere are needed to obtain metal nanoparticles. Thus, the high yield of nanoparticles is characteristic for decomposition of silver carboxylates in the presence of hydrogen. Carboxylate groups are deprotonated followed with reduction of silver ions and formation of spherical nanoparticles of 4–6 nm in diameter [174].

The conditions to control size and structure of silver nanoparticles arised from the different types of precursors [175] including coordination polymers were determined [176].

Thermolysis of metal salts of dicarboxylic acids, in particular, oxalates has been investigated for a long time (see [177–181]).

Pre-history (temperature and duration of deposition, aging, morphology) affects essentially the structure of a pyrolyzed product as in case of iron oxalate. Thermal decomposition in air produces hematite ( $\alpha\text{-Fe}_2\text{O}_3$ ), deficiency of oxygen at 773–973 leads to the formation of  $\text{Fe}_3\text{O}_4$  nanoparticles of 35–55 nm of size [182–186]:



An oxidative interaction of ethylene glycol with  $\text{Cu}(\text{NO}_3)_2 \cdot 3\text{H}_2\text{O}$  with a nitric acid (pH & 1.5) additive yields polynuclear oxalate copper complexes [118, 119]. Their thermolysis at 563 K affords monovalent copper oxide (cuprite,  $\text{Cu}_2\text{O}$ ), while that at 1,273 K gives CuO. Polymeric structures of a similar type can also arise in case of 1,2- and 1,3-propandiol and other metal nitrates. Meanwhile, ethylene glycol reacts with manganese oxalate  $\text{MnC}_2\text{O}_4 \cdot x\text{H}_2\text{O}$  ( $x = 2$  or 3) with displacement of a water molecule giving rise to a new solvation complex,  $\text{MnC}_2\text{O}_4(\text{HOCH}_2\text{CH}_2\text{OH})$  [187]. Thermolysis of this crystal solvate in air produces a quazi-one-dimensional  $\text{Mn}_3\text{O}_4$ , or  $\text{Mn}_2\text{O}_3$  nanowhiskers, or MnO particles (in the inert atmosphere). The metastable MnO is obtained by thermolysis of manganese acetate in an oleic acid mixture with trioctylamine [188]. Decomposition of this salt in oleylamine at 473 K furnishes a 2D structure,  $10.2 \times 6.8$  nm nanoplates. The formation of MnO nanospheres from the  $\text{Mn}_2(\text{CO})_{10}$  complex with oleylamine upon the addition of trioctylphosphine was also reported [189]. The  $\text{Mn}_3\text{O}_4$  nanoparticles with the core-shell structure [190] were obtained by thermolysis of  $\text{Mn}(\text{acac})_2$  (acac is

acetylacetonate) in oleylamine [191] or by oxidation of MnO with trimethylamine-N-oxide [192–194]. Note that the MnO and Mn<sub>3</sub>O<sub>4</sub> nanoparticles reveal ferromagnetic properties at low temperatures and the coercive force is 8.9 kOe at 5 K; this is essentially more than that for the bulk Mn<sub>3</sub>O<sub>4</sub>. Nanoparticles of MnO of 5–10 nm in size possess weak ferromagnetism at low temperatures but the antiferromagnetic phase transition of bulk MnO occurs at about 120 K. Superparamagnetic particles of iron oxide were obtained by thermal decomposition of iron acetylacetonate (at 538 K) in the presence of phenyl ether, oleylamine, and 1,2 hexadecandiol [195] or by the same way from anhydrous iron oleate (at 573 K) [196, 197].

Thermolysis of the complex Eu[C<sub>6</sub>H<sub>3</sub>(CO<sub>2</sub>)<sub>3</sub>-1,3,5]-6H<sub>2</sub>O obtained from an aqueous solution of europium nitrate and benzene-1,3,5-tricarboxylic acid affords 10–20 nm-thick one-dimensional Eu<sub>2</sub>O<sub>3</sub> nanorods with a 50–100 nm width and a length ranging from hundreds nanometres to several micrometres [198–200]. At temperature below 873 K, the TGA curves show two main weight loss stages, one at 383 K (elimination of water molecules) and one at 742 K (elimination of the organic ligand); as this takes place, the one-dimensional crystalline thread of the nanomaterial being formed (Eu<sub>2</sub>O<sub>3</sub>) is retained. The oxide Eu<sub>2</sub>O<sub>3</sub> was also obtained as nanoparticles of different shape: rods [201], nanowires [202], hollow spheres [203] and nanotubes [204]. The interest in these structures is caused by their unusual physical and chemical properties [205]. For example, europium-doped yttrium oxide (Eu<sup>3+</sup> in the Y<sub>2</sub>O<sub>3</sub> host lattice) is a red inorganic lumiphore efficient for the use in plasma displays as hollow spheres and inefficient when has the ‘core-shell’ morphology.

Thermal decomposition of europium acetate at 923 K for 3 days in a steel reactor in the self-generated atmosphere affords single-phase crystalline hexagonal nanoplates of europium oxycarbonate Eu<sub>2</sub>O<sub>2</sub>CO<sub>3</sub> [206]. Lanthanide oxycarbonates Gd<sub>2</sub>O<sub>2</sub>CO<sub>3</sub>, Sm<sub>2</sub>O<sub>2</sub>CO<sub>3</sub>, Y<sub>2</sub>O<sub>2</sub>CO<sub>3</sub>, La<sub>2</sub>O<sub>2</sub>CO<sub>3</sub> obtained by this way have attracted considerable attention because of their versatile applications [207, 208]. Under similar conditions, zinc acetate is converted to nanopencil-shaped luminescent ZnO [209].

Scattered data on the thermal decomposition of metal acetates in polymer matrices were published. For example, metallopolymer composites are formed in the high-temperature (1,273 K) thermolysis of cobalt acetate in the presence of polystyrene (PS), poly(acrylic acid) (PAA) or poly(methyl vinyl ketone) (PMVK) [210]. Carbonization of the organic part affords a material containing metallic cobalt clusters.

Worthy of note is the synthesis of monodisperse oxide nanoparticles from submicrone oxide powders based on controlled dissolution – recrystallization processes. Thus on slow dissolution of a haematite powder in an oleic acid – octadec-1-ene mixture followed by decomposition of the resulting salt, Fe<sub>3</sub>O<sub>4</sub> and γ-Fe<sub>2</sub>O<sub>3</sub> nanoparticles are formed in 3:2 ratio with an average diameter of 12.1 nm [211]. Colloid nanocrystals of transition metal oxides of well-defined sizes, shape, morphology, and crystallinity, and having ability to self-assembling are widely used in various fields, especially in catalysis, biomedicine, as sensors and so on [212, 213].

### 6.3.3 Thermolysis of Metal Complexes

One of the most facile and convenient methods for the preparation of monodisperse metal nanoparticles is thermal decomposition of their complexes, for example, acetylacetonates, carbonyls, and so on, in high-boiling solvents. In the presence of surfactants, oleic acid or oleylamine (in some cases, metal oleates dissolved in octadecene are used), thermolysis of these compounds results in the formation of evenly shaped monodisperse particles. Long-chain amines, thiols, carboxylic acids, phosphine oxides are efficient stabilizing agents both of noble metal nanoparticles in different solvents (see, for example [214–218]) and nickel, cobalt, iron [219, 220], and silver [174] nanoparticles and so on. They prevent aggregation of nanoparticles formed during thermal decomposition. Usually, the process is carried out at 573 K under  $N_2$  atmosphere. Long-chain acids or amines can serve as alternatives to surfactants. For example, stabilization of cobalt nanoparticles of diameter 25–35 nm was observed during the thermal transformation of cobalt (II) bis(salicylidene) in the presence of oleylamine [221]. Oleylamine complex of nickel acetate was decomposed at 488 K yielding monodisperse sphere nanoparticles of nickel or its oxide [222]. Similar syntheses are numerous. Worthy of note is the formation of nanocrystalline nickel (18.1 nm) at the controlled thermolysis of ethylene diamine (en) complex  $[Ni(en)_2(H_2O)_2](NO_3)$  [223]. Under static conditions an autogenic decomposition occurs at 473 K, the kinetics of its oxidation follows the Johnson–Mehl–Avrami mechanism, the activation energy is 135.1 kJ/mol. The product is stable and not oxidized up to 623 K. The kinetics of deamination is retraced for a solid phase thermolysis of tris (ethylenediamine)nickel(II) sulfate [224].

Thermal decomposition of the coordination three-dimensional polymer  $[Pb(phen)(I-N_3)(I-NO_3)]_n$  containing an azide-anion ligand gave PbO nanoparticles [225]. The controlled thermolysis of  $Fe_3(CH_3COO)_6(OH)_2(CH_3COO)$  in a closed reactor in an inert atmosphere at 973 K affords ferromagnetic magnetite nanoparticles [226]. Thermal decomposition of iron(III) oxalate tetrahydrate in a dynamic inert atmosphere is accompanied by the formation of small amounts of superparamagnetic iron(III) oxide. The key intermediate formed at 483 K is  $FeC_2O_4$  [227]. The yield products are FeO (wustite),  $\alpha$ -Fe, magnetite. Thermolysis of the starting complex in an oxidative atmosphere comprises dehydration, reduction to Fe(II) and the subsequent decarboxylation to hematite.

Components of the reaction medium can have a considerable influence on the specific growth mechanism and the nanoparticle shape. Thermolysis of iron(III) oleate in the presence of tetraoctylammonium bromide yields octahedral iron oxide nanocrystals, the transformation of the quaternary ammonium salt into trioctylammonium bromide being the rate-determining step [228, 229].

The different mechanisms of thermolysis of such precursors are postulated on the assumption of the composition and structure of the yield products though many of them are inconsistent. First of all, it concerns bipyridine complexes Zn(II) and Cd(II) [230, 231] as well as Ni(II) [232] and Fe(II) [233] (and references there in).



For all these complexes it has been ascertained the formation of self-organizing nanocomposites comprising of crystal sulphide cobalt clusters ( $\text{Co}_9\text{S}_8$ ) (thermolysis at 593 K) and  $\text{Co}_6\text{S}_5$  (thermolysis at 873 K);  $\text{Ni}_3\text{S}_2$  and NiC, or nanocrystalline Cu with the structure of core-shell. The Cu particles of 2–3 nm or even bigger combined into aggregates make the core; the shell is the destruction products of ligand.

Metal nanocrystals, metal oxides, and metal sulphides were obtained by thermal decomposition of corresponding metal-surfactants [235].

It is interesting that silver nanoparticles with an average size of 60 nm and spherical morphology can be synthesized by thermolysis of 2-pyridine carboxylate complex  $\text{Ag}(\text{PPh}_3)_2(2\text{-pyCOO})$  in the presence of oleic acid. Meanwhile, without the surfactant only large particles of the bulk silver of a granulated shape are formed [236].

A comparative simple route for synthesis of nanosized  $\text{Co}_3\text{O}_4$  being one of the important p-type semiconductor with high gas-sensor, catalytic and electrochemical properties [237–239] is suggested. This is a solid-phase thermolysis of the organometallic precursor – bis[(salicylaldehyde)<sub>2</sub>cobalt(II)] at 773 K for 5 h in air [240, 241]. Thermolysis of N,N-(bis(salicylidene)ethylene-1,2-diamine)nickel in the absence of any template or surfactant was proven to be useful for synthesis of uniform NiO particles at temperature 700 K [242].

A simple large-scale method to synthesize high-purity Zn nanowires using a biomass as carbon source in a carbothermal process has been reported [243]. The process in which ZnO and *Eucalyptus sp.* tar pitch were used as source materials was carried out in inert atmosphere, without vacuum or catalyst, at temperatures (1,073–1,173 K) lower than those required in the carbothermal reduction of ZnO with graphite. Note that reoxidation of the Zn nanowires obtained in air at 573–673 K affords the nanostructured hexagonal ZnO with a high purity and crystallinity [244].

Thermolysis of bis-aqua-tris-salicylaldehyde zirconium(IV) nitrate in oleynimine is useful for obtaining single-phase  $\text{ZrO}_2$  ceramics with a cubic shape [245]. The addition of triphenyl phosphine to the reaction mixture allowed one to control the size of particles. Under certain conditions zirconyl nanoparticles of the quasi-spherical shape and about 30 nm of size are formed.

Analysis of thermal transformations of metal complexes has been performed in recent work [28]. Below in Sect. 6.4 we consider the thermolysis of such metal complexes in polymer matrices as well as polymerization conjugated with a thermolysis process of acrylamide complexes is discussed (Sect. 6.5).

## 6.4 The Conjugate Thermolysis – Nanoparticle and Polymer Matrix Formation Process

Currently, various methods for stabilizing nanosized particle are available [246]; some of them have already been mentioned. The self-regulated stabilization of highly dispersed metal particles either as metal-containing precursors or as monomers, which are then subjected to polymerization and thermolysis, seems especially promising.

### 6.4.1 Thermal Transformations of Salts of Unsaturated Carboxylic Acids

Thermolysis of metal-containing monomers (salts of unsaturated mono- and dicarboxylic acids) is poorly studied but vigorously developing line of research and the best embodiment of the idea of nanoparticle stabilization in situ. The monomers include alkali, alkaline earth and transition metal acrylates ( $\text{MAcr}_n$ ), maleinates ( $\text{MMal}_n$ ), itaconates ( $\text{MItac}_n$ ) and fumarates ( $\text{MFum}_n$ ) [247–249], their polysalts [250, 251]. This series can be extended for salts of acetylenecarboxylic acids [252]. Such compounds capable to polymerization have been named metallomonomers.

Most of the results of investigations of thermal transformations of metal-containing monomers are qualitative [253–260].

For example, the initial decomposition temperatures of acrylates increase in the sequence of metals:  $\text{Fe} < \text{Cr} < \text{Ni} < \text{Co} < \text{Mn}$ ; however, these temperatures are lower than the decomposition temperature of polyacrylic acid. Probably, this is caused by the catalytic influence of metal ions or nanoparticles on the destruction of the polyacrylate fragments. Preliminary  $\gamma$ -irradiation (200–600 kGy) of Ni (II), Co (II) and Cu(II) polyacrylates and increase in the irradiation dose lead to a decrease in the initial decomposition temperatures [261]. The stage mechanism of thermolysis has been proposed for complex acrylates of the composition of  $\text{M}(\text{phen})(\text{Acr})_2(\text{H}_2\text{O})_y$ , where phen is phenanthroline,  $\text{M} = \text{Mn}(\text{II})$  ( $y = 0$ ),  $\text{Ni}(\text{II})$  ( $y = 2$ ),  $\text{Cu}(\text{II})$  ( $y = 1$ ),  $\text{Zn}(\text{II})$  ( $y = 2$ ) (TG, DTG, air, 293–1,273 K, rate heating 10 deg./min) [262]. For these acrylates, except for Zn- complex, all of the macrostages were exothermic. The solid products are  $\text{Mn}_2\text{O}_3$ , NiO, CuO and ZnO, respectively.

Studies of the thermolysis of metal salts of unsaturated carboxylic acids both in the thermal analysis (TA) and SGA modes revealed the general pattern of their transformations. They tend to decompose via a sequence of three macro stages occurring at different temperature: [155] dehydration (desolvation) of the initial monomers (403–473 K); solid-state homo- or copolymerization of the dehydrated monomer (monomers) (473–573 K); decarboxylation of the polymer thus formed to give a metal-containing phase and oxygen-free polymer matrix (at temperatures of  $>523$  K, or for copper carboxylates  $>453$  K) accompanied by vigorous gas evolution.

The most informative quantitative data on the kinetics and the physicochemistry of thermal transformations of such precursors were derived from a SGA process in a non-isothermal closed reactor [263–270]. The studied compounds included  $\text{Cu}_2(\text{CH}_2=\text{CHCOO})_4$  ( $\text{CuAcr}_2$ ),  $\text{Co}(\text{CH}_2=\text{CHCOO})_2 \cdot \text{H}_2\text{O}$  ( $\text{CoAcr}_2$ ),  $\text{Ni}(\text{CH}_2=\text{CHCOO})_2 \cdot \text{H}_2\text{O}$  ( $\text{NiAcr}_2$ ),  $\text{Fe}_3\text{O}(\text{OH})(\text{CH}_2=\text{CHCOO})_6 \cdot 3\text{H}_2\text{O}$  ( $\text{FeAcr}_3$ ), cocrystallites  $[\text{Fe}_3\text{O}(\text{OH})(\text{CH}_2=\text{CHCOO})_6] \cdot [\text{Co}(\text{CH}_2=\text{CHCOO})_2]_{2,4}$  ( $\text{FeCoAcr}_2$ ) and  $[\text{Fe}_3\text{O}(\text{OH})(\text{CH}_2=\text{CHCOO})_6] \cdot [\text{Co}(\text{CH}_2=\text{CHCOO})_2]_{1,5} \cdot 3\text{H}_2\text{O}$  ( $\text{Fe}_2\text{CoAcr}_2$ ),  $\text{Co}(\text{OCOCH}=\text{CHCOO}) \cdot 2\text{H}_2\text{O}$  ( $\text{CoMal}_2$ ),  $[\text{Fe}_3\text{O}(\text{OH})(\text{OCOCH}=\text{CHCOO})_6] \cdot 3\text{H}_2\text{O}$  ( $\text{FeMal}_3$ ).

The time dependence of gas evolution  $\eta(t)$  for these compounds is described satisfactorily by the approximating relation

**Table 6.8** Kinetic parameters of thermolysis of transition metal salts of unsaturated carboxylic acids

Compound	Temp, K	Parameter	$\eta_{1f}, \Delta\alpha_{\Sigma f} = A \exp[-\Delta H/(RT)]$		$k$	$k = k_0 \exp[-E_a/(RT)]$		References
			A	$\Delta H$ , kJ/mol		$k_0, s^{-1}$	$E_a$ , kJ/mol	
CuAcr <sub>2</sub>	463–513	$\eta_{1f}$	$1.8 \cdot 10^4$	48.1	$k_1$	$9.5 \cdot 10^{11}$	154.7	[263]
		$\Delta\alpha_{\Sigma f}$	3.6	12.5	$k_2$	$9.2 \cdot 10^{11}$	163.0	
CoAcr <sub>2</sub>	623–663	$\eta_{1f}$	1.0	0	$k_1$	$3.0 \cdot 10^{14}$	238.3	[264]
		$\Delta\alpha_{\Sigma f}$	1.55	0	$k_2$	0	0	
FeAcr <sub>3</sub>	473–573	$\eta_{1f}$	1.0	0	$k_1$	$4.2 \cdot 10^{21}$	246.6	[266]
		$\Delta\alpha_{\Sigma f}$	$1.6 \cdot 10^2$	25,5	$k_2$	0	0	
	$\eta_{1f}$	1.0	0	$k_1$	$1.3 \cdot 10^6$	127.5		
		$\Delta\alpha_{\Sigma f}$	$1.7 \cdot 10^2$	26,3	$k_2$	0	0	
NiAcr <sub>2</sub>	573–653	$\eta_{1f}$	2.6	1.1	$k_1$	$1.7 \cdot 10^{17}$	242.4	[265]
			$\Delta\alpha_{\Sigma f}$	$1.4 \cdot 10^{11}$				
		$\Delta\alpha_{\Sigma f}$	1.2	10.5 (>613 K)	$k_2$	$7.5 \cdot 10^8$	156.8	
FeCoAcr	613–663	$\eta_{1f} = 0.65(613 \text{ K}) \div 0.45(663 \text{ K})$		$k_1$	$2.3 \cdot 10^{12}$	206.9	[267, 268]	
		$\Delta\alpha_{\Sigma f}$	$5.25 \cdot 10^2$	7.5	$k_2$	$6.0 \cdot 10^8$		137.9
Fe <sub>2</sub> CoAcr	613–663	$\eta_{1f} = 0.50(613 \text{ K}) \div 0.3(663 \text{ K})$		$k_1$	$2.6 \cdot 10^{12}$	204.8	[267, 268]	
		$\Delta\alpha_{\Sigma f}$	$1.9 \cdot 10^2$	6.0	$k_2$	$6.6 \cdot 10^5$		125.4
CoMal <sub>2</sub>	613–643	$\eta_{1f}$	1.0	0	$k_1$	$1.6 \cdot 10^6$	125.4	[269]
		$\Delta\alpha_{\Sigma f}$	$1.3 \cdot 10^2$	23.4	$k_2$	0	0	
FeMal <sub>3</sub>	573–643	$\eta_{1f}$	$0.59 \cdot 10^2$	23.4	$k_1$	$3.3 \cdot 10^7$	133.8	[270]
		$\Delta\alpha_{\Sigma f} = 4.78(673 \text{ K}) \div 7.4(643 \text{ K})$		$k_2$	$1.0 \cdot 10^7$	110.8		

Note.  $\eta = \Delta\alpha_{\Sigma f}/\alpha_{\Sigma f}$  is the degree of conversion where  $\Delta\alpha_{\Sigma f} = \alpha_{\Sigma f} - \alpha_{\Sigma 0}$ ;  $\Delta\alpha_{\Sigma f} = \alpha_{\Sigma f} - \alpha_{\Sigma 0}$ ;  $\alpha_{\Sigma f}$ ,  $\alpha_{\Sigma t}$ ,  $\alpha_{\Sigma 0}$  are the final, current and initial total numbers of the gaseous decomposition products evolved per mole of the starting compound at room temperature, respectively ( $\alpha_{\Sigma 0}$  is related to dehydration and polymerization processes);  $\eta_{1f} = \eta(t)$ ,  $k_2 t \rightarrow 0$ ,  $k_1 t \rightarrow \infty$ .

$$\eta(t) = \eta_{1f}[1 - \exp(-k_1\tau)] + (1 - \eta_{1f})[1 - \exp(-k_2\tau)], \quad (6.9)$$

where  $k_1, k_2$  are the effective rate constants for the transformation ( $W = d\eta/dt$ ) at the corresponding stage,  $\eta_{1f} = \eta(t)$  for  $k_2\tau \rightarrow 0$  and  $k_1\tau \rightarrow \infty$ ,  $\tau = t - t_0$ ,  $t_0$  are the heating time of the sample. Note that the ratio  $m_0/V$  has almost no influence on the transformation rate, which is indicative of thermolysis in the condensed phase.

Table 6.8 summarizes the kinetic characteristics of the thermal transformations of the studied compounds. Attention is attracted by the fact that thermolysis of FeAcr<sub>3</sub> comprises two temperature-separated gas evolution regions with different kinetic parameters: low-temperature (<573 K) and high-temperature (>573 K) regions. A possible explanation of this phenomenon is the occurrence of two parallel gas evolution processes. In terms of decreasing gas evolution ability of



the acrylates  $\text{MAcr}_n$ , metals can be arranged in the series:  $\text{Cu} \geq \text{Fe} > \text{Co} > \text{Ni}$ . The thermal transformation of  $\text{MAcr}_n$  and  $\text{MMal}_n$  in the gas phase produces [254, 271]  $\text{CO}_2$ ,  $\text{CO}$ ,  $\text{H}_2$ ,  $\text{H}_2\text{O}$  vapour, acrylic (from  $\text{MAcr}_n$  thermolysis) or maleic (from  $\text{MMal}_n$ ) acid vapour,  $\text{C}_2\text{H}_4$  (for  $\text{CuAcr}_2$ ),  $\text{CH}_4$  (for  $\text{CoAcr}_2$  and  $\text{NiAcr}_2$ ). The solid products of transformation are particles of the corresponding metal and/or metal oxide embedded in the decarboxylated polymer (in the case of co-crystallized  $\text{FeCoAcr}_2$  and  $\text{Fe}_2\text{CoAcr}_2$ , cobalt ferrite,  $\text{CoFe}_2\text{O}_4$ , is formed).

Analysis of the chemical transformation pathways shows that under the assumption of energetic non-equivalence of the  $\text{M}_7\text{O}$  bonds in unsaturated metal carboxylates, the primary decomposition step is the formation of radicals: acrylic ( $\text{CH}_2=\text{CHCOO}^\cdot$ ) and maleic ( $\text{OOCCH}=\text{CHCOO}^\cdot$ ) radicals for acrylates and maleates, respectively. The radicals initiate polymerization, which is followed by decarboxylation of the metallopolymer. As an example, Scheme 6.5 presents the mechanism of thermal decomposition of acrylate.

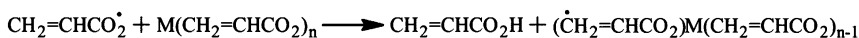
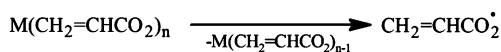
Taking account of Scheme 6.5, the material balance equations and quantitative data on the yields of gaseous and volatile products of thermolysis, it was found that the composition of the solid phase changes during the transformation. It can be represented by the following balance relation: for acrylates  $\text{MO}_r(\text{CH}_2\text{CHCOO})_{p-k}(\text{CH}_2\text{CH})_k(\text{CHCHCOO})_{q-l}(\text{CHCH})_l$  and for maleates  $\text{MO}_r(=\text{CHCOO})_{2p-k}(=\text{C}-)_k(=\text{CCOO})_{2q-l}(=\text{C}-)_l$  where before decarboxylation,  $r=k=l=0$  ( $r \neq 0$  for  $\text{FeAcr}_3$ ),  $p$  and  $q$  are the numbers of internal and terminal (hydrogen-depleted) carboxylate groups, respectively.

An important problem, although rarely discussed, is the morphology and topography of the solid products of carboxylate thermolysis the knowledge of which would extend the understanding of the physicochemistry of this process. The initial  $\text{MAcr}_n$  and  $\text{MMal}_n$  samples are optically transparent crystal-like porous particles without crystallinity at distances comparable with the transmitted light wavelength. They have relatively great specific surface area ( $S_{\text{sp}}^0 = 9\text{--}30 \text{ m}^2/\text{g}$ ), which does not change significantly upon thermolysis. However, in some cases (for  $\text{CuAcr}_2$ ,  $\text{CoAcr}_2$  and somewhat for  $\text{NiAcr}_2$ ), large aggregates are dispersed. As a result, the average particle size decreases and  $S_{\text{sp}}$  increases 2–3-fold and then decreases again due to the sintering of particles [263, 264].

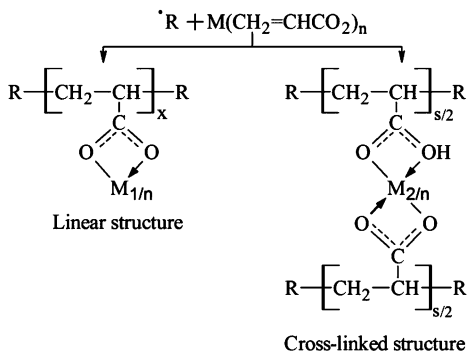
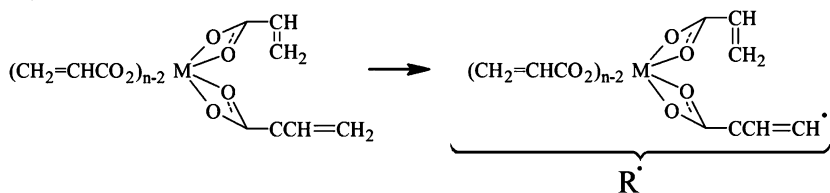
Even at early stages (during the sample warming-up), the particles lose transparency and their surface becomes sugar-like, probably as a result of desolvation processes, which may attest to a significant contribution of a bulk homogeneous reaction. Thus, thermolysis of these compounds is a heterogeneous-homogeneous process [265, 266, 268].

The average size of decarboxylated metallopolymer particles ( $S_{\text{sp}}$  measurement data) is estimated as  $\sim 20\text{--}30 \text{ nm}$  for  $\text{CuAcr}_2$  and  $\sim 30\text{--}50 \text{ nm}$  for  $\text{CoAcr}_2$ . Electron microscopy and electron diffraction studies [265, 269] of the sample microstructure have shown (Fig. 6.13a) a rather narrow particle size distribution, a 4–9 nm mean diameter of particles (Fig. 6.13b) and a 8–10 nm mean distance between particles in the matrix. The even particle distribution in the matrix and the narrow particle size distribution may be indicative of a high degree of pseudo-homogeneity of decarboxylation and the formation of a new phase. Note that the mean size of the

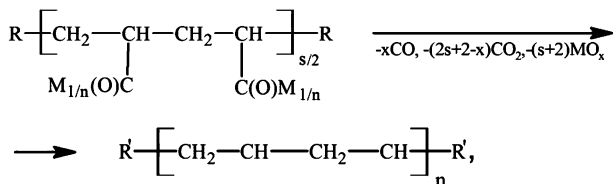
## I. Initiation



## II. Polymerization



## III. Decarboxylation

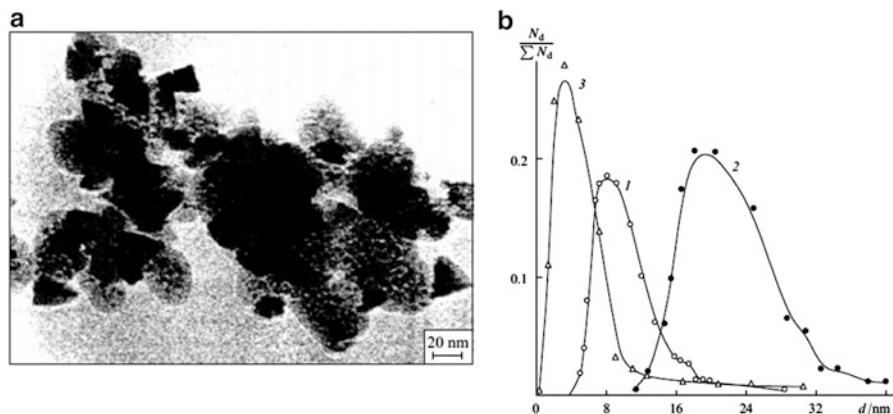


$\text{R}' = \text{CH}_2=\text{CH}-\text{CH}=\text{CH}$  is hydrogen-depleted decarboxylated diacrylate fragment;  $\text{MO}_x$  is the metal ( $x=0$ ) or its oxide ( $x>0$ ).

**Scheme 6.5** The main routes of thermal transformations of metal acrylates

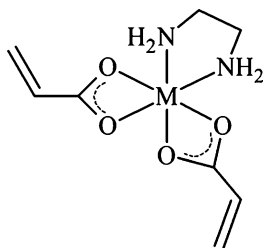
thermolysis products is much greater for the salts of saturated carboxylic acids than for the unsaturated acid salts (see Fig. 6.13b).

Of interest are lanthanide acrylates due to their specific optical properties [272–275]. The coordination vacancy of transition metals of acrylates can be occupied not only by water molecules but also by other ligands such as amines. In this



**Fig. 6.13** Electron microscopic image of the thermolysis product of  $\text{Co}(\text{O}_2\text{CCH}=\text{CHCO}_2)\cdot 2\text{H}_2\text{O}$  at 623 K (a) and size distribution of metal-containing particles (b) [269] (1)  $\text{Fe}_3\text{O}(\text{OH})(\text{CH}_2=\text{CHCOO})_6\cdot 3\text{H}_2\text{O}$ , (2)  $\text{Fe}(\text{HCOO})_2\cdot 2\text{H}_2\text{O}$ , (3)  $\text{Co}(\text{OCOCH}=\text{CHCOO})_2\text{H}_2\text{O}$

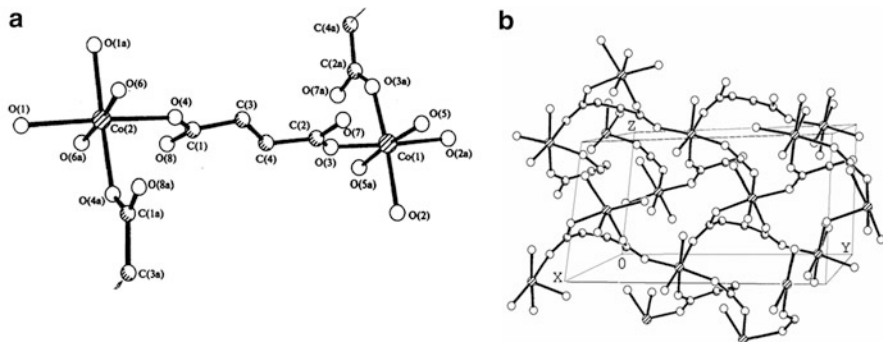
connection of interest is the work [276] in which the thermal stability of mixed acrylate and ethylenediamine metal complexes is investigated



$[\text{M}(\text{en})(\text{CH}_2=\text{CHCOO})_2]\cdot n\text{H}_2\text{O}$  ((1)  $\text{M}=\text{Ni}$ ,  $n=2$ ; (2)  $\text{M}=\text{Cu}$ ,  $n=0$ ; (3)  $\text{M}=\text{Zn}$ ,  $n=2$ ; en = ethylenediamine).

After dehydration and elimination of ethylenediamine a metal oxide yield product is formed except metallic copper arising from the copper complex. The complexes of acrylates with tetradentate tripodal ligands are known [277–279]. Such complexes reveal a superoxidedismutase-like activity, particularly, those with aromatic amines (2,2'- or 4,4'-dipyridil, 1,10-phenanthroline) which model different biological objects. However, in these works the stage of polymerization, the peculiarity of thermolysis of such complexes and, consequently, the properties of the resulting nanoparticles is ignored.

Synthetical approaches and structure of pre-thermolized carboxylates of unsaturated dicarboxylic acids are different from those of monocarboxylic acids. Firstly, already on the stage of their synthesis (as shown for metal maleates, fumarates, itaconates, acetylenedicarboxylates [252, 280]) coordination polymers are formed.



**Fig. 6.14** Molecular structure of coordination polymers of Co(II) fumarate pentahydrate (a) and maleate (b)

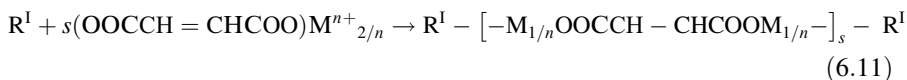
Thus, according to the X-ray analysis unsaturated metal dicarboxylates have both monomeric (Co(II) and Fe(II) hydromaleates,  $M(C_4H_3O_4)_2 \cdot 4H_2O$ ) and chain- (Co(II) fumarate,  $CoC_4H_2O_4 \cdot 5H_2O$ ) or three-dimensional (Co(II) maleate,  $CoC_4H_2O_4 \cdot 3H_2O$ ) polymeric structure (Fig. 6.14) multiple bonds of which are not coordinated with metal.

However the mechanism of their thermal transformations is similar to that of unsaturated monocarboxylic acid salts [269, 271]. One can assume that with the rise of the level of heat vibrations in the lattice of monomer the rupture of the weakest M–O bonds is the most probable. As the result the biradicals  $\cdot OOCCH=CHCOO\cdot$  are formed from maleates, for instance. The formed radicals react with the metal-containing maleate fragments to give corresponding acids and H-depleted radical  $R^\cdot$  of maleic groups by the following scheme:

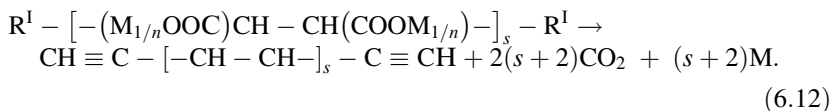


Where  $RH = (CHCOO)_2M^{n+}_{2/n}$ ,  $R^I = (\cdot CCOO)_2M^{n+}_{1/n}$ .

The formed  $R^I$  initiates the polymerization to produce the linear or networked polymers.



With temperature the metal-containing fragments of formed polymers decompose to produce a metal (or its oxide) and  $CO_2$ .



The polymers resulted in the decarboxylation reaction can be additionally thermopolymerized to form the net structure with conjugated multiple bonds.

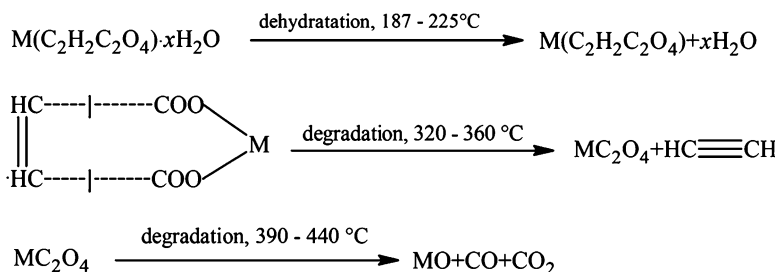
In general, the composition of solid phase products of thermolysis can be represented as a sum of the C–H–O-fragment fractions:

$$\text{MO}_z(=\text{CHCOO})_{2p-x}(=\text{CCOO})_{2q-y}(=\text{CH-})_x(\equiv\text{C-})_H, \quad (6.13)$$

where  $x = y = z = 0$  ( $z \neq 0$  in the case of Fe(III)-maleate),  $p$  and  $q$  are the amounts of intra-chain and H-depleted terminal groups ( $p + q = 1$ ), respectively.

Thermolysis of Cu(II) and Zn(II) [281] maleates and fumarates was studied by non-isothermal methods (TGA, DTG, DTA) in the temperature range 273–873 K (heating rate 5 deg./min). Dehydration of the complexes demonstrated that the thermal stability of copper and zinc fumarates was higher than the stability of the corresponding maleates, the dehydrated copper fumarates and maleates were equivalent in stability and zinc fumarate was more stable than zinc maleate.

Comparative analysis of thermolysis of geometry isomers (*cis*- and *trans*-) was carried out for Zn(II) and Cu(II) [282] and Mn(II), Co(II), and Ni(II) [281] maleates and fumarates, respectively, to study the influence of the ligand structure on the thermal stability and mechanism of thermolysis of the corresponding complexes. In the case of the nickel salts dehydration starts at 403 K and ends at 498 K. The second stage comprises the quickly oxidative decomposition (mass loss 69 % at 663 K) up to NiO. This indicates that the yield product arises directly from nickelfumarate. The following scheme has been proposed for this reaction (Scheme 6.6).



**Scheme 6.6** A scheme of thermolysis of metal maleates and fumarates in air

Probably, this mechanism should be defined more precisely making allowance for a polymer structure of the salts being formed during the decomposition. Secondly, the weakest carboxylic group bond should be also considered because the decomposition of a dehydrated complex starts from its rupture.

In a study of thermolysis of ferrimaleates  $\text{M}_3[\text{Fe}(\text{Mal})_3]_2 \cdot x\text{H}_2\text{O}$  ( $\text{M} = \text{Mn}, \text{Co}, \text{Ni}, \text{Cu}$ ) in a static air atmosphere at temperatures of up to 873 K, general characteristics of the decomposition process were established [258]. This is a multistage transformation starting with dehydration of ferrimaleates to ferrites; after dehydration, the Fe(III) precursor is converted to an intermediate Fe(II) derivative,  $\text{M}_3[\text{Fe}(\text{Mal})_2]_2$ ; after that, the monomer destruction yields iron(III) oxide and the metal

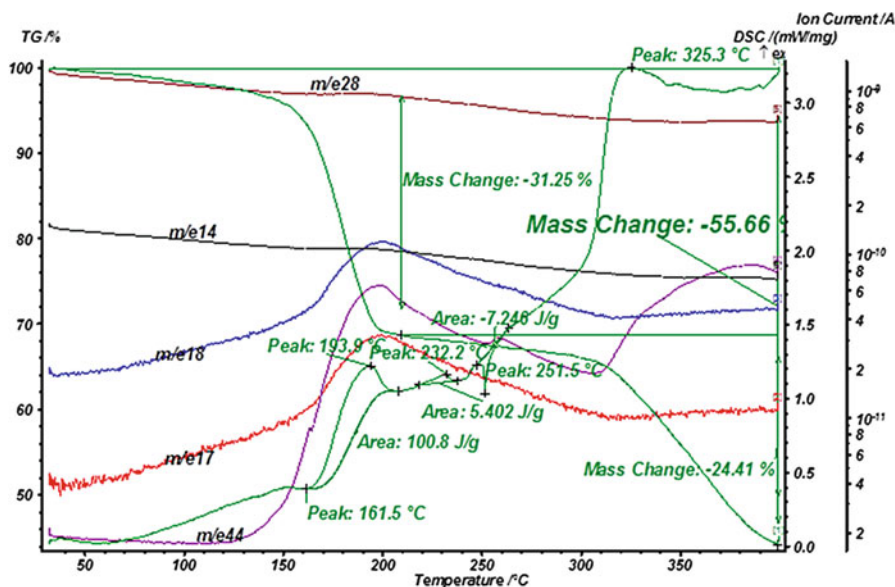
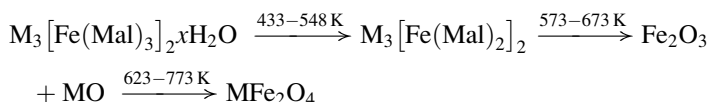


Fig. 6.15 TGA, DSC and mass-spectra of Co(II) acetylenedicarboxylate (heating rate 5 deg./min, argon)

oxide (MO). The formation of the ferrite  $MFe_2O_4$  can be described by the following reactions:



Synthesis of multimetallic ceramics via polymer-assisted transformations of unsaturated carboxylates will be analyzed in Sect. 6.6.

The major gaseous products of thermal decomposition of Co(II) acetylenedicarboxylate (CoADC) in the temperature range 413–1,223 K are  $CO_2$ ,  $C_2H_2$ ,  $C_6H_6$  which can be attributed to a decarboxylation process occurred already under polymerization of the monomer salt (Fig. 6.15) [252].

In the range of temperatures 413–453 K the rate of gas evolution at thermolysis of CoADC is satisfactorily approximated by the first-order equation  $W = d\eta/dt = k(1-\eta)$  where  $\eta = (\alpha_t - \alpha_0)/(\alpha_\infty - \alpha_0)$  is the degree of conversion;  $\alpha_t$ ,  $\alpha_0$ ,  $\alpha_\infty$  are the current, initial and final total numbers of the gaseous decomposition products evolved per mole of the starting CoADC,  $k = 1.6 \cdot 10^{15} \exp[-35,800/(RT)]$ ,  $s^{-1}$ . It was found that the total decarboxylation of metal-containing fragments of the CoADC completes over 673 K and the total gas evolution ends at  $>1,073$  K. In this case, a significant mass loss of the sample (up to 70 % at 1,223 K) was observed.

Thus, thermolysis of the salts of unsaturated carboxylic acids and the properties of the products attest to simultaneous “one-pot” occurrence of two processes: nanoparticle synthesis and their stabilization by the formed decarboxylated matrix of a controlled thickness.

### 6.4.2 Co-condensation of Metal and Monomer Vapours

It appears promising to combine thermolysis with low-temperature methods of nanoparticle insertion into polymerization-active monomers, for example, for preparing metal nanoparticles in poly(p-xylylene) films. This method implies co-condensation of vapours of the metal (and/or semiconductor) and the monomer, p-xylylene, which is prepared by pyrolysis of cyclic di-p-xylylene ([2, 2] paracyclophane), on a liquid nitrogen-cooled substrate [283–285]. The co-condensed product is subjected to low-temperature solid-state polymerization; this prevents the aggregation of metal particles at the stage of nanocomposite formation; the metal content in nanocomposite films reaches 50 vol.%. The block diagram for implementation of this method for nanocomposite preparation is shown in Fig. 6.16. The cyclophane molecules pass through the pyrolysis zone (~870 K) being converted to an active intermediate, which is deposited on a cooled substrate together with metal and/or semiconductor atoms. Then poly(p-xylylene) or its derivative is formed upon thermal polymerization, while nanoparticles or 1–20 nm clusters (depending on the chemical structure of the precursor and polymerization conditions) are formed in the polymer matrix. The particles having rather narrow size distribution are mainly located in amorphous areas of the polymer [286–290].

This method was used to stabilize the Ag, Zn, Cd, Pb [291], Cr [292], Mn [293] and other nanoparticles in poly(p-xylylene) films. The nanoparticle stabilization can be attained by both the formation of a metal cluster in the polymer matrix and the formation of *d*-metal  $\pi$ -complexes with the quinonoid form of the p-xylylene monomer. The complex formation between the polymer and *d*-metals brings about modification of the polymer properties, and the material becomes homogeneous rather than consisting of two phases. A similar reaction with p-xylylene can be proposed for other metals of the chromium, manganese and iron groups [293]. However, the targeted investigation of the thermal stability of these supramolecular assemblies is only at an early stage.

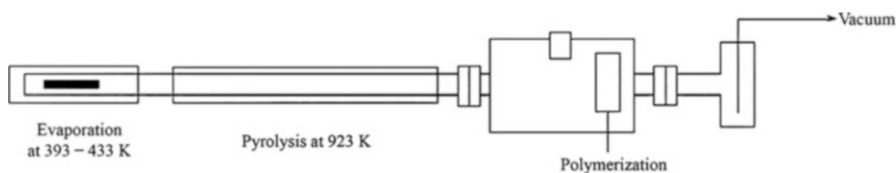


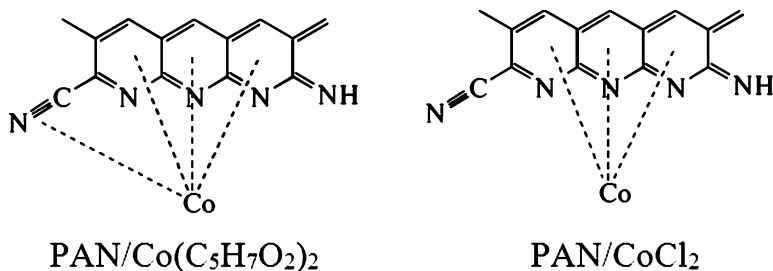
Fig. 6.16 Setup for the production of nanocomposite films [287]

### 6.4.3 The Methods of Formation of Metal – Carbon Nanocomposites

Metal - carbon nanocomposites can be prepared by pyrolysis of poly(vinyl chloride) (PVC), poly(vinyl alcohol) (PVA), PAN and cellulose hydrate fibres under carbonization conditions in the presence of metal-containing precursors. A typical procedure for the preparation of metal-carbon nanocomposites consists of several stages. The thorough mixing of the carbonaceous material with an aqueous solution of a metal salt (most often, nitrate) is followed by ultrasonic homogenization, filtration and drying in air; the process is completed by thermolysis at 870 K and pyrolysis at higher temperatures (in some cases, up to 2,070–2,270 K depending on the material composition) [294]. The chemical stability of these materials depends considerably on the nature of the initial polymer, conditions of thermolysis and the nature of additives (see, for example, Ref. [295, 296]).

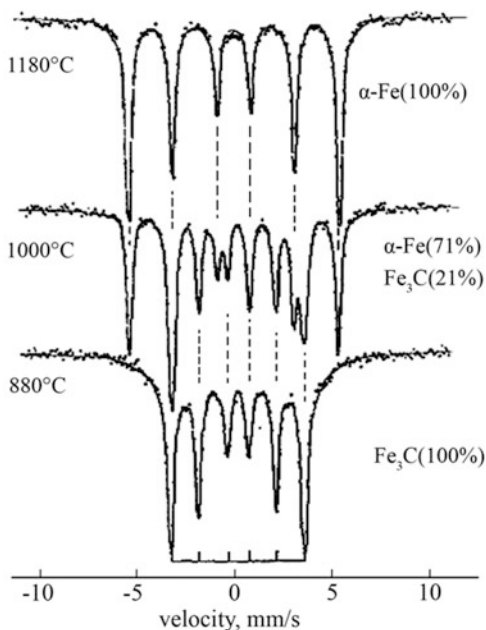
In recent years, vigorous studies of carbon (graphite) nanostructured membranes have been carried out, dealing with both optimization of the selective layer and the mechanisms of molecular transport in them. The preparation of composite membranes with enhanced mass exchange (selectivity, permeability) and service (mechanical strength and thermal and chemical stabilities) characteristics was reported [297, 298]. The membranes are formed upon carbonization of phenol formaldehyde resins on heating to 973 K on ceramic supports. Tubular or flat ceramics (with pore size of 40 nm to 5 mm) based on  $\alpha$ -Al<sub>2</sub>O<sub>3</sub>, TiO<sub>2</sub>, ZrO<sub>2</sub>, in particular those with additional metallic layers (Cr, Ti, Mo) are used as the supports. In the case of chromium additives, a graphite-resembling membrane structure is formed.

A thermally stable carbon nanocomposite with inclusion of metallic copper (nanoparticle size of 10–80 nm) is produced upon thermolysis of PAN and CuCl<sub>2</sub> in the presence of nitric acid [299]. This method is also suitable for preparing bimetallic nanocomposites. In particular, successive layering of the corresponding precursors (in 1:1 ratio) on PAN and thermolysis at 870 K results in the formation of the Au-Co/C metal-carbon nanocomposite [300]. Of some interest is the interaction of metal salts with a conjugated system of polymers. For example, Co(acac)<sub>2</sub> (acac is acetylacetonate) is predominantly coordinated with a conjugated system and slightly bounded with a terminal nitrile group of the conjugated chain. At the same time, CoCl<sub>2</sub> interacts with a conjugated system more strong playing the role of a dopant [301].

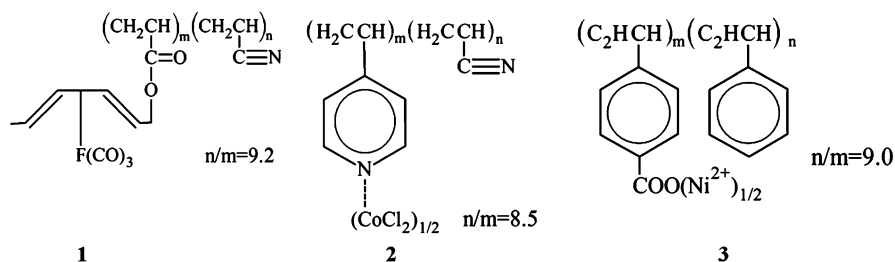




**Fig. 6.17** Mossbauer spectra of the products of thermolysis of hexadienyl-[tri(carbonyl)iron]acrylonitrile copolymer (molar ratio 9.2:1) obtained at different temperatures



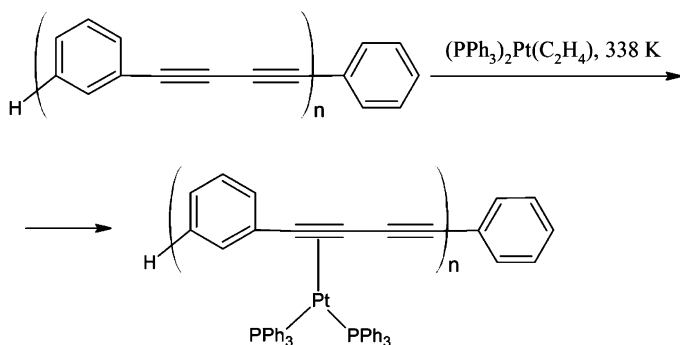
Comparatively on the early stages of the study of thermolysis attention was drawn the peculiarities of macromolecular complexes obtained by polymer-analogous transformations (see, for example, [302]). These macrocomplexes contain chemically bound metal compounds in the side chain. For example, the thermal treatment of hexadienyl-[tri(carbonyl)iron]acrylonitrile copolymer (the ratio of monomer units in polymer 9.2:1) (**1**) in air at 1373 K gives the uniform fine powder of nanocrystallites (80–120 nm) stabilized by a carbon matrix. Their phase composition (iron carbide or  $\alpha$ -Fe) depends on the temperature of thermolysis (Fig. 6.17).



Meanwhile, thermolysis of acrylonitrile and 4-vinylpyridine copolymers (molar ratio 8.5:1) with  $\text{CoCl}_2$  or nickel-bis(styrylcarboxylate) at 1,273 K for 24 h affords ultrasmall  $\beta$ -cubic Ni (52 nm) or  $\beta$ - and  $\alpha$ -Co (18 nm) nanoparticles.

The insertion of metal-containing precursors into glass–carbon matrices appears to be a promising approach. Thus thin films of platinum-doped glass carbon have

been obtained by immobilization (at 338 K) of mononuclear complexes of ethylenebis(triphenylphosphine)platinum(0) on the poly(phenylenediacyetylene) oligomer and subsequent pyrolysis (up to 873 K) (Scheme 6.7).



**Scheme 6.7** A scheme of synthesis of ethylenebis(triphenylphosphine)platinum(0)/poly(phenylenediacyetylene) oligomer

Platinum forms spherical particles with a mean diameter of 1.6 nm and a narrow size distribution [303]. It is significant that thermolysis of complexes not bound to the oligomer results in considerable enlargement (to 600 nm) of Pt particles.

Methods of this type are used rather often to obtain composite materials. For example, ceramics described as  $M_xSi_yC_z$  ( $M = \text{Fe}, \text{Co}$ ) was produced by high-temperature pyrolysis (1623 K) of diacetylene oligomers containing transition metal clusters [304]. Co-pyrolysis of ferrocene and thiophene (1,273–1,423 K) affords carbon nanotubes with Fe particles localized only inside the tube [305]; the metal clusters arising upon thermolysis of  $\text{Fe}(\text{CO})_5$  catalyze the formation of carbon nanoparticles [306]. Metal-carbon composites are also formed upon laser pyrolysis of a mixture of  $\text{Fe}(\text{CO})_5$  and  $\text{C}_2\text{H}_4$ , joint carbonization (1,173 K) of ferrocene and maleic anhydride or tetrachloroethylene [307, 308], controlled thermolysis of organocobalt compounds [309] and so on. Pyrolysis of poly(phenylcarbyne)  $(\text{PhC})_n$  mixed with  $\text{HAuCl}_4$  at 873 K under reducing atmosphere ( $\text{Ar} + 10\% \text{H}_2$ ) affords amorphous carbon nanocomposite films containing gold nanoparticles [310]. The key stage of these processes is the nanoparticle formation and mixing with the polymer. The presence of 1 % of metal carbonyl catalyzes the extensive destruction of mesogenic pitches (specific matrices with polycondensed aromatic structures, which can function as p-ligands stabilizing metal clusters) [311, 312]. An increase in the iron content to 5 % in ethylene polymerization and thermolysis at 520 K give rise to Fe-LDPE composites (LDPE is low-density polyethylene) with a considerable portion of structures resembling layered graphite compounds [313]. As the content of nanoparticles in the polymer increases, the degree of polymer amorphization increases, which is clearly demonstrated by Table 6.9.

**Table 6.9** X-Ray characteristics of Fe composite materials [313]

Polymer/iron components	RCS, nm	Content of the crystalline phase, %
Polycarbonate	8.0	65
+0.5 % Fe	9.0	60
+1.0 % Fe	9.0	60
+5.0 % Fe	10.0	50
+10 % Fe	10.0	40
Low-density polyethylene PELD	21.5	30
+1.0 % Fe	21.5	30
+5.0 % Fe	26.5	20
+10 % Fe	25.0	15

Note. RCS is the region of coherent scattering

A simple method for the preparation of ferromagnetic 1D nanofibres with a core–shell structure is based on the reaction of  $\text{Fe}(\text{CO})_5$  with elemental sulfur or tellurium at 970 K in a closed reactor under self-generated atmosphere (RAPET process) [314]. This produces  $\text{FeS}/\text{C}$  and  $\text{FeSe}/\text{C}$  nanoparticles several micrometres long with a diameter of 80–100 nm coated by a carbon shell. Presumably, under these conditions, the catalytic effect of iron is manifested, giving rise to oriented carbon nanotubes, which stabilize chalcogenide nanoparticles. The methods based on controlled carbonization of polymers followed by immobilization of metal nanoparticles (for example, to produce high-temperature filters and gas separating membranes [297]) are being currently successfully developed.

Worthy note a comparative simple method of preparing nano- and microparticles of  $\text{Zn}/\text{C}$ ,  $\text{Cd}/\text{C}$ ,  $\text{Al}/\text{C}$  stable in air by decomposition corresponding compounds of  $\text{Zn}(\text{C}_2\text{H}_5)_2$ ,  $\text{Cd}(\text{CH}_3)_2$ ,  $\text{Al}(\text{C}_2\text{H}_5)_3$  at 773–1,073 K in a self-generating atmosphere [315]. Morphology of these materials is a core-shell. Such approach appears to be perspective for obtaining the similar composites based on other metals (for example, from tetraalkyltin); thermolysis of molybdenum alkoxide affords  $\text{MoO}_2/\text{C}$  [316]. From such precursors under certain conditions (high temperature, reduction atmosphere  $\text{H}_2/\text{C}_x\text{H}_y$ ) it is possible to prepare metal carbides in one-stage route. These are  $\text{SiC}$  (at 1,073 K) as nanorods, nanotubes of  $\text{WC}$  (from  $\text{W}(\text{CO})_6$  at 1,173 K), micro- and nanospheres of  $\text{Mo}_2\text{C}$  (from  $\text{Mo}(\text{CO})_6$  at 1,073 K) or even composites of  $\text{SiC}/\text{C}$  [317]. Thermolysis of powder cellulose (PC) in the presence of hydrolyzing tetraethylsilane gave rise to the nanocomposite  $\text{PC}/\text{SiO}_2$  [318].

The above-mentioned thermolysis of solid/liquid mixtures in the case of metal/polytetrafluoroethylene (M/PTFE) offers a number of the advantages such as one-stage self-supporting process with a high rate and selectivity, no additional consuming of heating, the relatively simplicity of apparatus. Structure of carbon particles containing metals and Si nanofibers formed can be adjusted by a heating regime [58].

The aerosol thermolysis in solution is an easy method to produce ceramic electrolytes of oxide fuel elements (for example, on basis of yttrium (8–10 mol. %)- or gadolinium (10–20 mol.%) stabilized zirconia) [319].

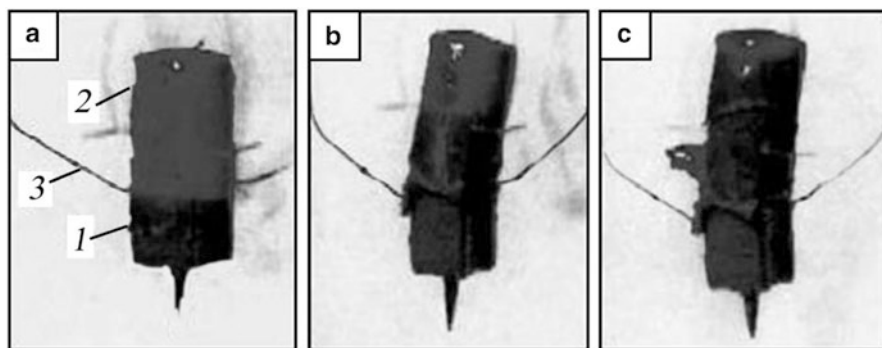
The above-analyzed data is only a brief illustration of the potential of thermolysis in the construction of metal/carbon nanocomposites.

## 6.5 Thermolysis of Metal-Containing Monomers in the Frontal Mode

A promising trend in the self-controlled synthesis of metallopolymer nanocomposites is frontal polymerization (FP) of solid metal-containing monomers [320–324]. Frontal polymerization is a layer-by-layer self-maintained chemical transformation where the localized zone of intense reaction (polymerization front) travels over the bulk of the polymerizing compound. As compared with the usual bulk polymerization, FP has a number of important advantages: lower energy expenditure, high rates and low reaction times, greater degrees of conversion and the possibility of the solid-state process.

The FP mode is implemented as follows. For a short period of time (~10 s), the system is subjected to thermal perturbation (ignition) by heating a small portion of the reacting volume with an electric heating device or a stationary external heat-transfer agent set to a specified temperature. Further polymerization is maintained by system inner resources proceeding in a narrow temperature range close to adiabatic heating of the reaction mixture. The appearance of a melt zone (1st order phase transition) and a colour change can be observed visually; the migration of the colour change boundary is used to monitor the reaction rate. The dynamic pattern of transformation of this polymerization wave is presented in Fig. 6.18.

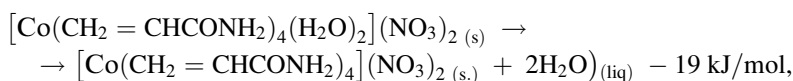
The FP phenomena in solid monomers are little described in the literature [325, 326]. The first and still the only one reported case of purely thermal initiation of FP in the condensed phase is decomposition of acrylamide (AAm) complexes of transition metal nitrates  $[M(\text{CH}_2=\text{CHCONH}_2)_4](\text{NO}_3)_n \cdot x\text{H}_2\text{O}$ , where  $M = \text{Cr(III)}, \text{Mn(II)}, \text{Fe(III)}, \text{Co(II)}, \text{Ni(II)}, \text{Cu(II)}, \text{Zn(II)}, \text{Pd(II)}$   $n = 2, 3; x = 0, 2$ . The isothermal gas evolution rate ( $W$ ) in a static non-isothermal reactor (SGA mode) as a function of the degree of conversion ( $\eta$ ) is approximated satisfactorily (up to  $\eta \leq 0,9$ ) by a first-order autocatalysis equation  $W = d\eta/dt = k(1 - \eta)(\eta + \xi_0)$  where the constants  $k = 4.2 \cdot 10^7 \exp[-24,000/(RT)] \text{ s}^{-1}$ ,  $\xi_0 = 1.9 \cdot 10^{-2}$ .



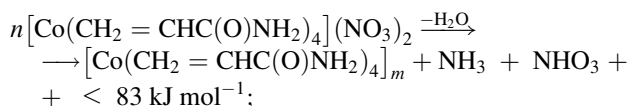
**Fig. 6.18** Dynamics of the polymerization front propagation for Co(II) acrylamide complex [322]. (a) after 20 s, (b) after 45 s, (c) after 55 s. (1) monomer, (2) polymer, (3) thermocouple

The transformation includes three stages:

1. dehydration of the monomer ( $333 \pm 358$  K)



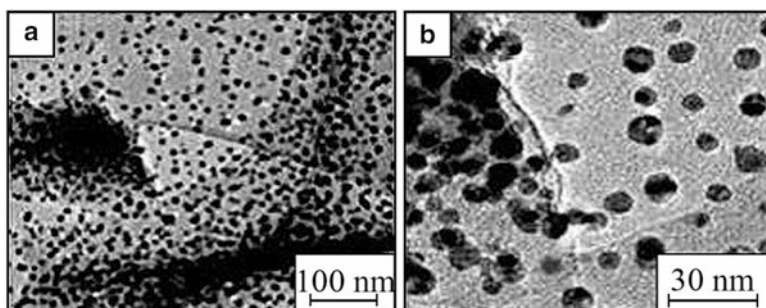
2. polymerization of the dehydrated complex (373–413 K) accompanied by the reaction of  $\text{H}_2\text{O}$  vapour with the  $\text{NO}_3^-$  anion and the  $\text{NH}_2$  group of the AAm ligand yielding  $\text{NH}_3$  and  $\text{HNO}_3$  vapours.



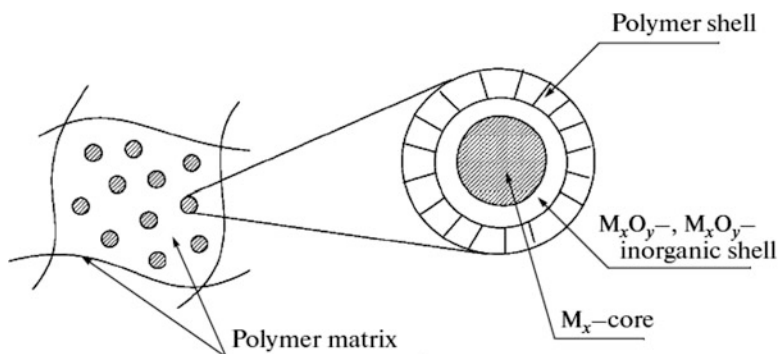
3. thermooxidative destruction of the resulting polymer (5,453 K) through interaction with  $\text{HNO}_3$  vapour and with reactive decomposition products thereof.

The last two stages are exothermic, which is a key cause of initiation of polymerization and development of the FP mode. The X-ray diffraction pattern of the product formed upon thermolysis of the cobalt complex at 673 K has peaks corresponding to the characteristic lines of the  $\beta$ -cobalt face-centred cubic lattice. The microstructure of the cobalt-containing product (Fig. 6.19) is composed of spherical nanoparticles with a mean size of 5–9 nm evenly distributed in the polymer matrix [327, 328].

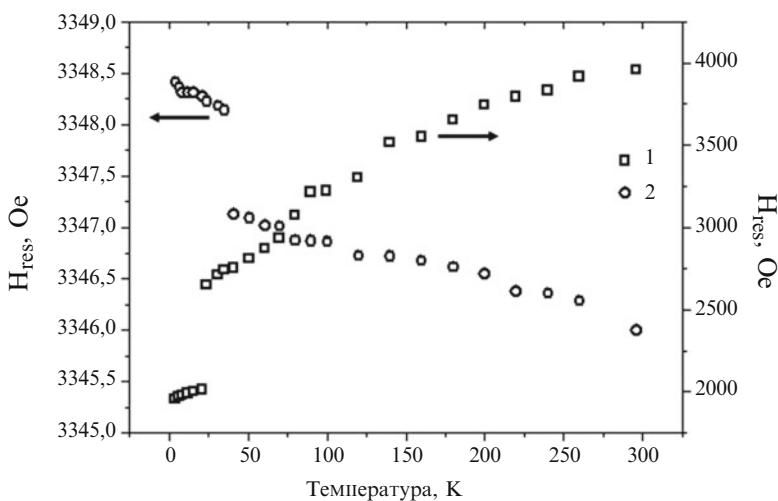
Polymer-assisted synthesis of metallopolymer nanocomposites allows one to control precisely the size of nanoparticles as well their composition and structure. Thus, unlike the products of thermolysis of metal carboxylates, nanocomposites based on acrylamide complexes contain highly dispersed metal phase or, at higher temperatures of thermolysis, metal carbide phase. Such difference may be caused by the character of chemical processes occurring at thermolysis of the starting



**Fig. 6.19** TEM images (on different scales) of spherical cobalt nanoparticles in the polymer matrix [327]



**Fig. 6.20** A schematic view of the structure of nanocomposites obtained by frontal polymerization [329]

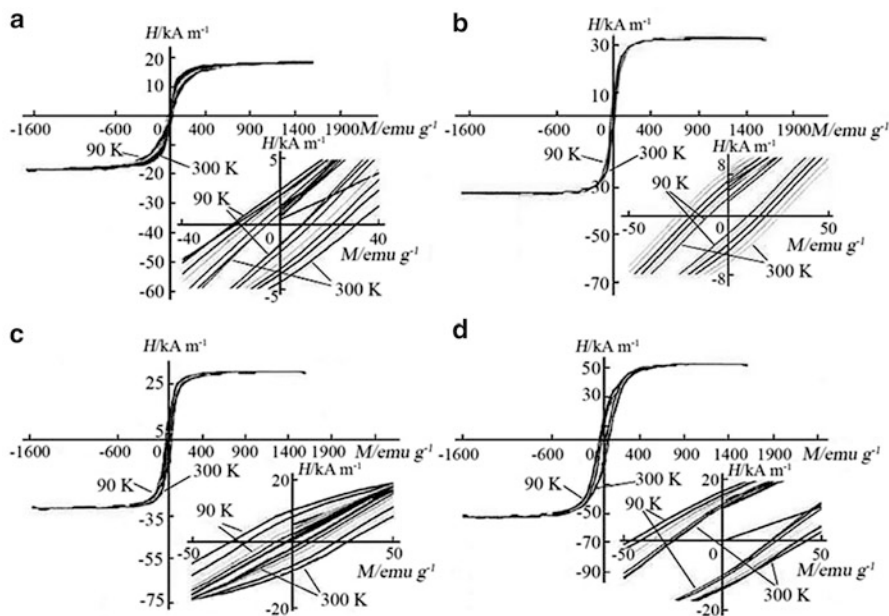


**Fig. 6.21** Temperature dependences of resonant field  $H_{\text{res}}$  for (1) cobalt nanoparticles and (2) polymer shell

monomers and intermediates formed [329, 330]. The nanoparticles in such systems have a specific structure of a core-shell which comprises metal-containing core and the surface layer from a polymer (Fig. 6.20).

The correlation of the temperature dependences for ferromagnetic resonance (FMR) line widths and the resonant field  $H_{\text{res}}$  values of the polymer shell and a cobalt nanoparticle, which it surrounds, is indicative of an interaction between them (Fig. 6.21) [327, 329].

Variation of the thermolysis conditions allows adjusting the sizes and composition of nanoparticles as well as properties of nanocomposites formed. For example, it is of interest to track the magnetic properties of the products of thermal transformations of CoAAm obtained at temperatures of 673, 773, 873, and 1,073 K. The



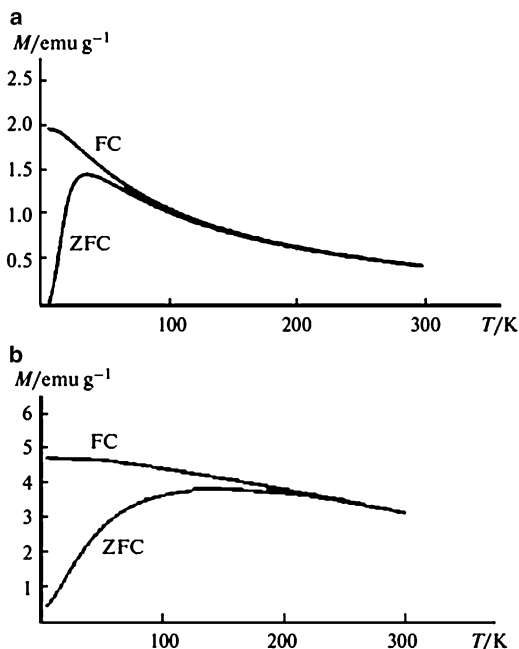
**Fig. 6.22** Magnetization vs. magnetic field in the temperature 90–300 K for the CoAAm thermolysis products formed at 673 (a), 773 (b), 873 (c), and 1,073 K (d)

hysteresis loops measured in the temperature range of 90–300 K attest to the ferromagnetic behavior of the thermolysis products (Fig. 6.22) [330]. However, the pattern of the curves, especially in the case of thermolysis product formed at 673 K, indicate the probable presence of a disordered interfacial layer with a skewed spin structure on the surface of magnetic particles. At the same time, the nanocomposites on the basis of Ni(II) complex obtained under the same conditions reveal superparamagnetic properties with the blocking temperature  $T_b \approx 40$  K (Fig. 6.23) [331]. An increase in the thermolysis temperature results in an increase in the particle size of Ni-containing nanocomposites from 6–7 nm (673 K) to 8–14 nm (773 K) and 12–17 nm (873 K). The sharp increase in  $H_c$  for the product obtained at 873 K indicates that at this temperature, the material switches from superparamagnet to ferromagnet.

Note that this approach for synthesis of nanocomposite materials immediately during FP of metal-containing monomers is an effective method for obtaining polymer-immobilized catalysts including hybrid types [332, 333].

In parallel with FP experiments, theoretical views on the modelling of this process have also been developed. Currently, various model FP mechanisms are discussed. The development of the polymerization front in a relatively porous monomer is ideologically similar to the formation of the combustion front [334]. It is not surprising that the theory of thermal mechanism of propagation of the polymerization front (as well as the combustion front) became predominant, although alternative (diffusion) mechanisms of front development [335] and a

**Fig. 6.23** Magnetization vs. temperature in the FC and ZFC modes in a  $8 \text{ kA m}^{-1}$  field ( $0.008 \text{ T}$ ) for the products of thermolysis of the acrylamide complex of Ni(II) nitrate formed at temperatures of  $673 \text{ (a)}$  and  $773 \text{ K (b)}$



mathematical model of FP [336] were proposed. The latter concentrates on the investigation of heat transfer complicated by phase transitions in the travelling narrow layer of the system (one-dimensional conjugate problem for two semispaces with a heat evolution source at the moving conjugate boundary). An analytical functional dependence of the temperature at the wave front on the velocity of the phase transition boundary that was in agreement with experimental data was obtained.

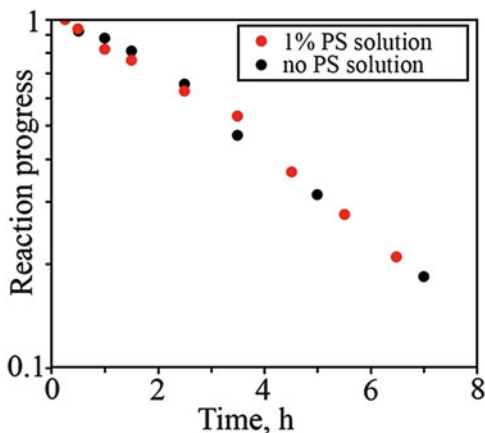
## 6.6 Thermolysis of Precursors in the Polymer Matrices

There are two choices for the insertion of metal-containing precursors into a polymer matrix: *ex situ* and *in situ* [246]. The *ex situ* (in a second moment) process comprises the addition of micro- or nanoparticles of the inorganic precursor to the finished polymer and mixing. According to the *in situ* method, the initial nanoparticles are generated directly in the polymer matrix upon decomposition of the proper macromolecular metal complex or the products of its transformation.

As a rule, a polymer matrix affects the rate of decomposition of a thermolizing compound. However, at the low concentrations of polymer when the viscosity of a system is not high the kinetics of the precursor decomposition in a polymer solution and in a free polymer solution is the same. Such behavior was observed at the

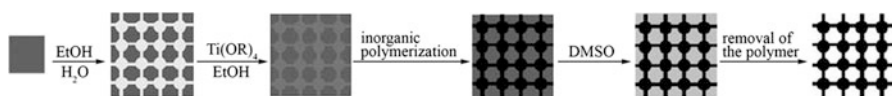


**Fig. 6.24** The kinetics of decomposition of  $\text{Cr}(\text{CO})_6$  in a toluene solution in the presence and without of polystyrene (PS) [337]



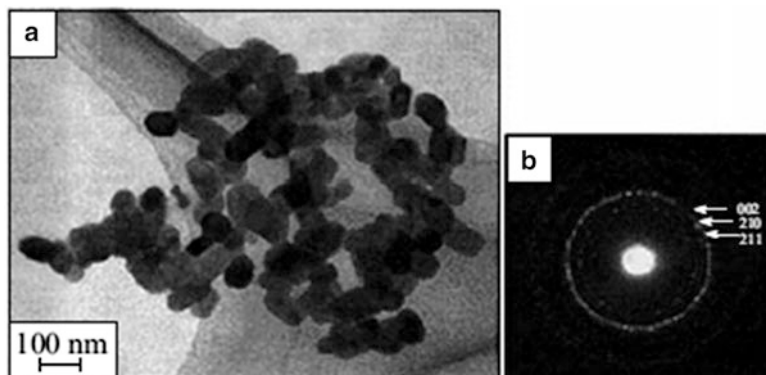
decomposition of  $\text{Cr}(\text{CO})_6$  at 363 K in a polystyrene solution in toluene [337] (Fig. 6.24).

Of interest from the practical standpoint is the use of thermolysis of polymers serving as templates for the manufacture of porous inorganic membranes [22–24]. The latter are usually produced by the sol-gel method [10]. After burning-out of the organic part, 1.5–10 nm channels are formed in the  $\text{SiO}_2$ ,  $\text{TiO}_2$ ,  $\text{SnO}_2$ ,  $\text{ZrO}_2$ ,  $\text{Nb}_2\text{O}_5$ , etc. membranes. These membranes can be used in nanocatalysis or solar cells or as nano-sized reactors [338]. The use of natural or synthetic polymers as the template agents has been reported, in particular, agarose gel (1.5–2.0 mass %) [339], partially cross-linked polyacrylamide gel prepared by a reported procedure [340] or gelatin with cell diameter of 10–100 nm [341]. After the formation of inorganic Ti network, the polymer is burned out at 773–873 K; at the same stage, the membrane is sintered to form a porous monolithic structure. The  $\text{TiO}_2$  (rutile) phase with a mean particle size of 23.6 nm is formed, whereas high-temperature (1,223 K) annealing is accompanied by particle enlargement to reach a size of 50.4 nm. The general pattern of the process is shown in Scheme 6.8.



**Scheme 6.8** Pattern of formation of an inorganic Ti network from a polymer gel [339]

Yet another example of this approach is the formation of nanocrystals of hydroxyapatite  $\text{Ca}_{10}(\text{PO}_4)_6(\text{OH})_2$ , the main bone and tooth structural material (see Chap. 7). Aqueous solutions of  $\text{Ca}(\text{OH})_2$  and  $\text{Ca}(\text{H}_2\text{PO}_4)_2$  are mixed in the presence of a sonicated colloid solution of bovine serum albumin ( $M_w = 66$  kDa) [342]. This gives rise to amorphous nanoparticles with a fibrous network structure with a broad size distribution. Apparently, sonication turns the protein globular structure into a linear structure, and the arising  $\text{HO}^\cdot$  radicals cross-link the chain through oxidation



**Fig. 6.25** Electron microscopic image of hydroxyapatite nanocrystals with bull serum albumin (a) and electron diffraction pattern (b) [342]

of the SH groups, while the negatively charged  $\text{COO}^-$  groups stabilize the calcium phosphate particles. The calcination of this precursor results in destruction of the protein to give nanoparticles the size of which depends on the albumin concentration. At a concentration of 5 g/L, nearly spherical  $25 \pm 100$  nm particles and short rod-like crystals with size ranging from  $40 \text{ nm} \times 75 \text{ nm}$  to  $70 \text{ nm} \times 150 \text{ nm}$  are formed (Fig. 6.25).

During pyrolysis, polymers can also act as reactants. For example, the formation of metal carbides with the polymer matrix serving as the source of carbon has been repeatedly noted. In addition,  $\text{H}_2$ , CO and other gaseous products of polymer thermolysis serve as reducing agents for reaction mixture components.

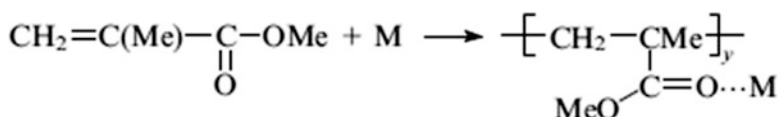
### 6.6.1 *Effect of Metal-Containing Components on the Destruction of the Polymer Matrix*

The thermal destruction of polymers is associated with the development of the chain process that is initiated by the formation of carbon-centered radicals ( $\text{R}\cdot$ ) upon chemical bond cleavage in the macromolecule [48, 49, 343, 344]. The products of thermodestruction include low-molecular-mass volatile compounds of complex composition, in particular monomers, and a non-volatile residue, which turns into a carbonized (coke-like) material at high temperatures. During the thermooxidative destruction of polymers, hydroperoxides are formed as the primary products; they decompose to give  $\text{RO}_2\cdot$  radicals, which induce autocatalytic destruction of the polymer. One of the ways of stabilization of the polymer matrix that decomposes by a radical mechanism is to provide kinetic chain termination upon the reaction of an inhibitor with the  $\text{R}\cdot$  or  $\text{RO}_2\cdot$  radicals, which are thus converted to low-activity or inert products.

**Table 6.10** Kinetic parameter (pre-exponential factor in the Arrhenius equation and activation energy) and decomposition temperature of metal-containing poly(methyl methacrylates) (Mol. weight  $(2.7 \div 5.0) \cdot 10^5$ ) [345]

Metal	$A/s^{-1}$	$E_a/kJ\ mol^{-1}$	$T_d/K$
Au	$2.6 \cdot 10^4$	99.3	573
Bi	$2.3 \cdot 10^2$	78.9	598
In	$1.4 \cdot 10^2$	74.2	548
Cu	$2.4 \cdot 10^2$	70.6	513
Sb	25.0	63.9	548
Pd	15.0	61.5	523
Sn	14.0	61.0	523
Ga	4.3	51.5	473

Polymers can be stabilized by introducing acceptor agents. They either remove agents that initiate chains (oxygen, active impurities, etc.) from the polymer or deactivate these agents. An effective way of influencing the thermal and thermooxidative destruction is to introduce into the polymer matrix highly dispersed metal-containing precursors capable of both inhibiting and catalyzing the polymer decomposition. For example, introduction of pre-dispersed metal particles (up to 2 % of Au, Cu, Pd, Ga, In, Sn, Sb, Bi) into PMMA (molecular mass of 270–500 kDa) during polymerization has a pronounced effect on the kinetic parameters of destruction [345]. Probably, the metallopolymer is formed as shown below



Pyrolysis of the metallopolymer is a zero-order reaction. The best results (as regards the activation energy and the temperature of the onset of decomposition) were found for the Au–PMMA system, which is, like metallic gold, is fairly stable against oxidation. In the case of Ga (readily oxidizable metal), the lowest thermal stability parameters were found (Table 6.10).

The introduction of a small amount (0.05–1.00 %) of iron atoms into LDPE provides a considerable increase in the thermal stability of the composite as compared with the pure polymer, and the decomposition temperature of the nano- $\alpha$ - $Fe_2O_3$ –PS system obtained from an aqueous colloid solution of FeOOH upon stirring for many hours followed by evaporation is  $\sim 97^\circ$  higher than that for pure PS [346–348].

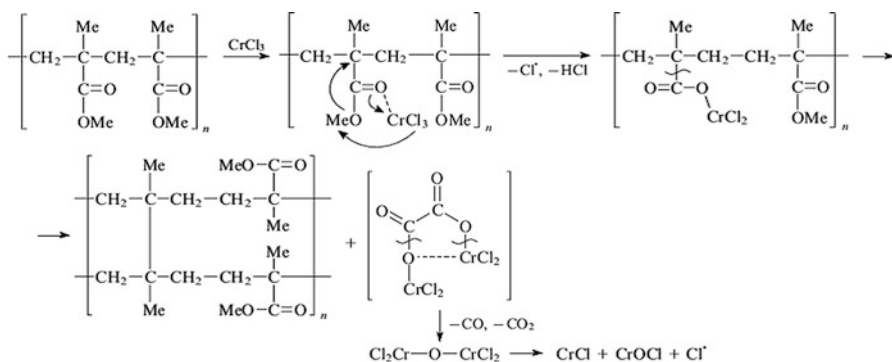
### 6.6.2 Metal Salt – Polymer Matrix System

Thermolysis of the polymer composites with metal halides  $MX_n$  ( $M = Cr, Mn, Zn$ ;  $X = Cl, Br$ ) inserted in the matrix, which is characterized by a complex pattern of transformations, has been reported [349]. Apart from the task of preparing highly

dispersed metal-containing products, investigations of this process are of interest for the protection of polymeric materials from the effect of flame and for the search for environmentally safe fire retardants (as alternative to toxic additives [350–352]).

Decomposition of the polymer matrix in the  $\text{MX}_n$  – PMMA composites ( $\text{MX}_n = \text{CrCl}_3, \text{MnCl}_2, \text{ZnBr}_2$ ) occurs, first of all, as destruction. This takes place at temperatures below the destruction temperature of pure PMMA (~647–690 K): at ~430 (for  $\text{ZnBr}_2$ ) [353], ~490 (for  $\text{MnCl}_2$ ) [353], ~520 K (for  $\text{CrCl}_3$ ) [354]. The replacement of  $\text{ZnBr}_2$  by  $\text{ZnCl}_2$  increases the destruction temperature to a value close to that of pure PMMA [354].

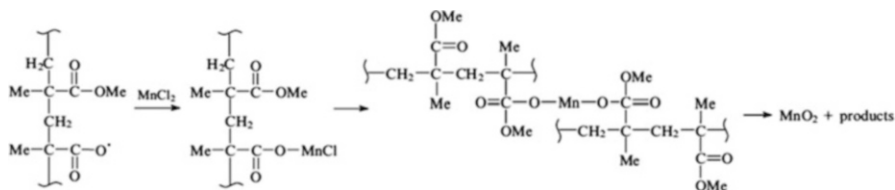
Heating of chromium(III) chloride as a composite with PMMA to 520–970 K leads to a ~62 % weight loss of the composite [355] caused by the removal of the volatile monomer, carbon oxides, HCl, traces of methane and unidentified low-molecular-mass organic products. Solid anhydride and chromium oxides, together with unsaturated oligomers remain in the condensed phase. Presumably [353–357] destruction of the  $\text{CrCl}_3$  – PMMA system follows a radical mechanism the main stages of which (Scheme 6.9) include pre-coordination of chromium to the carbonyl group of PMMA followed by elimination of the chlorine atom; reaction of the chlorine atom with a PMMA hydrogen atom; migration of the ester methyl group to the PMMA backbone to give a chromium carboxylate salt, which decomposes to the anhydride; polymer stabilization by chromium carboxylate or by cross-linking of polymer radicals generated in the previous stages.



**Scheme 6.9** Mechanism of the thermal destruction in the system of PMMA–CrCl<sub>3</sub>

The mechanism of thermal destruction of the  $\text{MnCl}_2$  – PMMA composite at 370–870 K has been discussed [357]. It is assumed that the process is initiated by the methoxyl and methyl radicals arising upon cleavage of ester bonds in PMMA; however, manganese chloride accelerates the initial depolymerization. Manganese oxide, which is one of the final solid products of thermolysis, results from the reaction of the carboxyl radical with  $\text{MnCl}_2$  and the subsequent conversion to the manganese intermediate connected to the PMMA chain (Scheme 6.10).

Such processes are intensively investigated.



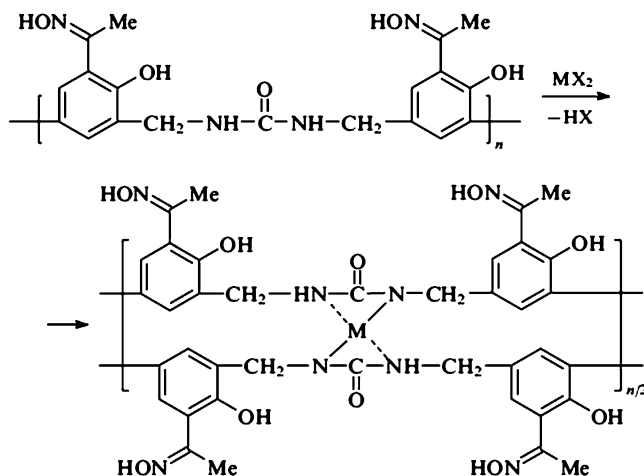
**Scheme 6.10** Mechanism of the thermal destruction in the system of PMMA–MnCl<sub>2</sub>

### 6.6.3 Thermolysis of Complex Compounds in Polymer Matrices

In recent years, considerable attention has been attracted by composites based on metal ions coordinated to the polydentate organic ligands of the framework (polymeric or inorganic) owing to their broad range of their practical applications. These materials are used as sensors [358, 359], in non-linear optics [360], for separation and molecular recognition [361], for gas storage [362, 363], in catalysis [364], in information and energy storage sources, in biomedicine, etc.

There are two basically different ways of performing thermolysis of coordination compounds in a polymer matrix, namely, the introduction of metal complexes into a traditional matrix and direct formation of a macromolecular metal complex, usually having a chelate structure.

The polymer matrices containing groups able to form complexes (amino, amido, hydroxyamino and hydroxyl groups) react with  $\text{MX}_n$  [365] ( $\text{M} = \text{Cu(II)}, \text{Ni(II)}, \text{Co(II)}, \text{Zn(II)}, \text{Mn(II)}, \text{VO(II)}, \text{UO(II)}, \text{Zr(IV)}, \text{Ti(IV)}$ ) to give the corresponding adducts (Scheme 6.11). The thermal stability of metal complexes decreases in the sequence of metals  $\text{Ni} > \text{Zn} > \text{Mn} > \text{Co} > \text{Cu} > \text{Ti} > \text{UO} > \text{Zr} > \text{VO}$ , and polymers



**Scheme 6.11** A scheme of the formation of polymer metal chelates

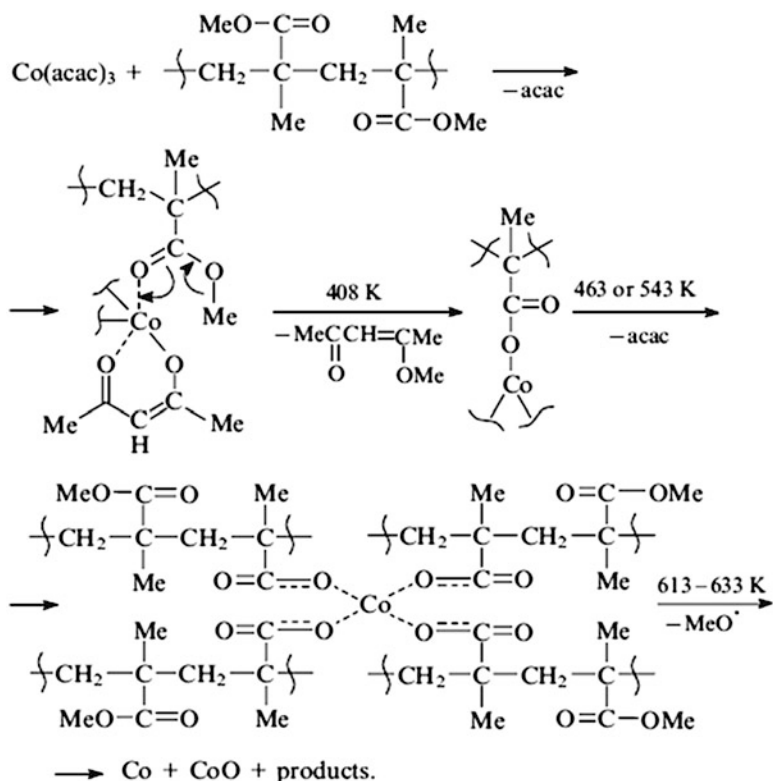
that do not coordinate metals are most stable. The same sequence holds for copolymers of diaminoalkanes with the Schiff base, 5,50-methylenebis(3-bromosalicylaldehyde) [366, 367].

The thermal transformation pathways of the macromolecular metal chelates have been analyzed [368–377]. Thermolysis of copper macrochelates with polyacrylamidoxime fibres comprises three temperature-separated stages: 398–603 K (weight loss 14.3 %), 603–715 K (10.8 %) and 715–965 K (10.8 %) [378]. The major weight loss is involved in the transformation of the starting polymer. The thermal behaviour (in the temperature range of 473–1,073 K) of the macromolecular Cu(II) and Co(II) chelates with the copolymer of N-phenylmaleimide with acrylic acid was studied; the ratio of comonomers was varied and various methods were used for metal binding [379]. An increase in the number of N-phenylmaleimide units in the copolymer chain increases in some cases the thermal stability and the glass transition temperature ( $T_g$ ) of the macrocomplex; however, this change is not so pronounced as might have been expected (in the optimal cases, from 623 to 646 K, and for some copolymer compositions, even a decrease to 488 K is observed).

The high-temperature pyrolytic carbonization processes of the precursors containing bulky organic ligands proceed in an unusual way. Under inert atmosphere, the ruthenium complexes  $[\text{RuL}_3]\text{X}_2$  (L is bipyridine (bipy), phenanthroline; X=OH, Cl) were converted to a ruthenium – carbon composite with a ruthenium content of 20–32 mass % [380]. This is a result of multistage destruction of the organic ligand. On heating to 873 K, vigorous decomposition of the complex with evolution of its fragments, pyridinium and bipyridinium ions, is completed. This is followed by the destruction of the condensed material thus formed to evolve light hydrocarbon species. The Ru-containing composites obtained at 873–973 K have a relatively great specific surface area (424–477  $\text{m}^2/\text{g}$ ), while ruthenium clusters are almost amorphous to X-rays. The highly dispersed ( $d \approx 1.5\text{--}2.0$  nm) ruthenium particles in the Ru/C composite are similar in size and are shaped like planar hexagons, which are associated. During pyrolysis, enveloping layers of turbostratic graphite-like carbon are formed around the hexagons as a result of organic ligand carbonization. The parallel-oriented turbostratic carbon layers with an interplanar spacing of  $\sim 0.34$  nm are tightly pressed to ruthenium particles, thus preventing their sintering under the drastic conditions of pyrolysis (973 K). Thus, obtained composite can be represented as a set of spheres (coils) each having a ruthenium nanoparticle (core) located at its centre and turbostratic carbon layers (shell) lining the outer surface.

Metal acetylacetonate – polymer matrix systems have found wide use. During thermolysis,  $\text{M}(\text{acac})_n$  can play a dual role. On the one hand, decomposition of  $\text{M}(\text{acac})_n$  produces metal-containing nanoprecursors, and on the other hand, the complex initiates depolymerization and destruction of the polymer matrix. In this respect, detailed thermovolumetric and thermogravimetric studies of the thermal decomposition of the  $\text{Co}(\text{acac})_3$  – PMMA and  $\text{Mn}(\text{acac})_3$  – PMMA systems over a broad range of  $\text{M}(\text{acac})_3$  : PMMA ratios (from 1:10 to 1:400) are illustrative [349,

381, 382] Decomposition of the Co composite includes four stages corresponding to maximum temperatures of 405, 460, 540 and 610–630 K (Scheme 6.12).



**Scheme 6.12** Mechanism of the thermal destruction in the system of PMMA–Co(AcAc)<sub>3</sub>

The first stage is associated with gradual reduction of Co(acac)<sub>3</sub> to give acetylacetone and Co(acac)<sub>2</sub>, which is coordinated by the unsaturated terminal groups of PMMA. Decomposition of this complex is accompanied by evolution of the monomer, which is the main decomposition product. The second and third stages continue accumulation of the monomer through the reduction of Co(III) to Co(II) and subsequent depolymerization of the remaining terminal groups. Simultaneously, Co(acac)<sub>2</sub> can be coordinated by ester groups, thus accelerating their destruction to give methoxy radicals (MeO<sup>·</sup>). The latter, in their turn, attack the ester groups thus converting them to anhydride fragments. The fourth stage is accompanied by the most pronounced gas evolution giving mainly non-condensed gases.

A similar situation is observed upon thermal decomposition of Mn(acac)<sub>3</sub> in PMMA: decomposition starts at 395 K (i.e., at a lower temperature than for pure PMMA); however, the major process takes place at higher temperatures. This is

**Table 6.11** Thermal stability of PMMA and its complexes with  $Mn(acac)_3$  [382]

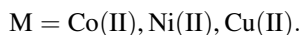
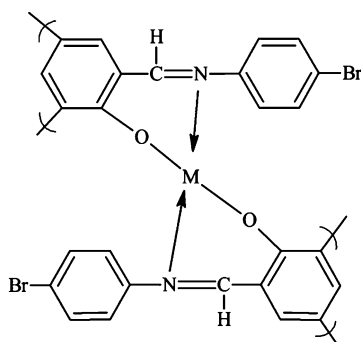
Polymer	The number of monomer units per $Mn(acac)_3$ molecule	$T_d$ / K	$T_{max}$ / K
High-molecular-mass PMMA	See <sup>a</sup>	483	623
	50	403	638
	10	398	673
Low-molecular-mass PMMA	See <sup>a</sup>	493	633
	50	403	638
	10	403	673

<sup>a</sup>Neat polymer

confirmed by comparison of the temperatures of the onset of decomposition ( $T_d$ ) and the major decomposition ( $T_{max}$ ) presented in Table 6.11.

For the formation of rhodium nanocrystals with different shapes (multipods, cubes, horns, cuboctahedra), thermolysis of  $Rh(acac)_3$  in the presence of polyols as reducing agents is of interest [383]. Yet another convenient method for the production of these polymer-protected monodisperse rhodium nanoparticles (size  $5 \pm 15$  nm) is one-stage reduction of the rhodium complex  $Rh(acac)_3$  in the presence of butane-1,4-diol and polyvinylpyrrolidone ( $M_w = 55$  kDa) at temperatures of  $240 \pm 300$  K [384]. This gives triangular, pentagonal and hexagonal particles, which can form Langmuir–Blodgett films on the silicon surface.

The polymer metal chelates of oligo-2-[(4-bromophenylimino)methyl]phenol (OBPIMP) with Co(II), Ni(II) and Cu(II) acetates [33] have been already mentioned when we discussed the kinetic peculiarities of thermolysis:



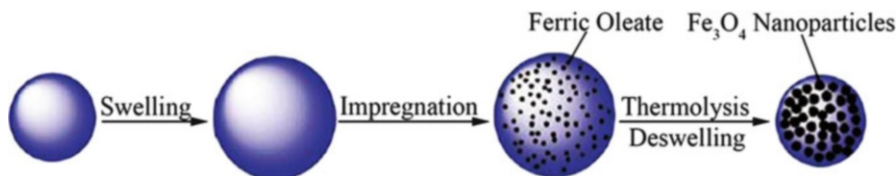
Thermodynamical and kinetic parameters of decomposition of these polymer metal chelates calculated with the Coats-Redfern equation are given in Table 6.12.



**Table 6.12** Thermodynamical and kinetic parameters of thermal decomposition of the OBPIMP-chelates

Compound	Stage <sup>a</sup>	The reaction order, <i>n</i>	<i>E<sub>a</sub></i> , kJ/mol	ln A, s <sup>-1</sup>	Δ <i>S</i> <sup>*</sup> , kJ/mol	Δ <i>H</i> <sup>*</sup> , kJ/mol	Δ <i>G</i> <sup>*</sup> , kJ/mol
BPIMP	I (458–602 K)	0.5	76.25	13.95	–134.6	71.28	151.6
OBPIMP	I (453–581 K)	0.9	96.31	19.53	–87.52	91.76	139.6
OBPIMP-Co	I (475–590 K)	0.2	39.84	5.81	–201.6	35.31	145.0
	II (626–997 K)	0.9	31.34	0.693	–248.4	23.75	250.3
OBPIMP-Cu	I (502–626 K)	0.5	100.2	18.16	–99.75	95.29	155.2
	II (626–997 K)	1.0	65.36	6.33	–201.3	57.96	235.5
OBPIMP-Ni	I (530–656 K)	0.8	62.04	6.48	–197.3	56.76	181.9
	II (656–899 K)	0.4	48.81	6.82	–195.7	42.65	187.5

<sup>a</sup>I and II are the temperature ranges of the starting and 50 % mass loss

**Fig. 6.26** Schematic diagram of the preparation of monodisperse magnetic polymer microspheres by swelling and thermolysis technique

Worthy of note is a recently elaborated method for the preparation of nanocomposites microspheres by combining swelling and thermolysis technique. The monodisperse polystyrene microspheres were first prepared by dispersion polymerization and swelled in chloroform. Then, ferric oleate was dispersed in chloroform as a precursor and impregnated into the swollen polymer microspheres. Subsequently, the iron oxide nanoparticles were formed within the polymer matrix by thermal decomposition of ferric oleate (at 583 K, for 0.5 h, nitrogen atmosphere) (Fig. 6.26) [385].

Iron oxide nanoparticles localized within polymer microspheres reveal unique superparamagnetic properties and can be used in various fields of biotechnology including purification of proteins, viruses, nucleic acids, in biosensors and enzyme immobilization, etc. [386–391] (see Chap. 7).

It should be noted that the polymer matrix, in turn, may influence thermal transformations of metal complexes. However, information concerning this matter is limited. Some peculiarities of thermal decomposition of  $(\text{NH}_4)_6\text{Mo}_7\text{O}_{24}\cdot 4\text{H}_2\text{O}$ ,

copper nitrate trihydrate, and polyoxymetallates in thin films (from 50 to 600  $\mu\text{m}$ ) of PVA can be assigned [392].

### 6.6.4 Thermolysis of Organometallic Compound – Polymer Matrix Systems

As noted above, thermal decomposition of single organometallic compounds affords metallic nanoparticles or (in oxidizing atmosphere) metal oxides. The products of thermolysis tend to be highly reactive especially during nucleation and at an early stage of growth of nanoclusters in the condensed phase. The most convenient method for the preparation of diverse metal oxide nanocrystals with well characterized size, morphology, phase composition and structure is the simple and economical non-hydrolytic bottom up process. This process includes thermolysis of alkoxometallates and their derivatives in high-boiling organic solvents (see, for example, Ref. [393]). This especially concerns the preparation of manganese oxides, which are important products for catalysis, electronics and production of magnetic materials.

Among rather simple methods, note the synthesis of vanadium oxide nanoparticles stabilized by carbon shells [394]. Thermolysis of oxovanadium triethoxide  $\text{VO}(\text{OEt})_3$  in a closed reactor and in self-generated atmosphere at 973 K affords carbon-coated nanoparticles of rhombohedral  $\text{V}_2\text{O}_3$  with a core-shell structure and a diameter of  $\sim 55$  nm. The subsequent thermal treatment of the product in air at 723 K for 2 h furnishes orthorhombic  $\text{V}_2\text{O}_5$  (<sup>5</sup> [395]), (particle size  $\sim 250$  nm), which is also coated. These materials have photoluminescent properties [396].

Spherical ruthenium nanoparticles are formed upon thermolysis in air of the organometallic copolymer  $\{[\text{NP}(\text{O}_2\text{C}_{12}\text{H}_8)]_x[\text{NP}(\text{OC}_5\text{H}_4\text{N})\text{CpRu}(\text{PPh}_2)_2]_{1-x}\}_n$  (Cp is cyclopentadienyl) [397].

On exposure of the cluster  $[\text{Ru}_6\text{C}(\text{CO})_{15}\text{Ph}_2\text{PC}_2\text{PPh}_2]_n$  ( $n \approx 1,000$ ) to accelerated electrons, a nanochain composed of ruthenium atoms was obtained [75]. Pyrolysis of the cluster  $\text{Os}_2(\mu\text{-I})_2(\text{CO})_6$  gives rise to rod-shaped metal particles [398]. The organometallic polymer  $[\text{Ru}(\text{CO})_4]_\infty$  with a planar structure and zigzag-like conformation is a potential precursor for the synthesis of various nanomaterials, in particular, for the formation of chain nanoparticles, upon removal of the carbonyl ligand [399]. Thermolysis of  $[\text{Ru}(\text{CO})_4]_\infty$  on a  $\text{SiO}_2$  surface at 443 K affords  $\sim 2$  mm-long and  $\sim 30$  nm-thick nanofibres. Upon thermal

---

<sup>5</sup> In the cited work it is not paid attention to the fact that components of the reactor wall may reveal some catalytic properties. As a rule, such reactors are lined by Teflon. Among the known vanadium oxides ( $\text{V}_2\text{O}_5$ ,  $\text{V}_2\text{O}_3$ ,  $\text{V}_3\text{O}_5$ ,  $\text{VO}_2$  and  $\text{VO}$ ), most stable is the oxide with the higher oxidation state of vanadium ( $\text{V}_2\text{O}_5$ ), an oxidant with amphoteric properties. A comparative simple procedure was elaborated for obtaining  $\text{VO}_2$  by thermolysis at  $\leq 683$  K of the precursor arising from the interaction of  $\text{VOCl}_2$  with  $\text{NH}_4\text{HCO}_3$  in solution [395].

decomposition of the cluster  $\text{Ru}_3(\text{CO})_{12}$  in the nanopores of  $\text{Al}_2\text{O}_3$  membranes (100 nm size), nanofibres of diameter 10 nm are formed. When the temperature increases to 553 K, the structure of such items becomes irregular as like to the  $\text{Os}_3(\text{CO})_{10}(\mu\text{-H})(\mu\text{-OH})$  thermolysis product.

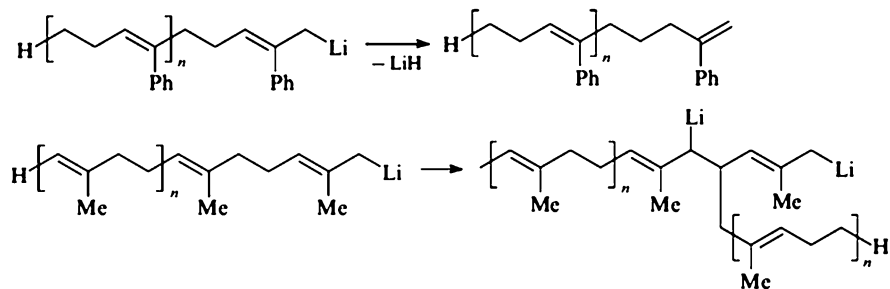
Of particular interest is the formation of refractory metal carbides upon the pyrolysis of various organometallic precursors. For example, the melting point of hafnium carbide is  $4,201 \pm 20$  K and that of tantalum carbide is 4,256 K. Metal carbides were formed [400] upon the pyrolytic (523–623 K) elimination of the cyclopentadienyl rings from the complexes  $\text{Cp}_2\text{HfR}_2$ , where  $\text{R} = \text{Cl}, \text{NET}_2, \text{Bu}_n$  (Ref. [401]), and upon high-vacuum thermal decomposition (523 K,  $\sim 1$  Pa) of tetra (neopentyl)titanium(IV)  $[\text{Ti}(\text{neo-C}_5\text{H}_{11})_4]$  vapour [402]. When decomposition is performed at 873 and 1273 K, the particle size of the formed nanocomposites is in the range of 10–50 nm [403]. They have a characteristic structure comprising a dense core (metal carbide and oxide) surrounded by less dense polymeric shell.

For preparing thin-layer high-temperature coatings by centrifugation on polished silicon substrates, ceramic matrix composite films containing highly dispersed tantalum carbide were formed [404]. A solution of  $\text{Ta}(\text{OC}_5\text{H}_{11-n})_5$  with phenol formaldehyde resin additive was used in an amount specified for providing a definite C:Ta ratio. The process was carried out at moderate temperatures (1,073–1,473 K) and reduced pressure ( $1 \cdot 10^{-3}$ – $1 \cdot 10^{-4}$  atm). The films thus obtained represented tantalum carbide and consisted of spherical particles with a mean diameter of  $\sim 50$  nm [405].

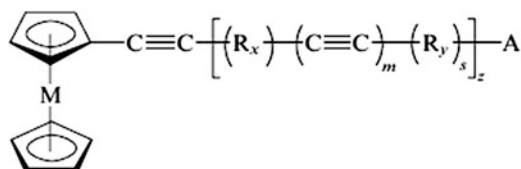
Similarly, other thermally unstable precursors – metal  $\pi$ -allyl complexes, carbonyls, nitrosyls, etc. decompose in the presence of polymers. Thus bis(arene) chromium chemically bonded to PAA is thermolyzed at 433 K to the oxidized species  $[\text{Ar}_2\text{Cr}]^+\text{OH}$ , while the polymer remains unchanged. Above 573 K evolution of cyano compounds and ammonium takes place [406] and a magnetic material is formed, while at 1,273 K product graphitization occurs to give a typical diamagnetic product.

Thermolysis of true organometallic polymers has been scarcely studied. Among the few examples, note decomposition of poly(styryl)lithium in the temperature range of 343–388 K and poly(isopropenyl)lithium (353–393 K) obtained by living anionic polymerization (initiated by  $\text{LiBu}_n$ ) [407]. The polymers have a molecular mass of 15–30 kDa and a low polydispersity index ( $M_w/M_n \approx 1.03$ ). A variety of reactions take place during thermolysis of poly(styryl)lithium, for example, elimination of  $\text{LiH}$  to give branched-chain intermediates (Scheme 6.13); these reactions follow first-order kinetics.

Apparently, a similar picture is observed as carbon-coated metallic iron particles are formed from iron phthalocyanine [404]. Nanoparticles of these metals were also obtained by vacuum thermolysis of other precursors: mesityl derivatives of copper  $\text{Cu}(\text{C}_6\text{H}_2\text{Me}_3\text{-2,4,6})_5$ , silver  $\text{Ag}(\text{C}_6\text{H}_2\text{Me}_3\text{-2,4,6})_4$  and gold  $\text{Au}(\text{C}_6\text{H}_2\text{Me}_3\text{-2,4,6})_5$  [408], metallocene – aromatic – acetylene complexes [409]



**Scheme 6.13** Thermal transformations of polystyryllithium



M = Fe, Sn, Co, Pd, Ni;  $R_x$  and  $R_y$  are phenylene or substituted phenylene; A = H, Ph; C:C, FcC≡C (Fc is ferrocenyl);  $m, s, z > 0$ .

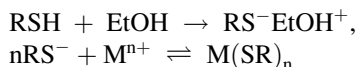
and metal acetylides [410].

Thus, thermolysis of organometallic compound – polymer matrix systems is a multistage process. As a rule, it proceeds along two key interrelated pathways: direct decomposition of the precursor and initiation of diverse transformations of the polymer chain (migration of double bonds, depolymerization, cross-linking, destruction, etc.). The arising nanoclusters may catalyze the carbonization and graphitization processes, i.e., later stages of decomposition of organic polymers. Their mechanisms are most often not entirely clear but they are being actively studied.

Only one fact is obvious: the degree of dispersion of nanoparticles upon thermal transformations is increased as the content of polar groups in the polymer increases [411].

### 6.6.5 Metal Thiolates and Sulfides in the Polymer Matrix

Metal chalcogenides are widely used precursors for the preparation of semiconductor quantum dots (isolated nanoobjects), which show size-dependent optical properties [412]. Thermolysis of the metal thiolate precursors  $M(C_nH_{2n+1}S)_x$  (M (n = 3, 5, 12, 16, 18) was studied in detail. These compounds are usually obtained by the following route:



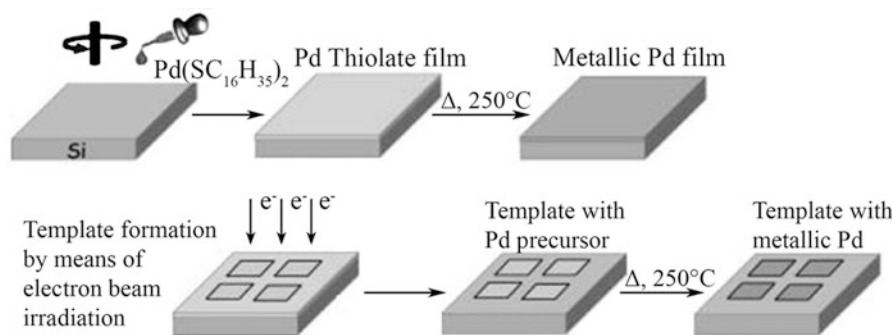
The metal–sulfur bond is fairly stable, the bond energy being in the range of 200–400 kJ/mol. The products that are formed are insoluble in common organic solvents as they are inorganic polymers.

Thermolysis of zinc, cadmium and nickel dodecanethiolates at 573 K with coordinating trioctylphosphine oxide as the solvent or without a solvent afforded ZnS and CdS nanocrystals with nanoparticle size of 1.5–3.0 nm coated by solvent molecules [413, 414] and NiS nanoparticles shaped as plates and rods [415]. Particles with similar size are formed in the thermolysis of  $\text{AgSC}_{12}\text{H}_{25-n}$  [416] while in the case of  $\text{Bi}(\text{SC}_{12}\text{H}_{25-n})_3$ , either layered nanostructures [417] or spheres and hexagonal plates are formed [418] as well as Ag(I), Cu(I) and Pb(II) alkanoates [419]. Thermolysis of copper dodecanethiolate in an inert atmosphere in the absence of solvent at 470–490 K results in the formation of CuS nanoparticles of diameter  $\sim 3$  nm and 12.7 nm-thick faceted nanodiscs of diameter 27.5 nm formed as a result of crystallization processes [420].

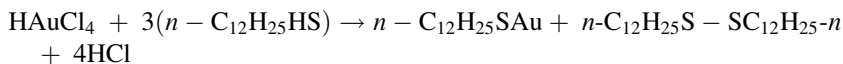
Thermolysis of Pd(II) cluster with a long-chain mercaptan  $[\text{Pd}(\text{SC}_{12}\text{H}_{25})_2]_6$  has been carried out in diphenylether (boiling temperature 532 K) in an argon atmosphere [421].

Palladium hexadecanethiolate  $\text{Pd}(\text{SC}_{16}\text{H}_{33-n})_2$  was decomposed in air at 520 K on the silicon surface to give 50–60 nm-thick nanofilms (the coating was applied by centrifugation or by spin coating) compatible with biomolecules [422] (Fig. 6.27).

Thermolysis of sulfur-containing derivatives of other noble metals, for example Pt, was carried out under analogous conditions [423]. Organogold derivatives  $[\text{RN}(\text{CH}_3)_3][\text{Au}(\text{SC}_{12}\text{H}_{25})_2]$  ( $\text{R} = \text{C}_8\text{H}_{17}$ ,  $\text{C}_{12}\text{H}_{25}$ , and  $\text{C}_{14}\text{H}_{29}$ ) were thermolized to spherical gold nanoparticles [424]. Similar reactions have been realized also in polymer matrices. Thus, gold(I) dodecanethiolate, a precursor of gold nanoparticles in a polystyrene matrix, was obtained in ethanol solution by the following route [425, 426]:

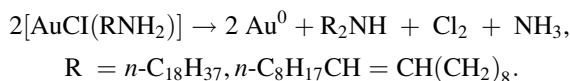


**Fig. 6.27** Spin-coating palladium hexadecanethiolate on the silicon surface followed by the Pd-film formation



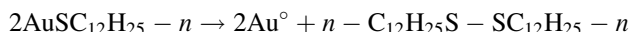
Two moles of thiol were consumed for the reduction of Au(III) to Au(I) and the formation of disulfide as a by-product.

Note that surface-bonded gold nanoparticles are also formed upon controlled thermolysis (348 K) of the surface-grafted complex obtained by adsorption of  $\text{Me}_2\text{Au}(\text{acac})$  on partially dehydrated (on heating to 673 K)  $\text{SiO}_2$  surface [427] while under milder conditions (at temperatures below 333 K), AuCl complexes with octadecylamine and oleylamine decompose [428]:



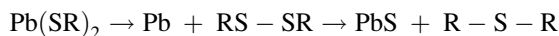
The resulting zerovalent gold particles nucleate and grow to a size of 12 nm with low (8 %) polydispersity, the particles being stabilized by the amine.

The addition of a solution of  $\text{AuSC}_{12}\text{H}_{25} - n$  in acetone to the PS matrix (molecular mass of 230 kDa) and intense sonication followed by casting on a glass surface produces a thin (0.1–0.3 nm) transparent film [426]. These films containing 5–10 % of dodecanethiolate and placed between aluminium foil sheets were subjected to short-term (40–105 s) thermolysis at 573 K. This gave gold nanoparticles according to the reaction:



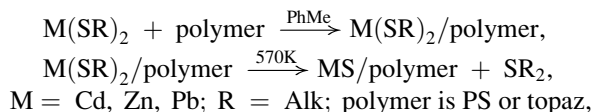
However, it cannot be ruled out that initially polynuclear complexes of the type  $(-\text{Au}^1\text{SR}-)_n$  are formed and then they are converted to nanocrystals. Finally, this gives polydisperse gold nanoparticles with a size of 1.8 nm (~150 gold atoms) evenly distributed in the PS matrix.

In the thermolysis of lead thiolate in PS, redox reaction is considered as the first stage and the formation of sulfide is the second stage [429]:



The crucial role in stabilization of such structures and in preventing their agglomeration is assigned to the polymer matrix. The resulting film nanocomposite of lead sulfide shows luminescent properties, it is stable for several months and is promising for the use in optoelectronics. Unfortunately, the study cited [429] like many other publications, does not consider the transformations of the matrix itself. Although the remainder of the ligand is often detected in PS, it is believed [413] that there is no chemical bond between the polymer chain and the nanoparticles.

Cadmium, zinc and lead alkanethiolates introduced in PS or topaz (thermoplastic copolymer of cycloalkene with ethylene and norbornene) matrix decompose in two stages as shown below



The mean size of the formed CdS nanoparticles is 2.4 nm and that of the ZnS nanoparticles is 1.9 nm. The photoluminescent properties of the particles depend on their size and shape, the maximum luminescence decay time being observed for the products obtained at thermolysis temperature of 553 K. The structure and phase composition of CdS nanocrystallites can be controlled by the thiourea/salt ratio and by thermolysis temperature (323–773 K). The transition of the cubic phase to the hexagonal one occurred at 473–573 K, whereas a pure hexagonal phase of CdS appeared at thermolysis over 873 K. These factors including the time of sintering affect dispersity, crystallinity, and average sizes of CdS nanoparticles. It is interesting that a photocatalytic activity in the synthesis of hydrogen is optimal for a mixture of cubic and hexagonal CdS apart from its pure phases [430].

Decomposition of  $\text{Sb}(n\text{-C}_{12}\text{H}_{25}\text{S})_3$  in polystyrene at 623 K affords Sb and  $\text{Sb}_2\text{S}_3$  nanoclusters (15–30 nm) evenly distributed in the amorphous polymeric phase [431].

As noted above [70] thermolysis of metal dithiolates to give sulfide semiconductors in thin films was performed successfully under the action of laser radiation or electron beam. The laser beam concentrating a 2 kW power was defocused over a small area (of diameter 4 mm), the pulsation time was 10–50 ms. The thin beam temperature is calculated proceeding from the polymer and beam parameters and can be controlled.

Thermolysis of the  $(n\text{-C}_{12}\text{H}_{25}\text{S})\text{Pd}/\text{PS}$  thin films occurs in 5 min at 443 K [423] and in air it can lead to the formation of metal oxides in the polymer matrix. For preventing this process, trioctylphosphine oxide is used as the stabilizing antioxidant (for example, for 2–4 nm CdS, ZnS, CdSe particles inserted *ex situ* into polyconjugated copolymers [432]). In fact, thermolysis of the  $\text{Fe}(n\text{-C}_{12}\text{H}_{25}\text{S})_2 - \text{PS}$  system at 473 K for 2 min is accompanied by the formation of fully transparent light-brown film (practically complete light transmission above 550 nm) in which nanoparticles with a mean size of 10 nm x 50 nm are evenly distributed [433].

Thermal decomposition of metal alkyldithiocarbamates in the presence of alkylamines can serve as a general method for the synthesis of metal sulfide nanoparticles [434]. For example,  $\text{Ag}_2\text{S}$  nanocrystallites were prepared by direct thermolysis of the corresponding precursor in air at 473 K [435]. The recent quite comprehensive review devoted to the thermal synthesis of silver nanoparticles in polymer matrices should be mentioned [436].

Scattered data on the synthesis of heterometallic sulfides can be found in the literature. Thermolysis of a solution of copper and indium oleates in dodecane-thiol in the presence of oleylamine gives  $\text{Cu}_2\text{S}$  and  $\text{In}_2\text{S}_3$ , while  $\text{CuInS}_2$  is not produced in this way due to different decomposition temperatures of the components [437].

### 6.6.6 *Polymer-Mediated Thermal Synthesis of Mono- and Multimetallic Alloys and Ceramics*

Of interest for obtaining bimetallic nanoparticles are the complex salts containing two metals, for example, of general formula  $[M_1A_n]_x[M_2B_m]_y$ , where  $M_1$  and  $M_2$  are the central metal atoms of the complex cations, A and B are the ligands. The composition of the solid solutions obtained can be easily adjusted by the stoichiometry ratio of the precursors. Bimetallic clusters are often served as alternative in the synthesis of nanoheterostructures with a defined composition. Other well-characterized complex salts are metal oxalates, citrates, tartrates which are high-crystalline and are readily decomposed at moderate temperatures.

Usage of suitable polymers allows applying the convenient techniques such as a film coating, spinning, photolithography, etc. before the end stages of thermolysis. This enables a hard control of the structure and size uniformity of particles, their density and so on. Using the metal salts and their oxides as precursors allows obtaining amorphous powders on the certain stages of thermolysis followed by their transformations into crystalline products.

Magnetic alloys FeCo are soft materials with high saturation magnetization (up to 2.45 T), low magnetostriction, relatively low coercive force, and high Curie temperature and energy of magnetic anisotropy (higher than the value predicted for FePt). These materials have a broad spectrum of practical applications. They are obtained using various approaches including RF-discharge plasma, chemical vapour deposition (CVD) [438], thermolysis of cobalt or iron carbonyls in the presence of surfactants [439–441]. The ferromagnetic behaviour of such optically transparent magnetic plastics corresponds to a multidomain magnetite structure; therefore, they could find use in magneto-optical technology (see, for example, Ref. [442]).

Monodispersed magnetic heterostructures  $MFe_3O_4$  ( $M = Ag, Au, Pt, Pd$ ) are well studied [443]. They were obtained by thermal decomposition of iron(III) oleate in the presence of oleylamine with a following deposition of  $Fe_3O_4$  formed on the surface of noble metal nanoparticles. Nanoparticles  $AuFe_3O_4$  having dumbbell-like shape reveal diagnostic and therapeutic features, and catalytic properties [444, 445]. The simplest route of their synthesis is thermolysis of iron pentacarbonyl in the presence of pre-formed gold nanoparticles in 1-octadecene followed by oxidation of iron in air at room temperature. An alternative way is a thermal decomposition of the mixture of iron oleate with a metal-oleylimine complex in the presence of 1,2-hexadecandiol at 583 K. Heterostructures  $AgFe_3O_4$  are formed from the silver nanoparticles on the surface of an amorphous  $Fe_xO_y$  [446]. By controlled co-thermolysis of palladium and iron acetylacetonates, in the presence of oleylamine and oleic acid  $PdFe_3O_4$  were obtained [447–451]. Reduction thermolysis of molecular complexes  $Pd(OOCMe)_4M(OH)_2$  ( $M = Ni(II), Co(II), Zn(II)$ ) or  $Pd(OOCMe)_4Ag_2(HOOCMe)$  and  $PdM(\mu-OOCR)_4L$  ( $M = Co(II), Ni(II), Mn(II), Zn(II)$ ;  $R = Me, Bu$ ;  $L = H_2O, MeCN$ ) affords bimetallic nanoparticles PdM [452, 453].

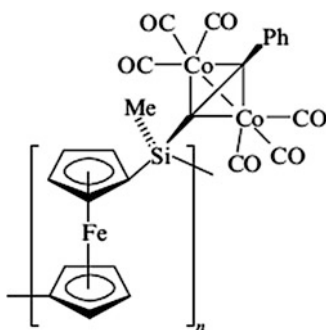


Under heating double complex salt  $[\text{Pd}(\text{NH}_3)_4][\text{AuCl}_4]_2$  in a helium atmosphere from the room temperature up to 623 K the reduction of Au(III) and Pd(II) occurred yielding heterometallic nanoparticles. The process in hydrogen was accompanied by the competitive formation and aggregation of Au and Pd individual nanoparticles up to 603 and 623 K, respectively [454].

The complexes of mixed types  $[\text{Zn}(\text{NH}_3)_4][\text{PtCl}_6]$  and  $[\text{Cd}(\text{NH}_3)_4][\text{PtCl}_6]$  were used as precursors for synthesis of heterometallic particles PtZn and PtCd [455].

A recent study [456] proposes a non-hydrolytic method for the synthesis of nanocrystalline magnetite ( $\text{Fe}_3\text{O}_4$ ) in the presence of rigid matrices, namely, linear  $\omega$ -functionalized polystyrenes ( $M_w$  from 5 to 39.4 kDa). Usually,  $\omega$ -sulfopolystyrene ( $\text{PS-SO}_3\text{H}$ ),  $\omega$ -thiopolystyrene and  $\omega$ -carboxypolystyrene ( $\text{PS-CO}_2\text{H}$ ) obtained by living-chain anionic polymerization are used. Thermolysis of iron(III) acetylacetonate is carried out in hexadecane-1,2-diol at 532–537 K.  $\omega$ -Carboxypolystyrene stabilizes iron nanoparticles more efficiently than  $\text{PS-SO}_3\text{H}$ ; the size of magnetite nanoparticles is 3–10 nm and decreases with increase in the content of the polymer. Ceramic materials incorporating  $\alpha$ - $\text{Fe}_2\text{O}_3$  nanocrystals were also obtained by thermolysis of hyperbranched poly(ferrocenylsilane) [457]. The synthesis and self-organization of the polymer-coated ferromagnetic cobalt, nickel and iron nanoparticles have been analyzed in considerable detail [458, 459]. For example, the corresponding composite is obtained by thermolysis of  $\text{Co}_2(\text{CO})_8$  in dichlorobenzene in the presence of polymeric surfactants with terminal functional groups ( $M_w = 5$ –10 kDa) at temperatures of 433–453 K [460, 461]. The process occurs in two stages: at higher temperature, the metal carbonyl decomposes, while at lower temperature (below 433 K), nanoparticles grow. The mean particle size (17–21 nm) depends on the nature of the surfactant and thermolysis conditions.

Pyrolysis of cobalt carbonyl silanes comprising cobalt carbonyls or cobalt clusters gives rise to soft materials with ferromagnetic properties [462]. Thin ceramic polymetallic films, for example, alloys of magnetic CoFe nanoparticles on a SiC/C film are obtained by thermolysis of high-metallized poly(ferrocenylsilanes) with grafted cobalt clusters at 773 K [463].



Under conditions of air oxidation at 873 K, the thickness of the ceramic film decreases from 200 to 40 nm and then remains almost invariable up to 1,173 K; as

this takes place, fine superparamagnetic particles are formed on the ceramic film surface.

The formation of  $\alpha$ -CoFe and Co(Fe)O phases was detected experimentally. In view of their magnetic properties, the thin films obtained at 773 and 873 K could find use in spintronic instruments as insulating magnetic layers.

The most convenient routes to monodisperse magnetite nanocrystals include co-precipitation in aqueous solutions of Fe(III) and Fe(II) ions, thermolysis of alkaline solutions of Fe(III) chelates in the presence of hydrazine, sonochemical decomposition of hydrolyzed Fe(II) salts followed by thermolysis [195, 464, 465].

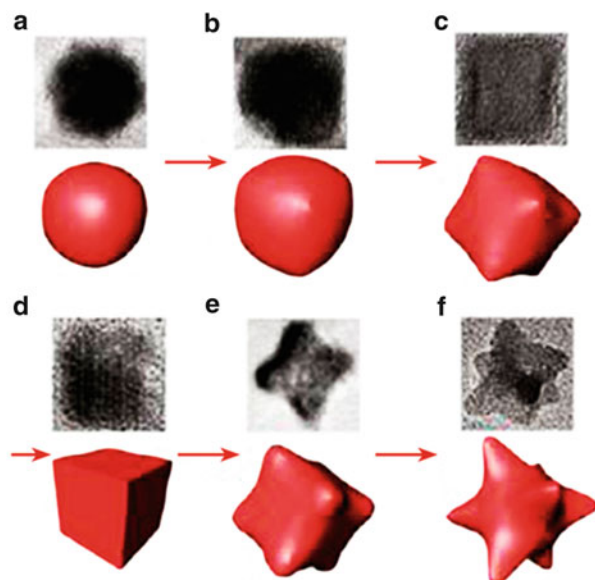
The most widely used method for the synthesis of monodisperse inorganic ferrites described as  $MFe_2O_4$  ( $M = Co, Ni, Mn, Fe, \text{etc.}$ ) is thermal decomposition of mixed organic compounds of the corresponding metal and Fe(III), such as acetylacetonates, carbonyls, carboxylates and so on. The process is carried out in the solid phase or in high-boiling solvents with addition of surfactants (oleic acid, oleylamine and so on) [163, 466].

Thus  $MFe_2O_4$  nanocrystals are formed upon the thermolysis of mixed oleate complexes dissolved in octadec-1-ene under  $N_2$  at 573 K [466]. The particle size depends on the nature of the ferrite and, according to transmission electron microscopy data, it is 9, 11 and 7 nm for  $M = Co, Ni$  and  $Mn$  and 24 nm for  $M = Fe$ . Prenucleation of  $CoFe_2O_4$  occurs at 523 K but without growth of nanocrystallites because the concentration of monomer is lower than the critical nucleation concentration. For reaction temperatures between 523 K and 593 K, the size and shape evolution of the nanocrystals are determined by the nucleation and growth dynamics. For temperatures in the range of 573–593 K which is above the thermolysis temperature of the mixed Co(II)-Fe(III)-oleate complex, the monomer concentration increases rapidly resulting in homogeneous nucleation. Atomic clusters of  $CoFe_2O_4$  with size  $< 2$  nm are initially formed at 587 K that then grow rapidly when the temperature is raised to 593 K in less than a minute. The shape of the  $CoFe_2O_4$  nanocrystals can be controlled by the aging time at 593 K, evolving from initial spherical, to spherical-to-cubic, cubic, corner-grown cubic, or starlike shapes (Fig. 6.28). Thus, by varying reaction conditions, such as the precursor concentration and the heating rate, it is possible to obtain shape-controlled monodisperse  $CoFe_2O_4$  nanocrystals with high yield [466].

The magnetic saturation of  $CoFe_2O_4$ ,  $NiFe_2O_4$ ,  $FeFe_2O_4$  (69.7, 34.2 and 58.6 emu/g, respectively) are close to theoretical values (71.2, 47.5 and 96.2 emu/g), whereas for  $MnFe_2O_4$  this value is much lower (23.9 instead of 120.8 emu/g). This circumstance may be related to the decrease in the particle size during the measurements or to the formation of antiferromagnetic layer on their surface.

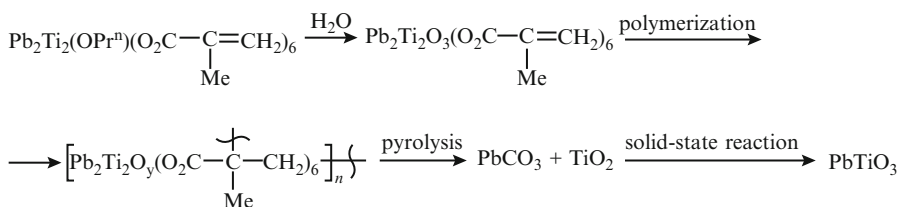
Thus, essential conditions for the formation of ferrites by thermolysis include: the possibility of molecular mixing of the components, their thermodynamic compatibility and similar decomposition temperatures. The failure of the formation of  $CuFe_2O_4$  ferrite is attributable to the fact that already at 523 K, CuO is formed. The

**Fig. 6.28** The shape evolution of  $\text{CoFe}_2\text{O}_4$  nanocrystals. (a) spherical, (b, c) spherical-to-cubic, (d) cubic, (e) corner-grown cubic and (f) star-like



polymer-mediated synthesis followed by thermolysis is free from this drawback. This method was used to prepare  $\text{BaSnO}_3$ ,  $\text{BaTiO}_3$ ,  $\text{SrTiO}_3$ ,  $\text{NdAlO}_3$ ,  $\text{SrBi}_2\text{Ta}_2\text{O}_9$  and other nanoparticles [467].

We developed [155] a method for the synthesis of nanoparticles consisting of combined polymerization of a metal-containing monomer with the thermolysis (CMPT). High-quality  $\text{BaTiO}_3$  ceramics with particle size from 10 nm to 1.5  $\mu\text{m}$ , which depended on the temperature (ranging from 873 to 1,623 K) and the type of atmosphere (inert or oxidizing one) was obtained using this method from organometallic precursors [468, 469]. The traditional way for the preparation of these ceramics, for example  $\text{PbTiO}_3$ , is solid-state mixing of  $\text{PbCO}_3$  and  $\text{TiO}_2$  in mills and subsequent annealing at temperatures above 873 K (ex situ synthesis). However, in the latter case, the process is accompanied by the formation of toxic  $\text{PbO}$  as a side phase. The CMPT production of the lead–titanium ceramics can be described by the following sequence of reactions (Scheme 6.14) [470]:



**Scheme 6.14** Preparation of  $\text{PbTiO}_3$  ceramics via the CMPT method

In the preparation stage of the monomer precursors (batch mixture), it is possible to add paramagnetic ions such as Mn(II), Gd(III) and Cr(III) as acetates or acetylacetonates. These additives are of interest not only for EPR measurements but also for modification of the material, which may thus acquire electrical conductivity, dielectric properties or other properties.

By combining the synthesis and pyrolysis processes, heterometallic ceramics of various types have been obtained, for example, perovskites  $ABO_3$ . The natural perovskite  $CaTiO_3$  mineral has a pseudocubic crystal lattice in which large cations (A) are located at cell vertices, small cations reside at the cell centres, and oxygen ions are at the midpoints of the faces. These materials are widely used in electronics owing to their specific ferro-, piezo- and pyroelectric properties; for example,  $BaTiO_3$  is used in the capacitor industry [411]. Perovskite type ferrites  $M_3Fe_2O_{7-x}$  ( $M = Sr, Ba$ ) with particle size of 50–55 nm are formed upon thermal decomposition of molecular citrate precursors at lower temperature (873 K) than that used in conventional ceramic production processes [471].

Polymetallic ceramics used as high-temperature superconductors (HTSC) also deserve attention. Currently HTSC ceramics are widely used in microlithography, UV-sensitive sensors, etc. [472]. The conventional approach to their production comprises several stages: mixing of compounds of the corresponding metals (oxides, carbonates, oxalates or nitrates), grinding of the mixture, multistage annealing of the batch mixture, including high-temperature annealing in an oxygen atmosphere. Each stage has considerable limitations as regards reproducibility, which is related not only to the quality of grinding and mixing of the initial solid components, but also to complex physicochemical and mechanochemical transformations that take place during the material preparation. This produces both inhomogeneities at the micro level and different phases, including non-conducting ones. As a result, low-quality HTSC ceramic with smeared superconducting junction is produced. The knowledge of thermoanalytical characteristics of decomposition of the precursors of HTSC ceramics would be helpful to optimize the conditions of pyrolysis and understand the mechanism of thermal decomposition.

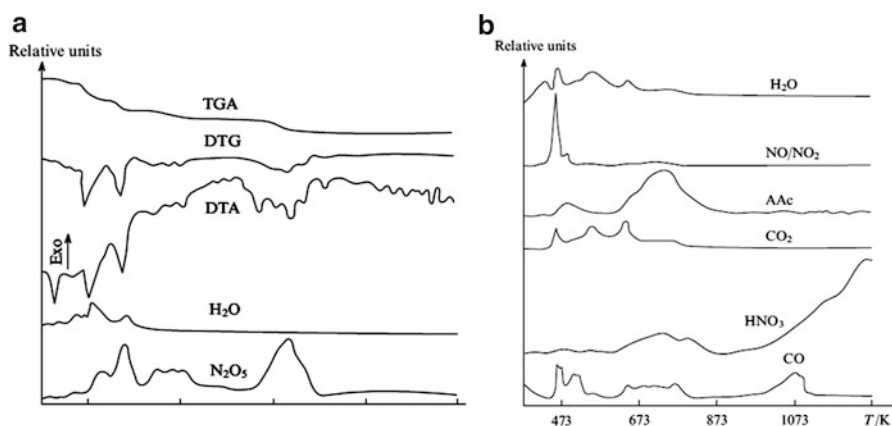
Different types of polymers are used for preparing HTSC materials: PMAA [473–475], PAN [476, 477], polyimides [478, 479], poly(N,N-dicarboxymethyl) allylamine [480, 481], copolymers of acrylic acid [482, 483] etc.

Several options of the polymer-mediated synthesis followed by thermolysis to produce HTSC ceramics have been proposed: preliminary synthesis of the corresponding metal complexes via polymer analogous transformations; polymerization of traditional monomers in the presence of aqueous solutions of Y(III), Ba(II) and Cu(II) nitrates, copolymerization of the corresponding metal-containing monomers and so forth [484]. Each of the approaches has its own advantages and shortcomings. For example, the formation of the copper complex of PAA decreases the thermal stability of the polymer. The process is multistage, including copper-catalyzed rupture of the polymer chain and depolymerization, the formation of macroradicals and low-molecular-mass organic products and anhydride structures, which are decarboxylated [476, 482]. No significant differences were found

between thermolysis of macrocomplexes at temperature below 613 K in argon or in air, complete decomposition taking place at 852 K.

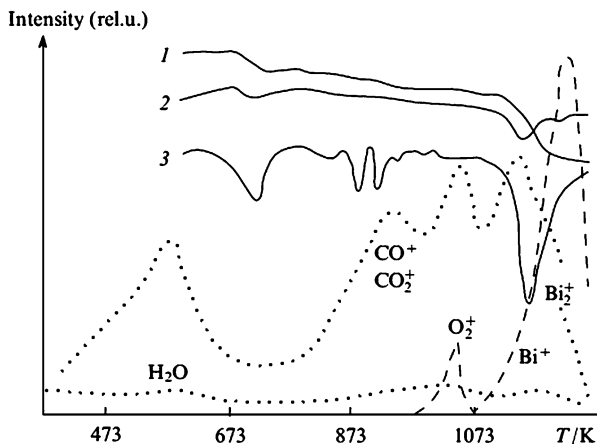
Thermolysis of a mixture of yttrium, barium and copper nitrates (atomic ratio 1:2:3) is known [483] to include five key stages: (1) dehydration (in the temperature range of 298–459 K with an exothermic peak at 400 K); (2) dehydration with copper denitration (in the temperature range of 459–517 K with a temperature maximum at 548 K), (3) completion of copper denitration and yttrium denitration (517–585 K), (4) final yttrium denitration (585–773 K with a maximum at 648 K) and (5) barium melting and denitration (above 773 K with an endothermic peak at 848 K). The denitration of the material reaches a maximum at 913 K, and the residual weight at 1,273 K is 41.6 %, which corresponds to the composition  $\text{YBa}_2\text{Cu}_3\text{O}_{6.5}$  (Fig. 6.29a).

Thermal decomposition of a PAA mixture with components of the HTSC ceramics also occurs in 5 main stages including: (1) dehydration and formation of the macrocomplex (298–419 K, the glass transition temperature of PAA is 401 K); (2) evolution of water, nitrogen oxides and  $\text{CO}_2$  (temperature range of 419–472 K); (3) intensive evolution of water,  $\text{CO}_2$ , CO, monomeric acrylic acid (AA) and nitrogen oxides (472–603 K, DTG peaks at 535 and 552 K (Fig. 6.29b)); (4) intensive destruction of PAA (603–663 K, DTG peak at 663 K). The last, fifth stage starts at 899 K and is accompanied by an exothermic peak with a maximum at 1,118 K corresponding to CO and  $\text{HNO}_3$  evolution, decomposition of the most stable barium nitrate and  $\text{BaCO}_3$  formed. The relatively large fraction of the residue (22.3 %) attests to incomplete oxidation of PAA in argon, whereas thermolysis in air inhibits the formation of barium carbonate and eliminates the fifth stage of pyrolysis. Thus, for optimization of the production process of high-quality HTSC ceramics, the initial stages of thermolysis (temperature below 773 K, heating rate 5 deg/min) should be carried out in an inert atmosphere, and the final stage (773–1,223 K, heating rate 10 deg/min) should be carried out in air. This prevents the formation of undesirable phases like  $\text{BaCO}_3$ ,  $\text{Y}_2\text{O}_3$ ,  $\text{BaCuO}_2$ ,  $\text{Y}_2\text{Cu}_2\text{O}_5$ , etc.



**Fig. 6.29** Thermal analysis data for a mixture of metal nitrates (Y:Ba:Cu = 1:2:3) (a) and mass spectra of their composition with polyacrylic acid (PAA:(Y, Ba, Cu) = 2:1) recorded during the analysis (b) [483]. The thermal analysis was performed under argon, heating rate 5/deg min

**Fig. 6.30** Thermal (continuous line) and mass spectral (dashed line) analysis data for samples 2223: (1) TGA curves, (2) DTA curves, (3) DTGA [484]. Heating rate 4 deg/min, the  $\text{CO}^+$ + $\text{CO}_2^+$  curves are enlarged 50-fold



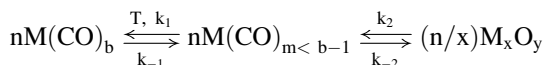
The polymer-mediated synthesis has been utilized [483] to prepare various ceramics. For example, decomposition of yttrium metallopolymer at 633–793 K affords  $\text{YBa}_2\text{Cu}_3\text{O}_{7-x}$  ceramics (123-ceramics), while in the case of bismuth metallopolymer, 2223 ceramics with the formula  $\text{Bi}_2\text{Sr}_2\text{Ca}_{n-1}\text{Cu}_n\text{O}_{2n+4-8}$  ( $n = 1-3$ ) is produced, the highest weight loss rates being achieved at 693–1,143 K. The mass spectrometric analysis of the gases evolved from the bismuth 2223 ceramics on vacuum heat treatment indicates (Fig. 6.30) that at 973–1,073 K, small amounts of oxygen and bismuth are formed, and are stabilized as  $\text{O}_2^+$ ,  $\text{Bi}^+$ ,  $\text{Bi}_2^+$  ions and traces of  $\text{H}_2\text{O}$ ,  $\text{CO}^+$ ,  $\text{CO}_2^+$ , etc. In terms of key characteristics (superconductivity at 87 K), 100 %-magnetic shielding, electrical conductivity at room temperature of  $800-1,000 \Omega^{-1}\cdot\text{cm}^{-1}$ , bulk density of  $4.7 \text{ g}\cdot\text{cm}^{-3}$ , critical current up to  $240 \text{ A}\cdot\text{cm}^{-3}$ , etc.), the yttrium ceramics obtained by the polymer-mediated method and the single-phase bismuth superconducting cuprate specimens synthesized by the combined polymerization – pyrolysis route can be assigned to the best HTSC ceramics formed under thorough oxygen annealing.

One of the promising methods of the HTSC synthesis, i.e. the YBCO-ceramics, is a thermal decomposition of novolac resins (*m*-cresol-formaldehyde) containing of corresponding metal nitrates [485–487]. The optimal thermolysis in an inert atmosphere starts at 1,023 K, however the formation of  $\text{BaCO}_3$  continues in  $\text{O}_2$  atmosphere yielding the orthorhombic YBCO-ceramics with a high superconductivity at 91 K. This polymer-mediated approach appears to be perspective for synthesis of HTSC-ceramics and requires further studies.

### 6.6.7 Thermolysis of Metal Carbonyls in Polymer Matrices

This is the earliest and popular method for preparing nanocomposites. Some typical examples of metal carbonyl decomposition have been noted repeatedly in this Chapter. Along with cobalt acetate, formate, acetylacetonate, the most widely used precursor is cobalt carbonyl  $\text{Co}_2(\text{CO})_8$ .

The general scheme of metal carbonyl decomposition including in the presence of a polymer matrix being a stabilizing agent of the metal or its oxide nanoparticles formed can be represented as follows [337]:

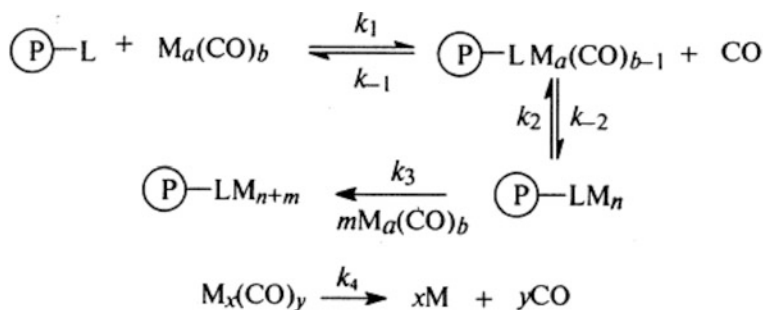


where  $k_1, k_{-1}, k_2, k_{-2}$  are appropriated constants.

Among other metal carbonyls  $Cr(CO)_6$ , and  $Fe(CO)_5$  are often used applying two methods of their decomposition in polymers: in solution and in their melt.

The most general approach comprises the dispersion of pre-synthesized nanoparticles in polymer matrices, i.e., method *ex-situ*. In the processes *in situ* more 'active' polymers which have the functional groups for complexation with a precursor are preferable.

The nucleophilic fragments of macroligands (particularly in styrene-N-vinylpyrrolidone copolymer) bring about a polymer-catalyzed decomposition of the metal carbonyl by scheme:



The main condition for a proper matching of a functionalized polymer is connected with the greater reaction rate on the polymer surface to reduce the decomposition in the solution to a minimum, i.e. to provide:

$$\begin{array}{l} k_1 + k_2 - k_{-1} - k_{-2} > k_4 \\ k_3 > k_4 \end{array}$$

If this condition is fulfilled, the main process takes place, i.e. particle growth and the formation of nanoparticles of 1–10 nm in size.

Coincidentally with the sizes of the forming nanoparticles the probability of termination of particle growth increases due to their noncovalent surface interactions with the macromolecule. The stronger the interaction the smaller the particle size; polymers having more polar groups promote the finest particles growth.

Of interest is an approach based on the decomposition of metal carbonyls in block-copolymers. Thermolysis of metal carbonyls in block-copolymers in the synthesis, for example,  $Cr_2O_3$ ,  $Fe_2O_3$ , and  $Co_2O_3$  nanoparticles in polystyrene-*b*-poly(methyl-

methacrylate) diblock copolymer (PS-PMMA) as a model system is studied in detail [488–492]. Results showed that the rates for reactions performed in a diblock copolymer solution are much faster than the rates of the same reactions performed in a homopolymer solution. The arrangement of the diblock copolymers in solution into spherical core-shell domains created self-assembled “nanoreactors” with PS acting as the surrounding shell and the internal PMMA domain (core) contained high precursor concentration, resulting in faster kinetics. Note that the size and shape of nanoparticles formed are similar to those generated at the thermolysis in pure PMMA solution. This may indicate that the particle morphology is determined not by the kinetic of their formation but by their interactions with their surrounding media and the presence of reactive stabilizing molecules, such that, in this case, PMMA segments, either as homopolymers or as part of a block-copolymer.

The formation of metallopolymers in a polymer melt with an addition of a high-boiling solvent [493, 494] is based on decomposition of the melt at the highest possible temperatures much exceeding the decomposition temperature of the precursor for the fastest possible and complete removal of the eliminated ligand from the reaction medium. Its main difference from ‘wet’ methods is that the short-range order of the structure of the initial polymer, PE, polypropylene (PP), PTFE, etc. is preserved in the melt, as opposed to solution, because in the case of the solid-state thermolysis, the polymer is destroyed to a lesser extent. The voids present in the polymer (due to density fluctuations) become accessible for the accumulation of the products. First of all, these are concentrated in the loosest disordered interspherulite areas of the organic matrix, in the space between the lamellas and at the centres of spherulites. Due to the decrease in the free polymer volume and the possible cross-linking, the segmental motion of the amorphous phase is hampered.

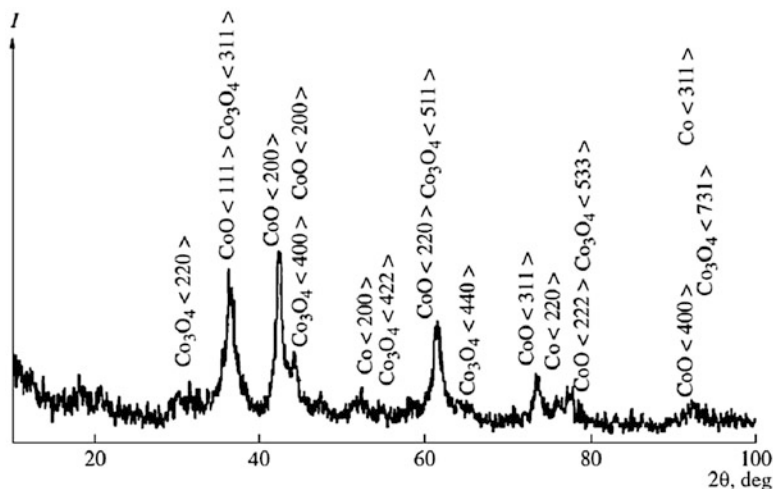
Cobalt-based nanoparticles (metallic cobalt, cobalt oxides, and cobalt alloys, such as CoFe) are very interesting varieties of magnetic nanoparticles. Cobalt-containing nanomaterials have the highest values of important magnetic characteristics (coercive force and saturation magnetization) among the magnetic materials [495]. In view of their relatively low cost and high efficiency, the most popular processes for manufacturing cobalt-containing nanoparticles involve the thermolysis of organocobalt compounds in organic solvents (octadecene, benzyl ether, tetraline, and heptadecane) with surfactants (fatty acids, amines, and organophosphorus compounds) [496].

X-ray powder diffraction is an effective method for studying for determining nanoparticle sizes and their phase composition in the Co nanocomposites. Examination of the X-ray diffraction pattern in Fig. 6.31 showed one metallic phase (very weak) and two oxide phases. This implies that CoO  $\langle 111 \rangle$ ,  $\langle 200 \rangle$  and Co<sub>3</sub>O<sub>4</sub>  $\langle 220 \rangle$  phases are the major components of the sample and the metallic cobalt percentage is low, the average size of the particles is  $9.0 \pm 0.8$  nm [461].

It cannot be ruled out that strong interaction of the polymer with the nanoparticle inserted into intermolecular voids of the matrix may lead to destruction of the crystalline portion and its transition to the amorphous state. In this material, no metal phase is detected, and it can be considered as a single-phase metallopolymer.

Using this method, the PE-based metallopolymer composites were obtained with iron clusters (nanoparticle size 9–12 and 20–22 nm) [497] with Fe<sub>0.85</sub>Mn<sub>0.15</sub> (size ~2.5–3.0 and 20 nm) [494, 497], with ZnO and CdS clusters (mean size 4–10 nm)





**Fig. 6.31** X-ray diffraction pattern for cobalt-containing nanoparticles. CoO,  $\text{Co}_3\text{O}_4$ , and Co peaks are indexed

[493, 498]. The formed iron-containing nanoparticles exist at room temperature in the superparamagnetic state and are multiphase structures: they consist of  $\alpha$ -Fe,  $\text{Fe}_3\text{C}$ ,  $\text{Fe}_3\text{O}_4$ ,  $\text{Fe}_2\text{O}_3$  [494]. According to the existing views, these particles are constructed as a core ( $\alpha$ -Fe) coated by a metal-containing shell ( $\text{Fe}_3\text{C}$ ,  $\text{Fe}_3\text{O}_4$ ,  $\text{Fe}_2\text{O}_3$ ).

Thermal decomposition of  $\text{Fe}(\text{CO})_5$  in organic solvents is accompanied by the formation of intermediates – clusters of the different composition such as  $\text{Fe}_2(\text{CO})_9$ ,  $\text{Fe}_3(\text{CO})_{12}$  and other; therefore, sometimes triiron dodecacarbonyl  $\text{Fe}_3(\text{CO})_{12}$  as precursor is used instead of  $\text{Fe}(\text{CO})_5$  [499].  $\text{Fe}(\text{CO})_5$  decomposes into highly active atom clusters and CO in a closed reactor at 972 K in an inert atmosphere in the presence of S or Se powders. CO undergoes a Boudard disproportionation reaction  $2\text{CO} \rightarrow \text{CO}_2 + \text{C}$ . Under these conditions FeS and FeSe nanoparticles covered by a carbon shell are formed [314]. The layered hexagonal structure of FeS is known to be an excellent solid lubricant.

Thermal decomposition of  $\text{Fe}_x(\text{CO})_y$  in imidazolium salts with long-chain N-alkyl substituents – an ionic liquid as solvent affords iron carbide nanoparticles with the size from 2 to 15 nm [499].

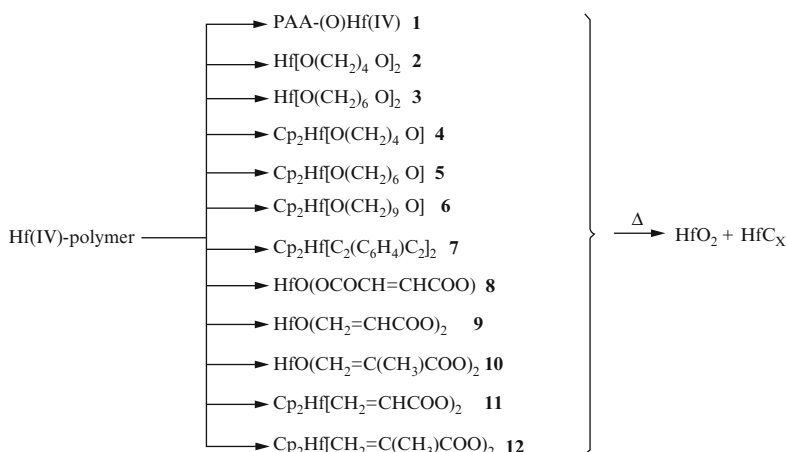
Thus, thermolysis of metal carbonyls in polymer matrices is a versatile and controlled approach to obtain nanocomposites with a complex of useful properties.

### 6.6.8 Comparison of Different Methods of Solid-State Thermolysis of Metallopolymers

Currently, there are three key methods for the preparation of metallopolymers [365] for polymer-mediated synthesis of nanoparticles: reactions of metal compounds

with linear functionalized polymers (so called polymer analogous transformations); polycondensation of the corresponding precursors to metallopolymers; polymerization and copolymerization of metal-containing monomers. Thermolysis of metallopolymers formed according to each of the methods listed above occurs in different ways.

This fact will be demonstrated in relation to hafnium-containing polymers obtained by polymer analogous transformations involving PAA (compound **1**), by condensation methods, viz., the reaction of hafnium compounds with diols (**2–6**) or condensation of cyclopentadienyl hafnium complexes with p-diethynylbenzene (**7**), and by polymerization of hafnium-containing monomers (**8–12**) [500–502]. The isothermal thermolysis of Hf(IV) – polymer systems (**1–12**) was studied at three characteristic temperatures: 1) 643 K (heating for 60–300 min) – the mean decomposition temperature where secondary transformations (pyrolysis of the decomposition products) are insignificant; 2) 873 K (150–200 min) – the mean temperature of the early stages of pyrolysis of the organic transformation products; 3) 1,273 K (~150 min) – the temperature of intense pyrolysis of organic products. The general pattern of controlled thermolysis of these polymers can be represented as follows:

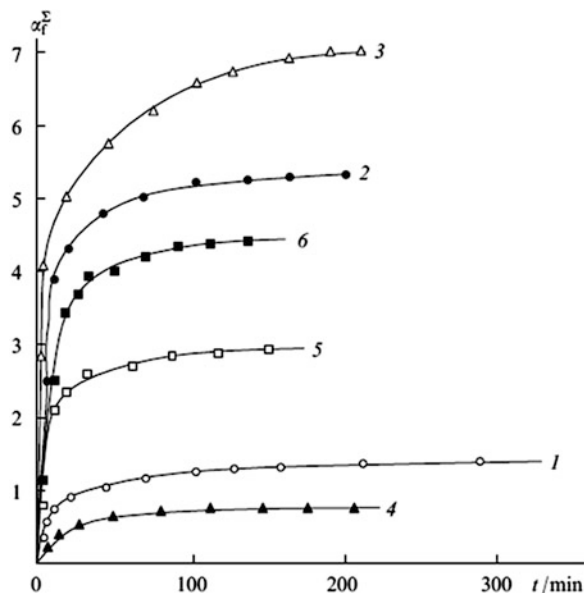


The formed composites tend to have different H:O atomic ratios covering a rather broad range and forming the series

$$14 (\text{for } \mathbf{6}) > 11, 0(\mathbf{5}) > 6, 0(\mathbf{3}) > 5(\mathbf{12}) > 4, 0(\mathbf{2}, \mathbf{11}) > 1, 2(\mathbf{9}) > 0, 4(\mathbf{8}).$$

The typical regular features of the thermolysis of metallopolymers **1–12** are as follows. The gas evolution kinetics are similar for all of the samples (Fig. 6.32): first, the reaction rate decreases monotonically with an increase in the time of thermolysis at a constant temperature; a temperature rise for similar transformation times induces non-linear increase in the gas evolution and weight loss rates. The major gaseous product in the thermolysis of Hf carboxylate polymers **8, 9, 11** at 643 K is CO<sub>2</sub>, while for polymer **11**, this is cyclopentadiene vapour. An increase in

**Fig. 6.32** Gas evolution kinetics during thermolysis of metallopolymers **12**: (1) 643, (2) 873, (3) 1,273 K and **2**: (4) 643, (5) 873, (6) 1,273 K [500]



the temperature of thermolysis (to 873–1,273 K) brings about considerable evolution of  $H_2$ , and in the case of Hf diol polymers **2–6**, the corresponding diols and a broad range of their oxygen-free fragments are formed even at 643 K.

The weight loss by the samples at the end of transformation is most often below the value expected for their decomposition to  $HfO_2$  or  $HfC$ . Out of this series, only for metallopolymer **11**, the weight loss at 873 and 1,273 K is close to that observed in the decomposition of  $HfO$  fumarate to  $HfC$ : apart from the  $HfO_2$  crystalline phases, the  $HfC$  phase is formed but no metallic hafnium (Table 6.13). The content of hafnium carbide in the composite and the degree of crystallinity of products depend on the ligand environment (the type of the bifunctional ligand used to prepare the polymer), the polymer composition and the conditions of thermolysis. At relatively low temperatures ( $\leq 643$  to  $\sim 873$  K), the transformation products are amorphous to X-rays; and temperature rise promotes crystallization. In view of the thermodynamic analysis of the  $Hf-C-O-H$  system, it appears unexpected [503, 504] that a well crystallized  $HfC$  phase was observed only in the thermal decomposition of polymer **8** formed from the complex  $Cp_2Hf(CH_2=CMeCO_2)_2$  with the minimum H:O atomic ratio (0.4). Possibly, in this case, the conditions of thermolysis are far from thermodynamic equilibrium.

For a thermodynamically equilibrium  $HfC_xO_yH_z$  system, the  $HfO_2(s) \rightarrow HfC(s)$  transition occurs in the temperature region of 1,973–2,023 K. However, under real conditions, this transformation starts with participation of the energy-saturated highly reactive nano-sized particles formed, the reacting system being far from equilibrium. This shifts the  $HfO_2(s) \rightarrow HfC(s)$  transition to lower temperatures, 873–1,273 K (see Table 6.13), for almost all types of metallopolymers.

Depending on the nature of the ligand and the conditions of thermolysis, several options of nano-sized particle conservation are available. They are related either to

**Table 6.13** Effect of the thermolysis temperature on the phase composition of the solid thermolysis products of Hf-containing polymers [500]

Polymer	Temperature of thermolysis, K		
	643	873	1,273
<b>2</b>	Amorphous	m-HfO <sub>2</sub> + HfC*	m-HfO <sub>2</sub> + HfC*
<b>3</b>	Amorphous	m-HfO <sub>2</sub> + t-HfO <sub>2</sub>	m-HfO <sub>2</sub> + t-HfO <sub>2</sub> * + HfC*
<b>5</b>	Amorphous	m-HfO <sub>2</sub> + t-HfO <sub>2</sub> * + HfC*	m-HfO <sub>2</sub> + HfC*
<b>6</b>	Amorphous	m-HfO <sub>2</sub> + t-HfO <sub>2</sub> * + HfC*	m-HfO <sub>2</sub> + t-HfO <sub>2</sub> * + HfC*
<b>8</b>	Amorphous + t-HfO <sub>2</sub> + HfC*	Amorphous + HfC + t-HfO <sub>2</sub> *	m-HfO <sub>2</sub> + HfC*
<b>9</b>	Amorphous	m-HfO <sub>2</sub> + t-HfO <sub>2</sub> + HfC*	m-HfO <sub>2</sub> + t-HfO <sub>2</sub> + HfC*
<b>11</b>	Amorphous	Amorphous	m-HfO <sub>2</sub> + t-HfO <sub>2</sub> + HfC*
<b>12</b>	Amorphous	Amorphous	m-HfO <sub>2</sub> + t-HfO <sub>2</sub> + HfC*

Note. The asterisk marks highly disordered phases, letters m and t stand for monoclinic and tetragonal systems, respectively

destruction and subsequent carbonization of the ligand or the mixture of the precursor with the polymer at high temperature or to transformations of the polymer catalyzed by metal clusters arising during the decomposition. Generally, all transformations of this type are self-regulated processes [505].

The research into thermal transformations of precursors in the solid phase is vigorously developing. On the one hand, the transformations most often resemble the pyrolysis in high-temperature liquids [411] and it can be considered as a pseudohomogeneous process. On the other hand, they bear specific features of solid-state reactions, which is manifested as influence of the topochemistry and crystal lattice defects on the transformation rate.

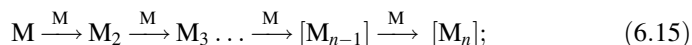
## 6.7 Computer Modelling of the Kinetics of Nanoparticle Formation During Solid-State Thermolysis

Despite the complexity of multistage physicochemical transformations that accompany the solid-state thermolysis of metallopolymers [506] three key macroscopic stages can be distinguished:

1. thermal decomposition of the metal-containing fragment



## 2. clusterization and nanoparticle growth



## 3. polymerization of the demetallized ligand



where M is the metal, M\* is a metal atom or metal compound, L is ligand, M<sub>n</sub> is metal-containing oligo(poly)mer, P is the product of polymerization or ligand destruction.

The published and experimental data mainly focus on the characteristics of the final thermolysis products (nanoparticle size distribution and spatial distribution in the matrix, physical and chemical properties of the obtained matrices, etc.). However, no studies considering the variation of the physicochemical parameters during the thermal transformation are available.

The most productive approach to the theoretical investigation of the thermolysis kinetics is computer modelling. In recent years, various solutions to problems of this type have been developed [507–509]; this allows one to follow the cluster formation dynamics in the matrix during the solid-state thermolysis, the temporal growth of particles and the topochemical behaviour of particles in the polymeric medium.

The kinetics of nucleation and particle growth are studied within the framework of the diffusion-controlled aggregation model using combined sweep and Monte–Carlo methods. As the basis of kinetic models, polymeric media of various structures, namely, isotropic (globular) and anisotropic (layer and fibrillar) structures, are considered. The aggregated particles come from the products of thermal decomposition of the metal-containing groups of the polymer chain: metal atoms or metal oxide particles. The medium in which the transformations and the motion and growth of cluster-forming particles take place is represented as a three-dimensional lattice consisting of L<sup>3</sup> (50 nm × 50 nm × 50 nm) cubic cells – reactive groups (1.25 × 10<sup>5</sup> reaction sites). The cell dimension (face α = 10<sup>−9</sup> – 10<sup>−8</sup> m) varies being determined by the size of the characteristic fragment of the regular polymer chain comprising one decaying metal-containing group. The determining algorithms of the model are as follows.

1. Decomposition of the metal-containing groups to give monoatomic metal particles (or oxide particles) at the rate

$$W_J = kC = C_0 k_0 \exp\left(-\frac{E_{a,J}}{RT}\right), \quad (6.17)$$

where k is the constant, C and C<sub>0</sub> are the current and initial numbers of the polymer reaction sites (C<sub>0</sub> = 1.25 × 10<sup>5</sup> monoatomic sites), E<sub>a,J</sub>, k<sub>0</sub> and T are the variable parameters (activation energy, pre-exponential factor and the temperature of the experiment, respectively). A definite (variable) probability that the decay of reaction sites is catalyzed by diffusing particles is taken into account.

2. Solid-state activated diffusion of monoatomic metal (or metal oxide) particles giving polyatomic cluster particles, the rate of diffusion being

$$W_{D,N} = D_N C^* = C^* D_1 \times N^{-1/3}, \quad (6.18)$$

where  $C^* = C/a$  is the current number of the reaction sites per cell with dimension  $a$ ,  $N$  is the size of  $N$ -atomic cluster,  $D_1 = D_0 \exp[-E_{a,D}/(RT)]$  is the diffusion coefficient for a monoatomic particle,  $E_{a,D}$  and  $D_0$  are the variable parameters (activation energy and entropy factor, respectively). As noted above, it is assumed that a single cell cannot accommodate two (or more) separate particles, i.e., they immediately coalesce to a unified cluster.

3. Considering dissociation of clusters by the reaction



to give monoatomic particles at a rate

$$W_N = k_N C_N, \quad (6.20)$$

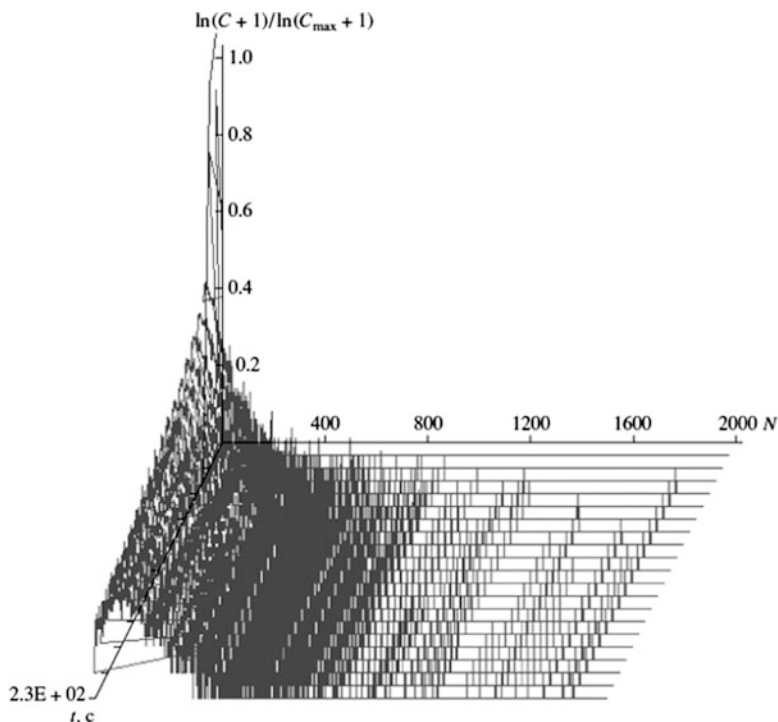
where

$$k_N = k_{0N} N \exp\left(-\frac{E_{a,N}}{RT}\right) \quad (6.21)$$

depends on the cluster dimension  $N$  and decreases as the cluster dimension increases,  $C_N$  is the current concentration of the cluster particles with dimension  $N$ ,  $E_{a,N}$  and  $k_{0N}$  are the activation energy of the  $N$ th cluster and the preexponential factor (equal to  $\sim 10^{13} \text{ s}^{-1}$ ), respectively. It is assumed that monoatomic particles can migrate to neighbouring cells.

4. Visualization of the formation of cluster particles. At the end of the experiment, the results are presented as the dependence of  $\ln(C+1)/\ln(C_{\max}+1)$  and  $J(N)$  on  $t$ , i.e., the time dependence of the cluster size distribution ((Fig. 6.33) [506, 509] where  $C_{\max}$  is the greatest number of clusters at time instant  $t$ ;  $J(N)$  is the cluster size distribution where  $J$  is the number of  $N$ -dimensional clusters. As a result, the accumulation kinetics of a specified  $N$ th cluster is obtained.

The time of the numerical experiment is  $t_\Sigma = Z t_p$ ,  $t_p = -k^{-1} \ln(C/C_0)$  is the time of decay of 95.5 % of the metal-containing groups of the polymer,  $Z$  is the relative (variable) time of cluster formation ( $Z \geq 1$ ). The values  $C_0 = 5 \times 10^{26}$  particles per  $\text{m}^3$  (for a metallopolymer with the density  $1.5 \text{ g m}^{-3}$  a chain fragment of which contains one reactive group in the cell with  $a = 10^{-9} \text{ m}$ ),  $E_{a,J} = 167 \text{ kJ mol}^{-1}$ ,



**Fig. 6.33** Evolution of cluster size distribution during the computer experiment (*gl*-structure):  $T = 653$  K,  $Z = 5$ ,  $W_{D, N} = 1 \times 10^{-18}$  particle  $\text{m}^2 \text{s}^{-1}$ ,  $W_1 = 2.2 \times 10^{25}$  particle  $\text{m}^{-3} \text{s}^{-1}$ ,  $W_2 = 1 \times 10^3$  particle  $\text{m}^{-3} \text{s}^{-1}$ , and  $W_\infty = 4 \times 10^{-14}$  particle  $\text{m}^{-3} \text{s}^{-1}$

$k_0 = 10^{13} \text{s}^{-1}$ ,  $E_{aN} = E_{a, \infty} - 2(E_{a, \infty} - E_{a,2})/N$ ,  $E_{a, \infty} = 420 \text{ kJ mol}^{-1}$  (the activation energy for the decay of the 'massive' cluster,  $E_{a, \infty} = E_{\text{sub}}$  is the sublimation energy of the metal or its compounds) and  $E_{a,2} = 170 \text{ kJ mol}^{-1}$  (dissociation energy of the two-particle cluster) are used as the basic kinetic parameters.

The results of the computer modelling of nanoparticle formation during the solid-state thermal decomposition of metal-containing monomers and polymers with different structural organization point to some general trends. For isotropic polymer media, an increase in the time of cluster formation leads to evolution of the particle size distribution spectrum: as  $Z$  increases, the transformation parameters being the same, the distribution maximum  $J_{\text{max}}(N)$  shifts to greater  $N$  values, from  $N \approx 80$  at  $Z = 2$  to  $N \approx 160$  at  $Z = 10$ , while the  $J_{\text{max}}$  value simultaneously diminishes. The formation of single clusters is a consecutive-parallel process. For example, over the experimental time  $t_\Sigma = 228$  s ( $Z = 5$ ), the yield of clusters with  $N \approx 2$  and 65 passes through a maximum, while for  $N \approx 125$  and 185, the number of clusters increases to reach a steady state, and smaller clusters ( $1 \leq N \leq 4$  and  $35 \leq N \leq 39$ ) do not disappear, their number reaching a steady value, apparently, as a result of dissociation of larger clusters.

An increase in the computing time results, first, in a shift of the distribution spectrum  $J(N)$  to greater  $N$  values, the mean value for the  $N$ -dimensional cluster reaching  $\sim 1,500$  as soon as for  $Z = 100$ , which may correspond to a spherical cluster with a size from 4.1 to 4.2 nm. Second, the distribution spectrum  $J(N)$  becomes simpler: the polymodal distribution typical of small  $Z$  values evolves already at  $Z = 100$  to a bimodal distribution with maxima at  $N \approx 540 - 550$  and  $N \approx 1,540$ . Presumably, further increase in the computing time ( $Z \gg 100$ ) may produce a unimodal particle size distribution with a much greater mean size. The considered results of modelling of the kinetics of formation of metallic clusters upon thermolysis of the metal-containing fragments of the polymeric media with different structural organization demonstrate [506, 509] the growth of nanoclusters, which may reach rather large sizes. These models are efficient and can be extended to other objects.

Of all the physical factors that can affect the behaviour of a chemical substance, temperature is most popular. Thermolysis of metallopolymers and their precursors provides almost infinite possibilities for the manufacture of various types of nanocomposites and it is the simplest and most widely used method for introducing up to 90 mass% of colloid particles of metals into a polymeric composite. It is possible, first, to subject a precursor to the thermolysis and, second, to blend it with the polymer matrix prepared beforehand (*ex situ* process). Alternatively, the researcher can perform joint thermolysis of a polymer blend with a metal compound present in a specified ratio (*in situ* process). Kinetically, the polymer-mediated synthesis of nanoparticles is a conjugate two-stage process related to multichannel transformations of the metal-containing precursor. It induces the evolution of the high-molecular-mass component: depolymerization, cross-linking, destruction, many reactions being catalyzed by the formed metal clusters [28]. The free energy of thermolysis is higher than the free energy absorbed upon the formation of metallopolymers; this is employed to perform other processes in conjugation with the thermolysis. As applied to solid-state reactions, transformations taking place in structural inhomogeneity sites (defects, dislocations) may induce other processes. The conjugate processes represent an approximation to self-assembly processes, i.e., processes with feedback [505].

The self-assembly of 'core-shell' type nanoparticles during thermolysis is one of the unique phenomena inherent in the rapidly developing supramolecular chemistry [510, 511]. Supermolecules (nanometre-sized molecules) are oligomolecular particles arising upon the intermolecular association of several components that form intricate structure of definite architectures according to the molecular recognition principle. The organization of such supermolecules is based on interaction types other than covalent bonds – hydrogen bonds, electrostatic and Van der Waals forces.

This chapter is restricted only to description of the formation of nanoparticles in organic matrices during thermolysis. Quite extended subject matter related to the thermal synthesis of inorganic matrices and the insertion of metal-containing clusters therein and production of metalloceramics remained beyond the scope of our consideration and is still waiting for being surveyed and analyzed.



## References

1. A.D. Pomogailo, I.E. Uflyand, *Makromolekulyarnye Metallokhelaty* (Macromolecular Metal Chelates) (Khimiya, Moscow, 1991)
2. Y. Kolytyn, N. Perkas, A. Gedanken, *J. Mater. Chem.* **14**, 2975 (2004)
3. X. Li, S.J. Tian, Y. Ping, D.H. Kim, W. Knoll, *Langmuir* **21**, 9393 (2005)
4. V. Prashant, *J. Phys. Chem. B* **106**, 7729 (2002)
5. X.F. Duan, C.M. Lieber, *Adv. Mater.* **12**, 298 (2000)
6. A.M. Morales, C.M. Lieber, *Science* **270**, 208 (1998)
7. Z.Q. Wang, X.D. Liu, J.F. Gong, H.B. Huang, S.L. Gu, S.G. Yang, *Cryst. Growth. Des.* **8**, 3911 (2008)
8. V.V. Kozlov, G.P. Karpacheva, V.S. Petrov, E.V. Lozovskaya, *Vysokomol. Soedin. Ser. A* **43**, 1 (2001)
9. G.P. Karpacheva, K.A. Bagdasarova, G.N. Bondarenko, L.M. Zemtsov, D.G. Muratov, N.S. Perov, *Vysokomol Soedin. Ser. A* **51**, 2037 (2009)
10. A.D. Pomogailo, *Kolloid. Zh.* **67**, 726 (2005)
11. J.H. Warner, *Adv. Mater.* **20**, 784 (2008)
12. H. Zhang, D.Y. Wang, B. Yang, M. Helmuth, *J. Am. Chem. Soc.* **128**, 10171 (2006)
13. V. Rotello, *Nanoparticles: Building Blocks for Nanotechnology* (*Nanostructure Science and Technology*) (Springer, Berlin, 2003)
14. A. Heilmann, *Polymer Film with Embedded Metal Nanoparticles* (Springer, Berlin, 2002)
15. P.M. Ajayan, L.S. Schadler, P.V. Braun (eds.), *Nanocomposite Science and Technology* (Wiley-VCH, Weinheim, 2003)
16. A.J. Gu, G.Z. Liang, *J. Appl. Polym. Sci.* **89**, 3954 (2003)
17. S.M. Pourmortazavi, I. Kohsari, M.B. Teimouri, S.S. Hajimirsadeghi, *Mater. Lett.* **61**, 4670 (2007)
18. N. Grassi, *Chemistry of High Polymer Degradation Processes* (Butterworths, London, 1956)
19. E. Themistou, A. Kanari, C.S. Patrickios, *J. Polym. Sci.: Part A: Polym. Chem.* **45**, 5811 (2007)
20. S.H. Kim, F. Nederberg, L. Zhang, C.G. Wade, R.M. Waymouth, J.L. Hedric, *Nano Lett.* **8**, 294 (2008)
21. J.D. Menczel, R.B. Prime (eds.), *Thermal Analysis of Polymers. Fundamentals and Applications* (Wiley, London, 2009)
22. P. Greil, *Adv. Eng. Mater.* **2**, 339 (2000)
23. S. Bernard, M. Weinmann, P. Gerstel, P. Viele, F. Aldinger, *J. Mater. Chem.* **15**, 289 (2005)
24. S. Duperrier, C. Gervais, S. Bernard, D. Cornu, F. Babboneau, C. Balan, P. Miele, *Macromolecules* **40**, 1018 (2007)
25. Y. Prosanov, F.F. Matvienko, *Fizika tverdogo tela* (Physics Sol. State) **53**, 824 (2011)
26. V.N. Kuznetsova, M.G. Malkin, *J. Appl. Spectr.* **67**, 762 (2000)
27. A.D. Pomogailo, V.S. Savost'yanov, *Synthesis and Polymerization Metal-Containing Monomers* (CRC Press, Boca Raton, 1994)
28. A.D. Pomogailo, A.S. Rozenberg, G.I. Dzhardimalieva, *Ros. Khim. Zh. (Mendeleev Chem. J.)* **53**, 140 (2009)
29. A.S. Shteinberg, *Fast Reactions in Energetic Materials: High-Temperature Decomposition of Rocket Propellants and Explosives* (Fizmatlit, Moscow, 2006)
30. D.A. Frank-Kamenetskii, *Diffuziya i Teploperedacha v Khimicheskoi Kinetike* (Diffusion and Heat Transfer in Chemical Kinetics) (Nauka, Moscow, 1987)
31. T. Cordero, J.M. Rodriguez-Maroto, J. Rodriguez-Miraso, J.J. Rodriguez, *Thermochim. Acta* **164**, 135 (1990)
32. A.Q. Gu, Z.L. Yu, Y.B. Li, *J. Appl. Polym. Sci.* **110**, 61 (2008); **114**, 911 (2009)
33. I. Kaya, A. Solguntekin, *J. Appl. Polym. Sci.* **113**, 1994 (2009)
34. F. Yao, Q. Wu, D. Zhou, *J. Appl. Polym. Sci.* **114**, 834 (2009)
35. J. Malek, *Thermochim. Acta* **355**, 239 (2000)

36. H. Pehlivan, F. Özmihiçi, T. Tihminlioglu, D. Balcöse, J. Appl. Polym. Sci. **90**, 3069 (2003)
37. H. Ismail, Z. Mohamad, A.A. Bakar, Polym. Plastics. Technol. Eng. **42**, 81 (2003)
38. H.S. Kim, H.S. Yang, H.J. Kim, H.J. Park, J. Therm. Anal. Calor. **76**, 395 (2004)
39. S.C. Turmanova, S.D. Genieva, A.S. Dimitrova, L.T. Vlaev, Express Polym. Lett. **2**, 133 (2008)
40. P.K. Roy, P. Surekha, C. Rajagopal, V. Choudhary, Express Polym. Lett. **1**, 208 (2007)
41. P.K. Roy, P. Surekha, R. Raman, V. Choudhary, J. Appl. Polym. Sci. **99**, 236 (2006)
42. O.F. Ozturk, D.A. Koze, A.N. Ay, B. Zumreoglu–Karan, J. Appl. Polym. Sci. **98**, 490 (2005)
43. F. Dogan, O.F. Ozturk, M. Yurekli, A.N. Ay, D.A. Koze, J. Appl. Polym. Sci. **106**, 1129 (2007)
44. R. Tannenbaum, S. King, J. Lecy, M. Tirrell, L. Potts, Langmuir **20**, 4507 (2004)
45. F. Yao, Q. Wu, D. Zhou, J. Appl. Polym. Sci. **114**, 834 (2009)
46. J. Opfermann, J. Therm. Anal. Calor. **60**, 641 (2000)
47. J. Opfermann, E. Kaisersberger, H.J. Flammersheim, Thermochim. Acta **391**, 119 (2002)
48. G.E. Zaikov, *Degradation and Stabilization of Polymers* (Nova Science Publication, New York, 1999)
49. G.E. Zaikov, Soros. Obrazov. Zh. (Soros Educat. J.) **12**, 48 (2000)
50. S.S. Batsanov, *Eksperimental'nye Osnovy Strukturnoi Khimii (Spravochnoe Posobie)* [Experimental Foundations of Structural Chemistry (The Handbook)]. (Izd. Standartov, Moscow, 1986)
51. R.A. Lidin, L.L. Andreeva, V.A. Molochko, *Spravochnik po Neorganicheskoi Khimii. Konstanty Neorganicheskikh Veshchestv* (The Handbook on Inorganic Chemistry. The Constants of Inorganic Substances). (Khimiya, Moscow, 1987)
52. N. Kubota, C. Serizawa, Propellants Explos. Pyrotech. **12**, 145 (1987)
53. T. Kuwahara, S. Matsuo, N. Shinozaki, Propellants. Explos. Pyrotech. **22**, 198 (1997)
54. A. Gocmez, A.G. Yilmaz, F. Pekel, Propellant. Explos. Pyrotech **24**, 65 (1999)
55. E.-C. Koch, A. Dochnahl, Propellant. Explos. Pyrotech. **25**, 37 (2000)
56. A. Gocmez, A.G. Yilmaz, F. Pekel, Propellants Explos. Pyrotech. **24**, 65 (1999)
57. S. Cudziło, A.W. Trzcilski, Polym. J. Appl. Chem. **26**, 25 (2001)
58. A. Huczko, H. Lange, G. Chojecki, S. Cudziło, Y.Q. Zhu, H.W. Kroto, D.R.M. Walton, J. Phys. Chem. B **107**, 2519 (2003)
59. V.V. Boldyrev, *Metody Izucheniya Kinetiki Termicheskogo Razlozheniya Tverdykh Veshchestv* (The Methods of Investigation of Kinetics of Thermal Decomposition of Solids) (Tomsk University, Tomsk, 1958)
60. V.A. Logvinenko, F. Paulik, I. Paulik, *Kvaziravnovesnaya Termogravimetriya v Sovremennoi Neorganicheskoi Khimii* (Quasi-equilibrium Thermogravimetry in Modern Inorganic Chemistry) (Nauka, Novosibirsk, 1989)
61. Z.A. Vnutschikh, A.A. Fedorov, Y.S. Chekryshkin, Z.R. Ismagilov, M.A. Kerzhentsev, Khim. Inter. Ustoich. Razv **9**, 621 (2001)
62. B. Delmon, *Introduction a la Cinetique Heterogene* (Technip, Paris, 1969)
63. J. Paulik, F. Paulik, Thermochim. Acta **100**, 23 (1986)
64. P.J. Haines, *Thermal Methods of Analysis* (Blackie Academic and Professional, London, 1995)
65. S.V. Pol, V.S. Pol, A. Gedanken, Chem. Eur. J. **10**, 4467 (2004)
66. J.Q. Sun, X.P. Shen, L.J. Guo, K.M. Chen, Q. Liu, Phys. E. Low Dimens. Syst. Nanostr. **41**, 1527 (2009)
67. J.Q. Sun, X.P. Shen, K.M. Chen, Q. Liu, W. Liu, Solid State Commun. **147**, 501 (2008)
68. M. Bowtell, Adhes. Age. **40**, 62 (1997)
69. G.P. Shveikin, I.V. Nikolaenko, Theor. Found. Chem. Eng. **43**, 553 (2009)
70. F. Antolini, A. Ghezlbash, C. Esposito, E. Trave, L. Tapfer, B.A. Korgel, Mater. Lett. **60**, 1095 (2006)
71. S. Cudziło, M. Bystrzejewski, H. Lange, A. Huczko, Carbon **43**, 1778 (2005)
72. D. Hulicova, K. Hosoi, S. Kuroda, A. Oya, Carbon **43**, 1246 (2005)

73. J. Delaunay, T. Hayashi, M. Tomita, S. Hirono, S. Umemura, *Appl. Phys. Lett.* **71**, 3427 (1997)
74. M.K. Corbierre, J. Beerens, R.B. Lennox, *Chem. Mater.* **17**, 5774 (2005)
75. B.F.G. Johnson, K.M. Sanderson, D.S. Shephard, D. Ozkaya, W.Z. Zhou, H. Ahmed, M.D.R. Thomas, L. Gladden, M. Mantle, *Chem. Commun.* 1317 (2000)
76. N.A. Tikhonov, I.V. Arkhangelsky, S.S. Belyaev, A.T. Matveev, *Thermochim. Acta* **486**, 66 (2009)
77. S.S. Belyaev, I.V. Arkhangelsky, I.V. Makarenko, *Thermochim. Acta* **507–508**, 9 (2010)
78. Y. Prosanov, F.F. Matvienko, *Fizika tverdogo tela (Physics Sol. State)* **52**(10), 2056 (2010)
79. S. Joden, *J. Chem. Chem. Eng.* **3**, 7 (2009)
80. L.M. Zemtsov, G.P. Karpacheva, M.N. Efimov, D.G. Muratov, K.A. Bagdasarova, *Vysokomol. Soedin. Ser. A* **48**, 977 (2006)
81. L.V. Kozhitov, A.V. Kostikova, V.V. Kozlov, V.I. Khursa, *Izv. VUZ'ov. Materialy elektronnoi tekhniki.* (3), 48 (2011)
82. L.V. Kozhitov, A.V. Kostikova, V.V. Kozlov, M.Ph. Bulatov, *J. Nanoelectron. Optoelectron.* (7), 419 (2012)
83. Y.C. Kang, S.B. Park, I.W. Lenggoro, K. Okuyama, *J. Mater. Res.* **14**, 2611 (1999)
84. I.W. Lenggoro, T. Hata, F. Iskandar, *J. Mater. Res.* **15**, 733 (2000)
85. H.K. Kammler, L. Mädler, S.E. Pratsinis, *Chem. Eng. Technol.* **24**, 583 (2001)
86. E.K. Athanassiou, R.N. Grass, W.J. Stark, *Nanotechnology* **17**, 1668 (2006)
87. M.T. Swihart, *Curr. Opin. Colloid Interf. Sci.* **8**, 127 (2003)
88. J. Lacson, *Inorganic Zinc Chemicals. Chemical Economics Handbook* (electronic release) (SRI International, Menlo Park, 2000)
89. C. Pacholski, A. Kornowski, H. Weller, *Angew. Chem. Int. Ed.* **41**, 1188 (2002)
90. L. Schmidt-Mende, J.L. MacManus-Driscoll, *Mater. Today* **10**, 40 (2007)
91. S.J. Peatron, D.P. Norton, *Prog. Mater. Sci.* **50**, 293 (2005)
92. K. Hara, T. Horiguchi, T. Kinoshita, *Adv. Mater.* **15**, 838 (2003)
93. L.E. Creene, W. Law, J. Goldberger, *Angew. Chem. Int. Ed.* **42**, 3031 (2003)
94. T.-J. Hsueh, C.-L. Hsu, *Sensors Actuators B. Chem.* **131**, 572 (2008)
95. A. Khan, M.E. Kordesch, *Physica E* **33**, 88 (2006)
96. M.D. Liedekerke, *Pigment, Inorganic, 2.3 Zinc Oxide (Zincwhite). Ullmann's Encyclopedia of Industrial Chemistry*, 6th edn. (Wiley-VCH Verlag GmbH, Weinheim, 2001)
97. T. Tani, L. Madler, S.E. Pratsinis, *J. Nanopart. Res.* **4**, 337 (2002)
98. R. Riedel, A. Gurlo, E. Ionescu, *Chem. Unserer Zeit.* **44**, 208 (2010)
99. N. Reuge, B. Caussat, N. Joffin, J. Dexpert-ghys, M. Verelst, H. Dexpert, *AIChE* **54**, 394 (2008)
100. D.S. Jung, S.B. Park, Y.C. Kang, *Korean J. Chem. Eng.* **27**, 1621 (2010)
101. J.-C. Lin, J.W. Gentry, *J. Aerosol Sci.* **31**(Supl.1), 797 (2000)
102. N. Reuge, B. Caussat, *Comput Chem. Eng.* **31**, 1088 (2007)
103. J.R. Sohn, Y.C. Kang, H.D. Park, *Jpn. J. Appl. Phys.* **41**, 3006 (2002)
104. H.S. Roh, Y.C. Kang, H.D. Park, S.B. Park, *Appl. Phys. A.* **76**, 241 (2003)
105. I.W. Lenggoro, Y. Itoh, K. Okuyama, T.O. Kim, *J. Mater. Res.* **19**, 3534 (2004)
106. W.-N. Wang, A. Purwanto, K. Okuyama, in *Handbook of Atomization and Sprays*, ed. by N. Ashgriz (Springer Sci. Business Media, LLC, New York, 2011), p. 861
107. Y.C. Kang, Y.S. Chung, S.B. Park, *J. Am. Ceram. Soc.* **82**, 2056 (1999)
108. K. Okuyama, I.W. Lenggoro, *Chem. Eng. Sci.* **58**, 537 (2003)
109. W.-N. Wang, I.W. Lenggoro, Y. Terashi, T.O. Kim, K. Okuyama, *Mat. Sci. Eng. B.* **123**, 194 (2005)
110. Y.C. Kang, S.B. Park, *Mater. Res. Bull.* **35**, 1143 (2000)
111. W.-N. Wang, I.W. Lenggoro, Y. Terashi, Y.C. Wang, K. Okuyama, *J. Mater. Res.* **20**, 2873 (2005)
112. I.W. Lenggoro, Y. Itoh, N. Iida, K. Okuyama, *Mater. Res. Bull.* **38**, 1819 (2003)
113. N.A. Luechinger, E.K. Athanassiou, W.J. Stark, *Nanotechnology* **19**, 445201 (2008)

114. G.B. Manelis, G.M. Nazin, Y.I. Rubtsov, V.A. Strunin, *Termicheskoe Razlozhenie i Gorenie Vzryvchatykh Veshchestv i Porokhov* (Nauka, Moscow, 1996)
115. A. Pivkina, P. Ulyanova, Y. Frolov, S. Zavyalov, J. Schoonman, *Propellant. Explor. Pyrotech.* **29**, 39 (2004)
116. G. Singh, D.K. Pandey, *Propellant. Explor. Pyrotech.* **28**, 231 (2003)
117. G. Sing, S.P. Felix, *Combust. Flame* **132**, 422 (2003)
118. M. Stefanescu, V. Sasca, M. Birzescu, *J. Therm. Anal. Calor.* **72**, 515 (2003)
119. M. Birzescu, M. Niculescu, R. Dumitru, P. Budrugaec, E. Segal, *J. Therm. Anal. Calor.* **94**, 297 (2008)
120. C.A. Strydom, C.P.J. Vuuren, *J. Therm. Anal.* **32**, 157 (1987)
121. M. Han, N.-E. Shi, W.-L. Zhang, B.-J. Li, J.-H. Sun, K.-J. Chen, J.-M. Zhu, X. Wang, Z. Xu, *Chem. Eur. J.* **14**, 1615 (2008)
122. M.A. El-Sayed, *Acc. Chem. Res.* **34**, 257 (2001)
123. Z.L. Wang, J.H. Song, *Science* **312**, 242 (2006)
124. H.P. Zho, Y.W. Zhang, H.X. Mai, X. Sun, Q. Liu, W.G. Song, C.H. Yan, *Chem. Eur. J.* **14**, 3380 (2008)
125. N. Joffin, *J. Lumin.* **113**, 249 (2005)
126. N. Joffin, B. Gaillier, J. Dexpert-Ghys, M. Verelst, G. Baret, A. Garsia, P. Guillot, G. Gali, R. Mauricot, S. Schamm, *J. Phys. D* **38**, 3261 (2005)
127. S.N. Rishikeshi, S.S. Joshi, *J. Therm. Anal. Calor.* **109**, 1473 (2012)
128. Z.W. Pan, Z.R. Dai, Z.L. Wang, *Science* **291**, 1047 (2001)
129. Z.X. Deng, C. Wang, X.M. Sun, Y.D. Li, *Inorg. Chem.* **41**, 869 (2002)
130. Z. Chen, L. Gao, *Mater. Res. Bull.* **42**, 1657 (2007)
131. C.A. O'Connell, D.J. Dollimore, *Thermochim. Acta* **357/358**, 79 (2000)
132. G. Reichmuth, E. Dubler, *Thermochim. Acta* **85**, 485 (1985)
133. R. Sasikala, S.K. Kulshreshtha, *J. Therm. Anal. Calor.* **78**, 723 (2004)
134. A.-S. Malik, M.J. Duncan, P.G. Bruce, *J. Mater. Chem.* **13**, 2123 (2003)
135. R.L. Frost, W. Martens, M.O. Adebajo, *J. Therm. Anal. Calor.* **81**, 351 (2005)
136. A. Valor, E. Reguera, E. Torres- Garcia, S. Mendoza, F. Sanchez-Sinencio, *Thermochim. Acta* **389**(133) (2002)
137. A. Valor, E. Reguera, F. Sanchez-Sinencio, *Powder Diffraction* **17**, 13 (2002)
138. W.Y. Yu, J.C. Falkner, C.T. Yavuz, V.L. Colvin, *Chem. Comm.* **20**, 2306 (2004)
139. H. Wang, X. Jiao, D. Chen, *J. Phys. Chem. C* **112**, 18793 (2008)
140. J. Park, E. Kang, S.U. Son, H.M. Park, M.K. Lee, J. Kim, K.-W. Kim, H.-J. Noh, J.-H. Park, C.J. Bae, J.-G. Park, T. Hyeon, *Adv. Mater.* **17**, 429 (2005)
141. Y. Goto, K. Taniguchi, T. Omata, S. Otsuka-Yao-Matsuo, *Chem. Mater.* **20**, 4156 (2008)
142. B.S. Randhawa, H.S. Dosanjh, N. Kumar, *J. Therm. Anal. Calor.* **95**, 75 (2009)
143. B.S. Randhawa, K.J. Sweety, *J. Radioanal. Nucl. Chem.* **247**, 513 (2001)
144. B.S. Randhawa, M. Kaur, *J. Radioanal. Nucl. Chem.* **261**, 569 (2004)
145. B.S. Randhawa, M. Kaur, in *Proceed. the 29th Int. Conf. on the Applications of the Mössbauer Effect (ICAME 2007) 14–19 October 2007*, ed. by N.S. Gajbhiye, S. K. Date (Springer, Dordrecht, 2008), p. 1329
146. A.S. Rozenberg, E.I. Aleksandrova, *Izv. Akad. Nauk. Ser. Khim.* **72** (1996)
147. A.S. Rozenberg, N.V. Chukanov, *Izv. Akad. Nauk, Ser. Khim.* **350** (1996)
148. A.S. Rozenberg, V.R. Stepanov, *Izv. Akad. Nauk, Ser. Khim.* **1406** (1996)
149. A.S. Rozenberg, *Doctoral Thesis in Chemical Sciences* (Institute of Problems of Chemical Physics, Russian Academy of Sciences, Chernogolovka, 1997)
150. S.V. Davidovich, A.A. Veher, E.A. Gusev, *Thermochim. Acta* **89**, 383 (1985)
151. I.V. Fedorova, V.A. Shurov, A.A. Fedorov, M.S. Gaisinovich, *Zh. Prikl. Khim.* **65**, 736 (1992)
152. I.V. Arkhangel'skii, L.N. Komissarova, A. Gorski, A. Kras'nicka, *J. Therm. Anal.* **32**, 1234 (1987)
153. A. Gorski, A. Kras'nicka, *J. Therm. Anal.* **32**, 1345 (1987)

154. K. Muraishi, T. Takano, K. Nagase, N. Tanaka, *J. Inorg. Nucl. Chem.* **43**, 2293 (1981)
155. A.S. Rozenberg, G.I. Dzhardimalieva, A.D. Pomogailo, *Dokl. Akad. Nauk* **356**, 66 (1997)
156. B.B. Bokhonov, Y.M. Yukhin, *Zh. Neorg. Khim.* **52**, 993 (2007)
157. V.V. Kireev, L.N. Demyanets, L.E. Li, V.V. Artemov, *Neorg. Mater.* **46**, 193 (2010)
158. R.-C. Wang, C.-C. Tsai, *Appl. Phys. A* **94**, 241 (2009)
159. S. Aghabeygi, F. Bigdeli, A. Morsali, *J. Inorg. Organomet. Polym.* **22**, 526 (2012)
160. C.S. Li, Y.N. Li, Y.L. Wu, B.S. Ong, R.O. Loutfy, *Sci. China. Ser E-Tech. Sci.* **51**, 2075 (2008)
161. W.J. Scharmach, R.D. Bucher, V. Papavassiliou, P. Pacouloute, M.T. Swihart, *Aerosol. Sci. Technol.* **44**, 1083 (2010)
162. E. Tirosh, G. Shemer, G. Markovich, *Chem. Mater.* **18**, 465 (2006)
163. N. Bao, L. Shen, Y. Wang, P. Padhan, A. Gupta, *J. Am. Chem. Soc.* **129**, 12374 (2007)
164. J.H. Park, N.M. Hwang, T. Hyeon, *Nat. Mater.* **3**, 891 (2004)
165. S. Sun, H. Zeng, D.B. Robinson, S. Raoux, P.M. Rice, S.X. Wang, G. Li, *J. Am. Chem. Soc.* **126**, 273 (2004)
166. K.J. Lee, B.H. Jun, J. Choi, Y.I. Lee, J. Joung, Y.S. Oh, *Nanotechnology* **18**, 335601 (2007)
167. N. Yang, K. Aoki, *J. Phys. Chem.* **109**, 23911 (2005)
168. M. Yamamoto, Y. Kashiwagi, M. Nakamoto, *Langmuir* **22**, 8581 (2006)
169. Y. Kashiwagi, M. Yamamoto, M. Nakamoto, *J. Colloid Interface Sci.* **300**, 16933 (2006)
170. M. Chen, Y.G. Feng, X. Wang, T.C. Li, J.Y. Zhang, D.J. Qian, *Langmuir* **23**, 5296 (2007)
171. S.J. Lee, S.W. Han, K. Kim, *Chem. Commun.* **5**, 442 (2002)
172. S. Navaladian, B. Viswanathan, R.P. Viswanath, T.K. Varadarajan, *Nanoscale Res. Lett.* **2**, 44 (2007)
173. L. D'Urso, V. Nicolosi, G. Compagnini, O. Puglisi, *Appl. Surf. Sci.* **226(c)**, 131 (2004)
174. P. Uznanski, E. Bryszewska, *J. Mater. Sci.* **45**, 1547 (2010)
175. B. Wiley, Y.G. Sun, Y. Xia, Y. Acc, *Chem. Res.* **40**, 1067 (2007)
176. A. Mehrani, A. Morsali, *J. Inorg. Organomet. Polym. Mater.* **21**, 476 (2011)
177. D. Dollimore, D.L. Griffiths, *J. Thermal Anal.* **2**, 229 (1970)
178. B. Malecka, E.D. Ciesla, A. Malechi, *J. Therm. Anal. Calor.* **68**, 819 (2002)
179. O. Carp, L. Patron, G. Marinescu, G. Pascu, P. Budrugu, M. Brezeanu, *J. Therm. Anal. Calor.* **72**, 263 (2003)
180. A. Angermann, J. Töpfer, *J. Mater. Sci.* **43**, 5123 (2008)
181. V.V. Boldyrev, *Thermochim. Acta.* **388**, 63 (2002)
182. R.L. Frost, M.L. Weier, *J. Therm. Anal. Calor.* **75**, 277 (2004)
183. W. Zhou, K. Tang, S. Zeng, Y. Qi, *Nanotechnology* **19**, 065602 (2008)
184. R. Zboril, I. Medrik, J. Pechousek, C. Gregor, *J. Am. Chem. Soc.* **129**, 10929 (2007)
185. M. Hermanek, M.A. Mohamed, A.K. Galwey, S.A. Halawy, *Thermochim. Acta* **29**, 57 (2005)
186. M. Hermanek, R. Zboril, M. Mashlan, L. Machala, O. Schneeweiss, *J. Mater. Chem.* **16**, 1273 (2006)
187. O.I. Gyrdasova, V.N. Krasilnikov, G.V. Bazuev, *Z. Neorg. Khim.* **54**, 1097 (2009)
188. M. Yin, S. O'Brien, *J. Am. Chem. Soc.* **125**, 10180 (2003)
189. J. Park, E. Kang, C.J. Bae, J.G. Park, H.J. Noh, J.Y. Kim, J.H. Park, H.M. Park, T. Hyeon, *J. Phys. Chem. B* **108**, 13594 (2004)
190. F. Jiao, A. Harrison, P.G. Bruce, *Angew. Chem. Int. Ed.* **46**, 3946 (2007)
191. F. Jiao, A. Harrison, P.G. Bruce, *Angew. Chem. Int. Ed.* **46**, 3946 (2007)
192. Y.-P. Du, Y.-P. Du, Y.-W. Zhang, L.-D. Sun, C.-H. Yan, *J. Phys. Chem. C* **113**, 6521 (2009)
193. A.H. Lu, E.L. Salabas, F. Schüth, *Angew. Chem. Int. Ed.* **46**, 1222 (2007)
194. Y.-P. Du, Y.-W. Zhang, L.-D. Sun, C.-H. Yan, *J. Phys. Chem. C* **113**, 6521 (2009)
195. S. Sun, H. Zeng, *J. Am. Chem. Soc.* **124**, 8204 (2002)
196. J. Park, K. An, Y. Hwang, J.G. Park, H.J. Noh, J.Y. Kim, J.H. Park, N.M. Hwang, T. Hyeon, *Nat. Mater.* **3**, 891 (2004)
197. M.M. Lin, D.K. Kim, *J. Nanopart. Res.* **14**, 688 (2012)

198. K. Liu, H. You, G. Jia, Y. Zheng, Y. Song, M. Yang, Y. Huang, H. Zhang, *Crystal Growth Design* **9**, 3519 (2009)
199. B.L. Chen, Y. Yang, F. Zapata, G.N. Lin, G.D. Qian, E.B. Lobkovsky, *Adv. Mater.* **19**, 1693 (2007)
200. J.R. William, M.L. Kathryn, H.Y. An, W.L. Lin, W.B. Lin, *J. Am. Chem. Soc.* **128**, 9024 (2006)
201. V.G. Pol, O. Palchik, A. Gedanken, I. Felner, *J. Phys. Chem. B* **106**, 9737 (2002)
202. K.-L. Wong, G.-L. Law, M.B. Murphy, P.A. Tanner, W.-T. Wong, P.K. Lam, L.M. Hon-Wah, *Inorg. Chem.* **47**, 5190 (2008)
203. L. Zhang, J. Luo, M. Wu, H. Jiu, Q.W. Chen, *Mater. Lett.* **61**, 4452 (2007)
204. H. Yang, D. Zhang, L. Shi, J. Fang, *Acta Mater.* **56**, 955 (2008)
205. J. Goldberg, R. Fan, P.D. Yang, *Acc. Chem. Res.* **39**, 239 (2006)
206. V.G. Pol, M. Popa, S. Acharya, K. Ariga, P. Thiyagarajan, *Inorg. Chem.* **48**, 5569 (2009)
207. N. Imanaka, T. Masui, Y. Mayama, K. Koyabu, *J. Solid State Chem* **178**, 3601 (2005)
208. K. Koyabu, T. Masui, S. Tamura, N. Imanaka, *J. Alloys Comp.* **408**, 867 (2006)
209. V.G. Pol, J.M. Calderon-Moreno, P. Thiyagarajan, *Langmuir* **24**, 13640 (2008)
210. M.C. Alves, G. Tourillon, *J. Phys. Chem.* **100**, 7566 (1996)
211. C.-J. Cheng, C.-C. Lin, R.-K. Chiang, C.-R. Lin, I.S. Lyubutin, E.A. Alkaev, H.-Y. Lai, *Crystal Growth Des.* **8**, 877 (2008)
212. M. Epifani, J. Arbiol, R. Díaz, M.J. Perálvarez, P. Siciliano, J.R. Morante, *Chem. Mater.* **17**, 6468 (2005)
213. E.V. Shevchenko, D.V. Talapin, N.A. Kotov, S. O'Brien, C.B. Murray, *Nature (London)* **439**, 55 (2006)
214. H. Hiramatsu, F.E. Osterloh, *Chem. Mater.* **16**, 2509 (2004)
215. L.-M. Lacroix, S. Lachaize, A. Falqui, M. Respaud, B. Chaudret, *J. Am. Chem. Soc.* **131**, 549 (2009)
216. Y. Wang, H. Yang, *Chem. Commun.* **2545** (2006)
217. P. Uznanski, C. Amiens, B. Chaudret, E. Bryszewska, *Polym. J. Chem.* **80**, 1845 (2006)
218. I. Quiros, M. Yamada, K. Kubo, J. Mizutani, M. Kurihara, H. Nishihara, *Langmuir* **18**, 1413 (2002)
219. N. Cordente, M. Respaud, F. Senocq, M.-J. Casanove, C. Amiens, B. Chaudret, *Nano Lett.* **1**, 565 (2001)
220. N. Wu, L. Fu, M. Su, M. Aslam, K.C. Wong, V.P. Dravid, *Nano Lett.* **4**, 383 (2004)
221. M. Salavati-Niasari, F. Davar, M. Mazaheri, M. Shaterian, *J. Magn. Magn. Mater.* **320**, 575 (2008)
222. J. Park, E. Kang, S.U. Son, H.M. Park, M.K. Lee, J. Kim, K.W. Kim, H.-J. Noh, J.-H. Park, C.J. Bae, J.-G. Park, T. Hyeon, *Adv. Mater.* **17**, 425 (2005)
223. P.R. Ponminiessary, A. Vasudevan, M. Sebastian, U.A. Chennampilly, K.M.Y. Karukapadath, *J. Therm. Anal. Calor.* **100**, 733 (2010)
224. K.S. Rejitha, S. Mathew, *J. Therm. Anal. Calor.* **93**, 213 (2008)
225. Y. Hanifehpour, B. Mirtamizdoust, A.R. Farzam, S.W. Joo, *J. Inorg. Organomet. Polym.* **22**, 957 (2012)
226. V.G. Pol, L.L. Daemen, S. Vogel, G. Chertkov, *Ind. Eng. Chem. Res.* **49**, 920 (2010)
227. P. Hermankova, M. Hermanek, R. Zboril, *Eur. J. Inorg. Chem.* **1110** (2010)
228. A. Shavel, B. Rodrigues-Gonzalez, J. Pacifico, M. Spasova, M. Farle, L.M. Liz-Marzan, *Chem. Mater.* **21**, 1326 (2009)
229. Y. He, Y. Sahoo, S. Wang, H. Luo, P.N. Prasad, M.T. Swihart, *J. Nanoparticle Res.* **8**, 335 (2006)
230. D. Czakis-Sulikowska, J. Radwańska-Doczekalska, M. Markiewicz, M. Pietrzak, *J. Therm. Anal. Calor.* **93**, 789 (2008)
231. D. Kumar, I.P.S. Kapoor, G. Singh, N. Geol, U.P. Singh, *J. Therm. Anal. Calor.* **107**, 325 (2011)
232. N. Parveen, R. Nazir, M. Mazhar, *J. Therm. Anal. Calor.* **111**, 93 (2013)

233. R. Nazir, M. Mazhar, T. Wakeel, M.J. Akhtar, M. Siddique, M. Nadeem, N.A. Khan, M.R. Shah, *J. Therm. Anal. Calor.* **110**, 707 (2012)
234. A.D. Pomogailo, A.S. Burlov, N.D. Golubeva, L.A. Petrova, S.A. Mishenko, S.I. Pomogailo, G.I. Dzhardimalieva, *A.D. Garnovskii, Neorg. Mater.* **47**, 969 (2011)
235. T. Hyeon, Y. Chung, J. Park, S.S. Lee, Y.-W. Kim, B.H. Park, *J. Phys. Chem. B* **106**, 6831 (2002)
236. M.M. Amini, O. Sadeghi, S.W. Ng, *J. Inorg. Organomet. Polym.* **23**, 826 (2013)
237. X. Wang, X.Y. Chen, L.S. Gao, H.G. Zheng, Z. Zhang, Y.T. Qian, *J. Phys. Chem. B* **108**, 16401 (2004)
238. J.Z.L. Zhang, H.R. Geng, L.S. Zheng, B. Du, *J. Alloys Compd.* **392**, 317 (2005)
239. M. Wang, C.M. Liu, H.Z. Zhang, C.P. Chen, L. Guo, *Appl. Phys. Lett.* **85**, 2080 (2004)
240. A. Khansari, M. Salavati-Niasari, A.K. Babaheydari, *J. Clust. Sci.* **23**, 557 (2012)
241. F. Mohandes, F. Davar, M. Salavati-Niasari, *J. Magn. Magn. Mater.* **322**, 872 (2010)
242. A. Khansari, M. Enhessari, M. Salavati-Niasari, *J. Clust. Sci.* **24**, 289 (2013)
243. J.V.D.S. Araujo, R.V. Ferreira, M.I. Yoshida, V.M.D. Pasa, *Solid State Sci.* **11**, 1673 (2009)
244. A.V. Maciel, W.N. Mussel, V.M.D. Pasa, *Mat. Sci. Appl.* **1**, 279 (2010)
245. M. Salavati-Niasari, M. Dadkhah, M.R. Nourani, A.A. Fazl, *J. Clust. Sci.* **23**, 1011 (2012)
246. A.D. Pomogailo, *Ros. Khim. Zh. (Mendeleev Chem. J.)* **46**, 64 (2002)
247. A.D. Pomogailo, V.S. Savost'yanov, *Synthesis and Polymerization Metal-Containing Monomers* (CRC Press, Boca Raton, 1994)
248. Y.Y. Wang, Q. Shi, Q.Z. Shi, Y.C. Gao, X. Hou, *Polyhedron* **19**, 891 (2000)
249. Y.Y. Wang, Q. Shi, Q.Z. Shi, *Acta Chim. Sinica* **58**, 675 (2000)
250. G.I. Dzhardimalieva, A.D. Pomogailo, *Usp. Khim.* **77**, 270 (2008); *Russ. Chem. Rev.* **77**, 259 (2008)
251. A.D. Pomogailo, G.I. Dzhardimalieva, *Monomernye I Polimernye Karboksilyaty Metallov* (Monomeric and Polymeric Metal Carboxylates) (Fizmatlit, Moscow, 2009)
252. V.A. Shershnev, G.I. Dzhardimalieva, D.P. Kiryukhin, V.A. Zhorin, A.D. Pomogailo, *Izv. RAN, Ser. Khim.* 1649 (2013)
253. J. Skupiska, H. Wilezura, H. Boniuk, *J. Therm. Anal.* **31**, 1017 (1986)
254. A.S. Rozenberg, G.I. Dzhardimalieva, A.D. Pomogailo, *Polym. Adv. Technol.* **9**, 527 (1998)
255. Z. Wojtczak, A. Gronowski, *J. Therm. Anal.* **36**, 2357 (1990)
256. P.A. Vasil'ev, A.L. Ivanov, A.N. Glebov, *Zh. Obshch. Khim.* **68**, 535 (1998)
257. J.M. Filipović, L. Katsicas, I.G. Popović, S.L. Velickovic, T.A. Djakov, D.M. Petrovic-Djakov, *J. Therm. Anal.* **49**, 335 (1997)
258. B.S. Randhawa, K.J. Sweetey, M. Kaur, J.M. Greneche, *J. Therm. Anal. Calor.* **75**, 101 (2004)
259. I.C. McNeill, A. Alston, *Angew. Makromol. Chem.* **261/262**, 157 (1998)
260. M. Badea, R. Olar, D. Marinescu, E. Segal, A. Rotaru, *J. Therm. Anal. Calor.* **88**, 317 (2007)
261. M. Zulfiqar, R. Hussain, S. Zulfiqar, D. Mohammad, I.C. McNeill, *Polymer Degrad. Stability* **51**, 167 (1996)
262. M. Badea, R. Jlar, D. Marinescu, G. Vasil, *J. Therm. Anal. Calor.* **80**, 683 (2005)
263. E.I. Aleksandrova, G.I. Dzhardimalieva, A.S. Rozenberg, A.D. Pomogailo, *Izv. Akad. Nauk. Ser. Khim.* 303 (1993)
264. E.I. Aleksandrova, G.I. Dzhardimalieva, A.S. Rozenberg, A.D. Pomogailo, *Izv. Akad. Nauk. Ser. Khim.* 308 (1993)
265. A.S. Rozenberg, G.I. Dzhardimalieva, N.V. Chukanov, A.D. Pomogailo, *Kolloid. Zh.* **67**, 57 (2005)
266. A.S. Rozenberg, E.I. Aleksandrova, G.I. Dzhardimalieva, A.N. Titkov, A.D. Pomogailo, *Izv. Akad. Nauk, Ser. Khim.* 1743 (1993)
267. A.S. Rozenberg, E.I. Aleksandrova, G.I. Dzhardimalieva, N.V. Kir'yakov, P.E. Chizhov, V.I. Petinov, A.D. Pomogailo, *Izv. Akad. Nauk, Ser. Khim.* 885 (1995)
268. A.D. Pomogailo, A.S. Rozenberg, G.I. Dzhardimalieva, Metal-containing polymers as precursors for the production of ferromagnetic and superconductive materials, in *Metal-*

- Containing Polymers Materials*, ed. by C.U. Pittman, C.E. Carraher Jr., M. Zeldin, B. Culberston (Plenum Press, New York, 1996), p. 313
269. A.S. Rozenberg, E.I. Aleksandrova, I.P. Ivleva, G.I. Dzhardimalieva, A.V. Raevskii, O.I. Kolesova, I.E. Uflyand, A.D. Pomogailo, *Izv. Akad. Nauk, Ser. Khim.* **265** (1998)
270. A.T. Shuvaev, A.S. Rozenberg, G.I. Dzhardimalieva, N.P. Ivleva, V.G. Vlasenko, T.I. Nedoseikina, T.A. Lyubeznova, I.E. Uflyand, A.D. Pomogailo, *Izv. Akad. Nauk, Ser. Khim.* **1505** (1998)
271. G.I. Dzhardimalieva, *Doctoral Thesis in Chemical Sciences*. (Institute of Problems of Chemical Physics, Russian Academy of Sciences, Chernogolovka, Moscow Region, 2009)
272. M.J. Yang, Q.D. Ling, M. Hiller, X.Z. Fun, L.H. Wang, W.G. Zhang, *J. Polym. Sci. Part A: Polym. Chem.* **38**, 34055 (2000)
273. V.T. Panyushkin, A.A. Mastakov, N.N. Bukov, A.A. Nikolaenko, M.E. Sokolov, *J. Struct. Chem.* **45**, 167 (2004)
274. F. Ramos-Lara, A.C. Lira, M.O. Ramirez, M. Flores, R. Arroyo, V. Caldino, *J. Phys. Condens. Mater.* **18**, 7951 (2006)
275. D.V. Kolechko, F.A. Kolokolov, A.I. Offidi, A.A. Pikula, V.T. Panyushkin, I.E. Mikhailov, G.A. Dushenko, *Dokl. Chem. Part 2* **441**, 374 (2011)
276. M. Badea, R. Olar, D. Marinesu, G. Vasile, *J. Therm. Anal. Calor.* **92**(1), 205 (2008)
277. H.L. Wu, W. Ying, L. Pen, Y.C. Gao, K.B. Yu, *Synth. React. Inorg. Met.-Org. Nano-Met. Chem.* **34**, 1019 (2005)
278. H.L. Wu, Y.C. Gao, K.B. Yu, *Trans. Met. Chem.* **29**, 175 (2004)
279. H.L. Wu, Y.C. Gao, *J. Coord. Chem.* **59**, 137 (2006)
280. N.P. Porollo, Z.G. Aliev, G.I. Dzhardimalieva, N.N. Ivleva, I.E. Uflyand, A.D. Pomogailo, N.S. Ovanesyan, *Izv. AN, Ser. Khim.* **375** (1997)
281. B.S. Randhawa, M. Kaur, *J. Thermal. Anal. Calor.* **89**, 251 (2007)
282. P.S. Bassi, B.S. Randhawa, C.M. Khajuria, S. Kaur, *J. Thermal Anal.* **32**, 569 (1987)
283. S.N. Chvalun, *Priroda* (7), **22** (2000)
284. V.A. Sergeev, A.Y. Olenin, U.F. Titova, A.S. Kogan, A.Y. Vasil'ev, *Zh. Fiz. Khim.* **66**, 1921 (1992)
285. M.T. Reetz, W. Helbig, *J. Am. Chem. Soc.* **116**, 7401 (1994)
286. G.N. Gerasimov, V.A. Sochilin, S.N. Chvalun, L.V. Volkova, I.Y. Kardash, *Macromol. Chem. Phys.* **197**, 1387 (1996)
287. H. Hopf, G.N. Gerasimov, S.N. Chvalun, V.I. Rozenberg, E.L. Popova, E.V. Nikolaeva, S.A. Zavjalov, L.I. Trakhtenberg, *Adv. Mater.* **3**, 197 (1997)
288. E.V. Nikolaeva, S.A. Ozerin, A.E. Grigoriev, E.I. Grigoriev, S.N. Chvalun, G.N. Gerasimov, L.I. Trakhtenberg, *Mat. Sci. Eng. C-Bio* **8-9**, 217 (1999)
289. P.V. Morozov, E.I. Grigor'ev, S.A. Zav'yalov, V.G. Klimenko, S.N. Chvalun, *Polym. Sci. Ser. A* **54**, 330 (2012)
290. I.A. Boginskaya, A.V. Gusev, K.A. Mailyan, S.N. Ozerin, A.V. Pebalk, I.A. Ryzhikov, M.V. Sedova, S.N. Chvalun, *J. Comm. Tech. Electr.* **56**, 66 (2011)
291. V.V. Zagorskii, A.E. Nasonova, M.A. Petrukhina, G.B. Sergeev, *Vestn. Mosk. Univ., Ser. 2, Khim.* **36**, 159 (1995)
292. V.A. Sergeev, L.I. Vdovina, Y.V. Smetannikov, A.Y. Vasil'kov, V.N. Gurishev, *Vysokomol Soedin Ser. B* **34**, 50 (1992)
293. V.V. Zagorskii, S.V. Ivashko, M.A. Petrukhina, G.B. Sergeev, *Vestn. Mosk. Univ., Ser. 2, Khim.* **39**, 276 (1998)
294. P. Harris, S. Tsang, *Chem. Phys. Lett.* **293**, 53 (1998)
295. P. Serp, V. Corrias, P. Kaick *Appl. Catal. A* **253**, 337 (2003)
296. E.A. Mel'gunova, Y.M. Balabina, A.N. Shmakov, M.S. Mel'gunov, *Zh. Fiz. Khim.* **77**, 510 (2003)
297. O.K. Alekseeva, A.A. Kotenko, M.M. Chelin, *Membrany* **36**, 3 (2007)



298. O.K. Alekseeva, A.A. Kotenko, E.V. Nefedova, Yu.S. Nechaev, M.M. Chelin, in *Nanochastitsy v Kondensirovannykh Sredakh* (Nanoparticles in Condensed Media) (Belarus State University, Minsk, 2008), p. 154
299. V.M. Novotortsev, V.V. Kozlov, Y.M. Korolev, G.P. Karpacheva, L.V. Kozhitov, *Zh. Neorg. Khim.* **53**, 1097 (2008)
300. H. Nabika, M. Mizuhata, A. Kajinami, S. Deki, K. Akamatsu, *J. Electroanal. Chem.* **559**, 99 (2003)
301. G.P. Karpacheva, K.A. Bagdasarova, G.N. Bondarenko, L.H. Zemstov, D.G. Muratova, N.S. Perov, *Vysokomol. Soedin.* **51**, 2037 (2009)
302. H. Yasuda, S. Miyanaga, A. Nakamura, H. Sakai, *J. Inorg. Organometal. Polym.* **1**, 135 (1991)
303. N.L. Pocard, D.C. Pocard, D.C. Alsmeyer, R.L. McCreery, T.X. Neenan, M.R. Callstrom, *J. Am. Chem. Soc.* **114**, 769 (1992)
304. A.A. Shutilov, *Candidate Thesis in Chemical Sciences*. (Institute of Catalysis, Siberian Branch of the Russian Academy of Sciences, Novosibirsk, 2008)
305. S.R. Liu, *Carbon* **43**, 1550 (2005)
306. S. Liu, X. Tang, Y. Mastai, I. Felner, A. Gedanken, *J. Mater. Chem.* **10**, 2502 (2000)
307. L. Xu, W. Zhang, Q. Yang, Y. Ding, W. Yu, Y. Qian, *Carbon* **43**, 1090 (2005)
308. E.P. Sajitha, V. Prasad, S.V. Subramanyan, S. Eto, K. Takai, T. Enoki, *Carbon* **42**, 2815 (2004)
309. L.J. Zhi, Y.S. Hu, H.B. El, X. Wang, I. Lieberwirth, U. Kolb, J. Maier, K. Mullen, *Adv. Mater.* **20**, 1727 (2008)
310. X. Yan, T. Xu, G. Chen, X. Wang, H. Liu, S. Yang, *Appl. Phys. A* **81**, 197 (2005)
311. R.A. Arents, Y.V. Maksimov, I.P. Suzdalev, Y.D. Amerik, *Hyperfine Interact.* **56**, 167 (1999)
312. Y.B. Amerik, Y.M. Korolev, V.N. Rogovoi, *Neftekhimiya* **36**, 304 (1996)
313. Y.M. Korolev, A.L. Bykova, Y.B. Amerik, *Vysokomol. Soedin., Ser. B* **39**, 1856 (1997)
314. S.V. Pol, V.G. Pol, A. Gedanken, *J. Phys. Chem. C* **111**, 16781 (2007)
315. A. Gedanken, E. Luvchik, *Eur. J. Inorg. Chem.* **2471** (2008)
316. S.V. Pol, V.G. Pol, A. Frydman, G. Churilov, A. Gedanken, *J. Phys. Chem. B* **109**, 9495 (2005)
317. V.G. Pol, S.V. Pol, A. Gedanken, *Eur. J. Inorg. Chem.* **709** (2009)
318. A.B. Shishmakov, Y.V. Mikushina, A.S. Seleznev, O.V. Koryakova, M.S. Valova, L.A. Petrov, *Russ. J. Appl. Chem.* **81**, 2180 (2008)
319. E. Papastergiades, S. Argyropoulos, N. Rigakis, N.E. Kiratzis, *Ionics* **15**, 545 (2009)
320. V.V. Barelko, A.D. Pomogailo, G.I. Dzhardimalieva, S.I. Evstratova, A.S. Rozenberg, I.E. Uflyand, *Chaos* **9**, 342 (1999)
321. A.S. Rozenberg, A.V. Raevskii, E.I. Aleksandrova, O.I. Kolesova, G.I. Dzhardimalieva, A.D. Pomogailo, *Izv. Akad. Nauk, Ser. Khim.* 862 (2001)
322. G.I. Dzhardimalieva, A.D. Pomogailo, V.A. Volpert, *J. Inorg. Organometal. Polym.* **12**, 1 (2002)
323. E. Sowka, M. Leonowicz, B. Andrzejewski, A.D. Pomogailo, G.I. Dzhardimalieva, *J. Alloys Comp.* **423**, 123 (2006)
324. A.D. Pomogailo, G.I. Dzhardimalieva, *Vysokomol. Soedin. Ser. A* **46**, 437 (2004)
325. J.A. Pojman, I.P. Nagy, C. Salter, *J. Amer. Chem. Soc.* **115**, 11044 (1993)
326. V.S. Savost'yanov, A.D. Pomogailo, B.S. Selenova, D.A. Kritskaya, A.N. Ponomarev, *Izv. Akad. Nauk SSSR, Ser. Khim.* 768 (1990)
327. R.B. Morgunov, A.I. Dmitriev, G.I. Dzhardimalieva, A.D. Pomogailo, A.S. Rozenberg, Y. Tanimoto, M. Leonowicz, E. Sowka, *Fiz. Tv. Tela* **49**, 1436 (2007)
328. E. Sowka, M. Leonowicz, J. Kazmierczak, A. Slawska-Waniewska, A.D. Pomogailo, G.I. Dzhardimalieva, *Physica B* **384**, 282 (2006)
329. G.I. Dzhardimalieva, A.D. Pomogailo, N.D. Golubeva, S.I. Pomogailo, G.F. Novikov, O.S. Roshchupkina, A.S. Rozenberg, M. Leonowicz, *Kolloid. Zh.* **73**, 457 (2011)

330. A.D. Pomogailo, G.I. Dzhardimalieva, A.S. Rozenberg, V.A. Shershnev, M. Leonowicz, Russ. Chem. Bull. **60**, 1476 (2011)
331. M. Izydorzak, A. Skumiel, M. Leonowicz, M. Kaczmarek-Klinowska, A.D. Pomogailo, G.I. Dzhardimalieva, Int. J. Thermophys. **33**, 627 (2012)
332. N.D. Golubeva, B.K. Dyusenalin, B.S. Selenova, S.I. Pomogailo, A.K. Zharmagambetova, G.I. Dzhardimalieva, A.D. Pomogailo, Kinetika I Kataliz **52**, 250 (2011)
333. A.D. Pomogailo, G.I. Dzhardimalieva. J. Catal., 2013, 12 pages, <http://dx.doi.org/10.1155/2013/276210>
334. A.G. Merzhanov, V.N. Sanin, V.G. Yukhvid, Dokl. Akad. Nauk **371**, 38 (2000)
335. V.V. Ivanov, E.V. Stegno, V.P. Mel'nikov, L.M. Pushchaeva, J. Polym. Sci., Ser. A **40**, 1017 (2002)
336. L.P. Kholpanov, S.E. Zakiev, A.D. Pomogailo, Dokl. Akad. Nauk **395**, 211 (2004)
337. O. Gazit, R. Khalfin, Y. Cohen, R. Tannenbaum, J. Phys. Chem. C **113**, 576 (2009)
338. S.H. Joo, C.S. Jhoi, I. Oh, K.J. Wak, Z. Liu, O. Terasaki, R. Ryon, Nature (London) **412**, 5835 (2001)
339. X. Fan, H. Fei, D.H. Demaree, D.P. Brennan, J.M. John, S.R. Oliver, Langmuir **25**, 5835 (2009)
340. T.L. Hsiung, H.P. Wang, H.P. Lin, J. Phys. Chem. Solids **69**, 393 (2008)
341. Z. Liu, X. Sun, S. Xu, J. Lian, Z. Xiu, Q. Li, D. Huo, J.-G. Li, J. Phys. Chem. C **112**, 2353 (2008)
342. Y. Han, S. Li, X. Wang, Cryst. Res. Technol. **44**, 336 (2009)
343. N.M. Emmanuel, A.L. Buchachenko, *Khimicheskaya Fizika Stareniya i Stabilizatsii Polimerov* (Chemical Physics of Ageing and Stabilization of Polymers) (Nauka, Moscow, 1982)
344. G.P. Gladyshev, O.A. Vasnetsova, N.I. Mashukov, Ros. Khim. Zh. **35**(5), 576 (1990)
345. G.-T. Cardenas, C.-C. Retamal, Termochim. Acta **176**, 233 (1991)
346. V. Djoković, J.M. Nedeljković, Macromol. Rapid Commun. **21**, 994 (2000)
347. J. Kuljanin, M. Marinović-Cincović, S. Zec, M.I. Comor, J.M. Nedeljkovic, J. Mater. Sci. Lett. **22**, 235 (2003)
348. M. Marinović-Cincović, Č.Z.V. Aponjić, V. Djoković, S.K. Milonjic, J.M. Nedeljkovic, Polym. Degrad. Stabil. **91**, 313 (2006)
349. L.V. Ruban, G.E. Zaikov, Usp. Khim. **63**, 373 (1994) [Russ. Chem. Rev. **63** 357 (1994)]
350. N.A. Khalaturinskii, Al.Al. Berlin, T.V. Popova, Usp. Khim. **53**, 326 (1984) [Russ. Chem. Rev. **53**, 197 (1984)]
351. Al.Al. Berlin, Soros. Obrazov. Zh. (9), 57 (1996)
352. R.M. Aseeva, G.E.T. Zaikov, Makromol. Chem. Makromol. Symp. **74**, 335 (1993)
353. I.C. McNeil, R.C. McGuinness, Polym. Degrad. Stabil. **9**, 2 (1984)
354. N.A. Kopylova, Y.D. Semchikov, S.D. Zaitsev, Z. Prikl. Khim. **81**, 678 (2008)
355. R.S. Beer, C.A. Wikie, M.N.L. Mittleman, J. Appl. Polym. Sci. **46**, 1095 (1992)
356. K. Kondo, M. Matsumoto, K. Okamoto, J. Chem. Eng. Jpn. **32**, 217 (1999)
357. L.E. Manring, Macromolecules **24**, 3304 (1991)
358. J.B. Beck, S.J. Rowan, J. Am. Chem. Soc. **125**, 13922 (2003)
359. Q.G. Meng, P. Boutinaud, H.J. Zhang, R. Mahiou, J. Lumin. **124**, 15 (2007)
360. S. Selvakumar, R.S.M. Kumar, K. Rajarajan, J.A.A. Pragasam, S.A. Rajasekar, K. Thamizharasan, P. Sagayaraj, Cryst. Growth. Des. **6**, 2607 (2006)
361. M.E. Kosal, J.N. Chou, S.R. Wilson, K.S. Suslik, Nat. Mater. **1**, 118 (2002)
362. K.L. Mulfort, J.T. Hupp, J. Am. Chem. Soc. **129**, 9604 (2007)
363. T.K. Maji, R. Matsuda, S. Kitagawa, Nat. Mater. **6**, 142 (2007)
364. B. Xing, M.F. Choi, B. Xu, Chem. Eur. J **8**, 5028 (2002)
365. D. Wöhrle, A.D. Pomogailo, *Metal Complexes and Metals in Macromolecules* (Wiley-VCH, Weinheim, 2003)
366. M.N. Patel, V.J. Patel, Indian J. Chem., A **28**, 428 (1989)
367. M.N. Patel, D.H. Sutaria, G.J. Patel, Synth. React. Inorg. Metal-Org. Chem. **24**, 401 (1994)

368. R. Coskun, M. Yigitoglu, M. Sacak, *J. Appl. Polym. Sci.* **75**, 766 (2000)
369. D. Bilba, L. Bejan, L. Tofan, *Croatica Chemica Acta* **71**, 155 (1998)
370. B.W. Zhang, K. Fischer, D. Bieniek, A. Kettrup, *React. Polym.* **24**, 49 (1994)
371. R.X. Liu, B.W. Zhang, H.X. Tang, *J. Appl. Polym. Sci.* **70**, 7 (1998)
372. N. Kabay, H. Egawa, *Sep. Sci. Technol.* **29**, 135 (1994)
373. R. Lei, X. Jie, X. Jun, Z. Ruijun, *J. Appl. Polym. Sci.* **53**, 325 (1994)
374. E.H. Rifi, M.J.F. Leroy, J.P. Brunette, C. Schloesserbecker, *Solvent. Extr. Ion Exch.* **12**, 1103 (1994)
375. H. Kubota, Y. Shigehisa, *J. Appl. Polym. Sci.* **56**, 147 (1995)
376. N. Pekel, N. Sahiner, O. Güven, *J. Appl. Polym. Sci.* **81**, 2324 (2001)
377. I.H. Park, J.M. Suh, *Angew. Makromol. Chem.* **239**, 121 (1996)
378. G. Moroi, D. Bilba, N. Bilba, C. Ciobanu, *Polym. Degrad. Stabil.* **91**, 535 (2006)
379. O.G. Marambio, G. Del, C. Pizzaro, M. Jeria-Orell, M. Huerta, C. Olea-Azar, W.D. Habiche, *J. Polym. Sci.:Part A. Polym. Chem.* **43**, 4933 (2005)
380. N.B. Shitova, P.G. Tsyrunnikov, D.A. Shlyapin, P.S. Barbashova, D.I. Kochubei, V.I. Zaikovskii, *J. Struct. Chem.* **50**, 268 (2009)
381. I.C. McNeill, J.J. Liggat, *Polym. Degrad. Stabil.* **29**(93), 370 (1990)
382. I.C. McNeill, J.J. Liggat, *Polym. Degrad. Stabil.* **37**, 25 (1992)
383. S.M. Humphrey, M.E. Grass, S.E. Habas, L. Niesz, G.A. Somorjai, T.D. Tilley, *Nano Lett.* **7**, 785 (2007)
384. Y. Zhang, M.E. Grass, S.E. Habas, F. Tao, T. Zhang, P. Yang, G.A. Somorjai, *J. Phys. Chem. C* **111**, 12243 (2007)
385. C. Yang, Q. Shao, J. He, B. Jiang, *Langmuir* **26**, 5179 (2010)
386. R. De Palma, G. Reekmans, C. Liu, R. Wirix-Speetjens, W. Laureyn, O. Nilsson, L. Lagae, *Anal. Chem.* **79**, 8669 (2007)
387. M. Kuhara, H. Takeyama, T. Tanaka, T. Matsunaga, *Anal. Chem.* **76**, 6207 (2004)
388. S.L. Lu, G.X. Cheng, H.C. Zhang, X.S. Pang, *J. Appl. Polym. Sci.* **99**, 3241 (2006)
389. H. Lei, W. Wang, L. Chen, X. Li, B. Yi, L. Deng, *Enzyme Microb. Technol.* **35**, 15 (2004)
390. H. Qian, Z. Lin, H. Xu, M. Chen, *Biotechnol. Prog.* **25**, 376 (2009)
391. S. Yang, K. Lien, K. Huang, H. Lei, G. Lee, *Biosens. Bioelectron.* **24**, 861 (2008)
392. A.A. Ostroushko, M.Y. Sennikov, *Russ. J. Inorg. Chem.* **50**, 933 (2005)
393. E.V. Schevchenko, D.V. Talapin, N.A. Kotov, S. O'Brien, C.B. Murray, *Nature (London)* **439**, 55 (2006)
394. V.G. Pol, S.V. Pol, J.M. Calderon-Moreno, A. Gedanken, *J. Phys. Chem. C* **113**, 10500 (2009)
395. C. Zheng, J. Zhang, G. Luo, J. Ye, M. Wu, *J. Mat. Sci.* **35**, 3425 (2000)
396. Y. Wang, G. Cao, *Chem. Mater.* **18**, 2787 (2006)
397. C. Diaz, M.L. Valenzuela, *Macromolecules* **39**, 103 (2006)
398. C.X. Li, Z.Y. Zhong, W.K. Leong, *Langmuir* **24**, 10427 (2008)
399. C. Li, W.K. Long, *Langmuir* **24**, 12040 (2008)
400. P. Hooker, D.J. Tan, K.J. Clabunde, S. Suib, *Chem. Mater.* **3**, 947 (1991)
401. J. Cheon, L.H. Dubois, G.S. Girolami, *J. Am. Chem. Soc.* **119**, 6814 (1997)
402. A.V. Grafov, E.A. Mazurenko, O.V. Mel'nik, V.Y. Kofman, *Ukr. Khim. Zh.* **59**, 1235 (1993)
403. A.D. Pomogailo, in *Macromolecules. Design and Applications*, ed. by A.S. Abd-El-Aziz, C.E. Carraher, C.U. Pittman, M. Zeldin (Springer, New York, 2008), p. 241
404. C. Klinke, K. Kern, *Nanotechnology* **18**, 215601 (2007)
405. E.P. Simonenko, V.G. Sevast'yanov, N.A. Ignatov, Yu.S. Ezhov, N.T. Kuznetsov, in *Tezisy Dokladov 2-i Vserossiiskoi Konferentsii po Nanomaterialam 'NANO 2007'* (Abstracts of Reports of the Second All-Russian Conferences on Nanomaterials 'NANO 2007', Novosibirsk, 2007) p. 79
406. G.A. Domrachev, W.E. Douglas, B. Henner, L.G. Klapshina, V.V. Semenov, A.A. Sorokin, *Polym. Adv. Technol.* **10**, 215 (1999)
407. G.T. Viola, M. Bortolotti, A. Zazzetta, *J. Polym. Sci.:Part A. Polym.Chem.* **34**, 13 (1996)

408. S.D. Bunge, T.J. Boyle. US 20056929675 (2005)
409. T.M. Keller, J. Perrin, S.B. Qadri, US 20056884861 (2005)
410. J. Nishijo, C. Okabe, O. Oishi, N. Nishi, *Carbon* **44**, 2943 (2006)
411. A.D. Pomogailo, A.S. Rozenberg, I.E. Uflyand, *Nanochastitsy Metallov v Polimerakh* (Nanoparticles of Metals in Polymers) (Khimiya, Moscow, 2000)
412. V. Biju, T. Itoh, A. Sujith, M. Ishikawa, *Anal. Bioanal. Chem.* **391**, 2469 (2008)
413. L. Mirengi, F. Antolini, L. Tapfer, *Surf. Interface Anal.* **38**, 162 (2006)
414. F. Antolini, T. Di Luccio, A.M. Laera, L. Mirengi, E. Piscopiello, M. Re, *Phys. Stat. Sol.* **244**, 2768 (2007)
415. K. Sung, S.H. Lee, T.M. Chung, C.G. Kim, *J. Nanosci. Nanotechnol.* **8**, 4873 (2008)
416. Y.B. Chen, L. Chen, L.M. Wu, *Inorg. Chem.* **44**, 9817 (2005)
417. J. Chen, L.M. Wu, L. Chen, *Inorg. Chem.* **46**, 586 (2007)
418. Y. Wang, J. Chen, L. Chen, Y.B. Chen, L.M. Wu, *Cryst. Growth Des.* **10**, 1578 (2010)
419. M. Yamamoto, M. Nakamoto, *J. Mater. Chem.* **13**, 206 (2003); N. Sandhyarani, T. Predeep, *J. Mater. Chem.* **11**, 1294 (2001)
420. Y.B. Chen, L. Chen, L.M. Wu, *Chem. Eur. J.* **14**, 11069 (2008)
421. Z. Yang, A.B. Smetana, C.M. Sorensen, K.J. Klabunde, *Inorg. Chem.* **46**, 2427 (2007)
422. T. Bhuvana, G.U. Kulkarni, *Small* **4**, 670 (2008)
423. G. Carotenuto, L. Nicolais, P. Perlo *Polymer Eng. Sci.* 1016 (2006)
424. M. Nakamoto, Y. Kashiwagi, M. Yamamoto, *Inorg. Chim. Acta* **358**, 4229 (2005)
425. G. Carotenuto, B. Martorana, P.B. Perlo, L. Nicolais, *J. Mater. Chem.* **13**, 2927 (2003)
426. A.S. Susha, M. Ringler, A. Ohlinger, M. Paderi, N. LiPira, G. Carotenuto, A.L. Rogach, J. Feldman *Chem. Mater.* **20**, 6169 (2008)
427. M. Hisamoto, R.C. Nelson, M.-Y. Lee, J. Eckert, S.L. Scott, *J. Phys. Chem. C* **113**, 8794 (2009)
428. X. Lu, H.-Y. Tuan, B.A. Korgel, Y. Xia, *Chem. Eur. J.* **14**, 1584 (2006)
429. E. Holder, N. Tessler, A.L. Rogach, *J. Mater. Chem.* **18**, 1064 (2008)
430. N. Bao, L. Shen, T. Takata, K. Domen, A. Gupta, K. Yanagisawa, C.A. Grimes, *J. Phys. Chem. C* **111**, 17527 (2007)
431. F. Capezzuto, G. Carotenuto, F. Antolini, E. Bursesi, M. Palomba, P. Perlo *Exp. Polym. Lett.* **3**, 219 (2009)
432. A. Petrella, M. Tamborra, M.L. Curri, M. Striccolli, P.D. Cozzoli, A. Adostano, *J. Phys. Chem. B* **109**, 1554 (2005)
433. G. Carotenuto, G. Pepe, D. Davino, B. Martorana, P. Perlo, D. Acierno, L. Nicolais, *Microw. Opt. Technol. Lett.* **48**, 2505 (2006)
434. Y.K. Jung, J.I. Kim, J.K. Lee, *J. Am. Chem. Soc.* **132**, 178 (2010)
435. T.X. Wang, H. Xiao, Y.C. Zhang, *Mater. Lett.* **62**, 3736 (2008)
436. D. Pullini, G. Carotenuto, M. Palomba, A. Mosca, A. Horsewell, L. Nicolais, *J. Mater. Sci.* **46**, 7905 (2011)
437. S. Chio, E.G. Kim, T. Hyeon, *J. Am. Chem. Soc.* **128**, 2520 (2006)
438. W.S. Seo, J.H. Lee, X. Sun, Y. Suzuki, D. Mann, Z. Liu, M. Terashima, P. Yang, M.V. McConnell, D.G. Nishimura, H. Dai, *Nat. Mater.* **5**, 971 (2006)
439. H. Bonnemann, R.A. Brand, W. Brijoux, H.-W. Hofstadt, M. Frerichs, V. Kempter, W. Maus-Friedrichs, N. Matoussevitch, K.S. Nagabhushana, F. Voigts, V. Caps, *Appl. Organomet. Chem.* **19**, 790 (2005)
440. S. Behrens, H. Bonnemann, N. Matoussevitch, A. Gorschinski, E. Dinjus, W. Habicht, J. Bolle, S. Zinoveva, N. Palina, J. Hormes, H. Modrow, S. Bahr, V. Kempter, *J. Phys. Condens. Mater.* **18**, 2543 (2006)
441. B.Y. Kim, I.B. Shim, Z.O. Araci, S.S. Saavedra, O.L.A. Monti, N.R. Armstrong, R. Sahoo, D.N. Srivastava, J. Pyun, *J. Am. Chem. Soc.* **132**, 3234 (2010)
442. Y.A. Barnakov, B.L. Scott, V. Golub, L. Kelly, V. Reddy, K.L. Stokes, *J. Phys. Chem. Solids* **65**, 1005 (2004)
443. F.-H. Lin, W. Chen, Y.-H. Liao, R. Doong, Y. Dong, *Nano Res.* **4**, 1223 (2011)

444. H. Yu, M. Chen, P.M. Rice, S.X. Wang, R.L. White, S.H. Sun, *Nano Lett.* **5**, 379 (2005)
445. S.H. Choi, B.H. Na, Y.I. Park, K. An, S.G. Kwon, Y. Jang, M. Park, J. Moon, J.S. Son, I.C. Song, W.K. Moon, T. Hyeon, *J. Am. Chem. Soc.* **130**, 15573 (2008)
446. S. Peng, C.H. Lei, Y. Ren, R.E. Cook, Y.G. Sun, *Angew. Chem. Int. Ed.* **50**, 3158 (2011)
447. H.W. Gu, Z.M. Yang, J.H. Gao, C.K. Chang, B. Xu, *J. Am. Chem. Soc.* **127**, 34 (2005)
448. Y. Jang, J. Chung, S. Kim, S.W. Jun, B.H. Kim, D.W. Lee, B.M. Kim, T. Hyeon, *Phys. Chem. Chem. Phys.* **13**, 2512 (2011)
449. C. Wang, C.J. Xu, H. Zeng, S.H. Sun, *Adv. Mater.* **21**, 3045 (2009)
450. J. Jiang, H.W. Gu, H.L. Shao, E. Devlin, G.C. Papaefthymiou, J.Y. Ying, *Adv. Mater.* **20**, 4403 (2008)
451. V. Mazumder, S.H. Sun, *J. Am. Chem. Soc.* **131**, 4588 (2009)
452. B.G. Ershova, A.V. Anan'eva, E.V. Abkhalimova, D.I. Kochubei, V.V. Kriventsov, L.M. Plyasova, I.Y. Molina, N.Y. Kozitsyna, S.E. Nefedov, M.N. Vargaftik, I.I. Moiseev, *Nanotechnol. Russ* **6**, 323 (2011)
453. N.S. Akhmadullina, N.V. Cherkashina, N.Y. Kozitsyna, I.P. Stolarov, E.V. Perova, A.E. Gekhman, S.E. Nefedov, M.N. Vargaftik, I.I. Moiseev, *Inorg. Chim. Acta* **362**, 1943 (2009)
454. T. Nedoseykina, P. Plyusnin, Y. Shubin, S. Korenev, *J. Therm. Anal. Calor.* **102**, 703 (2010)
455. A.V. Zadesenets, A.B. Venediktov, Y.V. Shubin, *Russ. J. Inorg. Chem.* **52**, 500 (2007)
456. L. Jiang, J. Kim, *J. Appl. Polym. Sci.* **101**, 186 (2006)
457. Q. Sun, K. Xu, H. Peng, R. Zheng, M. Haussler, B.Z. Tang, *Macromolecules* **36**, 2309 (2003)
458. G.Y. Yurkov, S.P. Gubin, E.A. Ovchenkov, in *Magnetic Nanoparticles*, ed. by S.P. Gubin (Wiley-VCH, Weinheim, 2009), p. 87
459. P.Y. Keng, I. Shim, B.D. Korh, J.F. Douglas, J. Pyun, *ACS Nano* **1**, 279 (2007)
460. G.Y. Yurkov, A.S. Fionov, Y.A. Koksharov, V.V. Kolesov, S.P. Gubin, *Inorg. Mater.* **43**, 834 (2007)
461. M.A. Zaporozhets, D.A. Baranov, N.A. Kataeva, I.I. Khodos, V.I. Nikolaichik, A.S. Avilov, S.P. Gubin, *Russ. J. Inorg. Chem.* **54**, 517 (2009)
462. M. Haussler, R. Zheng, J.W.Y. Lam, H. Tong, H. Dong, B.Z. Tang, *J. Phys. Chem. B* **108**, 10645 (2004)
463. K. Liu, B. Clendenning, L. Friebe, W.Y. Chan, X. Zhu, M.R. Freemann, G.C. Yang, C.M. Yip, D. Grozea, Z.-H. Lu, I. Manners, *Chem. Mater.* **218**, 2591 (2006)
464. G.T. Fried, G.S. Markovich, *Adv. Mater.* **13**, 1158 (2001)
465. R. Vijayakumar, Y. Kolytyn, I. Felner, A. Gedanken, *Mater. Sci. Eng. A* **286**, 101 (2000)
466. N. Bao, L. Shen, W. An, P. Padhan, C.H. Turner, A. Gupta, *Chem. Mater.* **21**, 3458 (2009)
467. R.W. Schwartz, *Chem. Mater.* **9**, 2325 (1997)
468. E. Erdem, R. Bottcher, H.-C. Semmelhack, H.-J. Glasel, E. Hartmann, D. Hirsch, J. Hormes, H. Rumpf, *J. Mater. Sci.* **34**, 2319 (1999)
469. H. Rumpf, J. Hormes, H. Modrow, H.-J. Glasel, E. Hartmann, E. Erdem, R. Bottcher, *J. Phys. Chem. B* **105**, 3415 (2001)
470. H.-J. Glasel, E. Hartmann, D. Hirsch, *J. Mater. Sci.* **38**, 3211 (2003)
471. B.S. Randhawa, M. Kaur, *Hyperfine Interact.* **188**, 1329 (2008)
472. L. von Lampe, D. Schultze, F. Zygalsky, M.S. Silverstein, *Polym. Degrad. Stab.* **81**, 57 (2003)
473. L. von Lampe, A. Schmalstieg, S. Götze, J.P. Muller, F. Zygalsky, H.J. Lorkowski, M. Matalla, *J. Mater. Sci. Lett.* **16**, 16 (1997)
474. L. von Lampe, A. Bruckner, S. Götze, *Die Angew. Makromol. Chem.* **251**, 157 (1997)
475. L. von Lampe, D. Schultze, F. Zygalsky, *Polym. Degrad. Stab.* **73**, 87 (2001)
476. M.S. Silverstein, Y. Najary, G.S. Grader, G.E. Shter, *J. Polym. Sci. Part B: Polym. Phys.* **42**, 1023 (2001)
477. M.S. Silverstein, Y. Najary, Y. Lumelsky, L. von Lampe, G.S. Grader, G.E. Shter, *Polymer* **45**, 937 (2004)
478. S. Maeda, Y. Tsurusaki, Y. Tachiyama, K. Naka, A. Ohki, T. Ohgushi, T. Takeshita, *J. Polym. Sci. Part A: Polym. Chem.* **32**, 1729 (1994)

479. J.C.W. Chien, B.M. Gong, X. Mu, Y.S. Yang, *J. Polym. Sci.: Part A: Polym. Chem.* **28**, 199 (1990)
480. K. Naka, K. Hagihara, Y. Tanaka, Y. Tachiyama, A. Ohki, S. Maeda, *J. Mater. Sci.* **31**, 6389 (1996)
481. K. Naka, Y. Tachiyama, A. Ohki, S. Maeda, *J. Polym. Sci.: Part A: Polym. Chem.* **34**, 1003 (1996)
482. S. Dubinsky, G.S. Grader, G.E. Shter, M.S. Silverstein, *Polym. Degrad. Stabil.* **86**, 171 (2004)
483. S. Dubinsky, Y. Lumelsky, G.S. Grader, G.E. Shter, M.S. Silverstein, *J. Polym. Sci.: Part B: Polym. Phys.* **43**, 1168 (2005)
484. A.D. Pomogailo, V.S. Savost'yanov, G.I. Dzhardimalieva, A.V. Dubovitskii, A.N. Ponomarev, *Izv. Akad. Nauk, Ser. Khim.* 1096 (1995)
485. Y. Lumelsky, M.S. Silverstein, *J. Mater. Sci.* **41**, 8202 (2006)
486. I. von Lampe, D. Schultze, F. Zygalsky, M.S. Silverstein, *Polym. Degrad. Stabil.* **81**, 57 (2003)
487. I. von Lampe, I.S. Götte, F. Zygalsky, *J. Low Temp. Phys.* **105**, 1289 (1996)
488. E.H. Tadd, J. Bradley, R. Tannenbaum, *Langmuir* **18**, 2378 (2002)
489. S. King, K. Hyunh, R. Tannenbaum, *J. Phys. Chem. B* **107**, 12097 (2003)
490. R. Tannenbaum, M. Zubris, E.P. Goldberg, S. Reich, N. Dan, *Macromolecules* **38**, 4254 (2005)
491. R.R. Netz, D. Andelman, *Phys. Rep.* **380**, 1 (2003); N. Dan, *Langmuir* **16**, 4045 (2000)
492. E. Tadd, A. Zeno, M. Zubris, N. Dan, R. Tannenbaum, *Macromolecules* **36**, 6497 (2003)
493. E.G. Nebukina, A.A. Arshakuni, S.P. Gubin, *Russ. J. Inorg. Chem.* **54**, 1685 (2009)
494. S.P. Gubin, G.Y. Yurkov, I.D. Kosobudsky, *Int. J. Mater. Product Technol.* **23**, 2 (2005)
495. H.T. Yang, C.M. Shen, Y.K. Su, T.Z. Yang, H.J. Gao, Y.G. Wang, *Appl. Phys. Lett.* **82**, 4729 (2003)
496. T. Hyeon, *Chem. Commun.* **927** (2003)
497. Y.A. Koshkarov, G.Y. Yurkov, D.A. Baranov, A.P. Malakho, S.N. Polyakov, S.P. Gubin, *Fiz. Tv. Tela* **48**, 885 (2006)
498. M.V. Radchenko, G.V. Lashkarev, V.I. Sichkovskiy, A.A. Arshakuni, S.P. Gubin, V.O. Yuhymchuk, V. Domukhovskii, T. Story, Y.P. Piryatinskii, G.Y. Yurkov, *Inorg. Mater.* **45**, 468 (2009)
499. D.L. Huber, *Small* **1**, 482 (2005)
500. A.D. Pomogailo, A.S. Rozenberg, G.I. Dzhardimalieva, A.M. Bochkin, S.I. Pomogailo, N.D. Golubeva, V.M. Grishchenko, *Neorg. Mater.* **42**, 164 (2006)
501. A.D. Pomogailo, in *Macromolecules. Design and Applications*, ed. by A.S. Abd-El-Aziz, C.E. Carraher, C.U. Pittman, M. Zeldin (Springer, New York, 2008), p. 241
502. A.D. Pomogailo, G.I. Dzhardimalieva, A.S. Rozenberg, V.N. Kestelman, *J. Thermoplastic Comp. Mater.* **20**, 151 (2007)
503. K. Hanko, G. Vass, I. Szepes, *J. Organomet. Chem.* **492**, 235 (1995)
504. V.A. Umilin, V.K. Vanchagova, in *Primenenie Metalloorganicheskikh Soedinenii dlya Polucheniya Neorganicheskikh Pokrytii i Materialov* (Applications of Organometallic Compounds for Production of Inorganic Coatings and Materials), ed. by G.A. Razuvaev. (Nauka, Moscow, 1986), p. 58
505. Yu.D. Tretyakov, *Usp. Khim.* **72**, 731 (2003) [Russ. Chem. Rev. **72**, 651 (2003)]
506. A.S. Rozenberg, A.A. Rozenberg, A.V. Lankin, G.I. Dzhardimalieva, A.D. Pomogailo, *Dokl. Akad. Nauk* **393**, 361 (2003)
507. N.D. Zhuravlev, V.I. Raldugin, A.P. Tikhonov, *Kolloid. Zh.* **61**, 322 (1999)
508. A.F. Shestakov, V.N. Solov'ev, V.V. Zagorskii, G.B. Sergeev, *Zh. Fiz. Khim.* **68**, 155 (1994)
509. A.S. Rozenberg, A.A. Rozenberg, G.I. Dzhardimalieva, A.D. Pomogailo, *Kolloid. Zh.* **67**, 70 (2005)
510. J.-M. Lehn, *Supramolecular Chemistry Concepts and Perspectives* (VCH, Weinheim, 1995)
511. P.M. Zorkii, I.E. Lubnina, *Vestn. Mosk. Univ., Ser. 2, Khim.* **40**, 300 (1999)